Master Thesis

The elevated metro structure in concrete, UHPC and composite

Design study

Rotterdam, October 2010

Author
R.J.A. Kenter
1213059

Delft University of Technology
Faculty of Civil Engineering & Geosciences
Department of Design & Construction
Section of Structural & Building Engineering

Rotterdam Public Works Engineering Office
Department of Civil Engineering

Graduation Committee

Prof.dr.ir. J.C. Walraven
Dr.ing. A. Romeijn
Ir. S. Pasterkamp

Dr.ir. C.B.M. Blom

TU Delft Delft University of Technology

Gemeente Rotterdam Gemeentewerken

Figure front page: the Bangkok Mass Transit System [i6]

Preface

This report presents the results of my design study of my graduation thesis. Together with my literature and preliminary study, this forms my Master graduation thesis. This project was performed to obtain my Masters degree in Civil Engineering at Delft University of Technology. The project was carried out at the engineering office of Rotterdam Public Works in cooperation with the Faculty Civil Engineering & Geosciences, Department of Design & Construction.

The graduation committee consisted of the following members:

- Prof.dr.ir. J.C. Walraven, Delft University of Technology
- Dr.ing. A. Romeijn, Delft University of Technology
- Ir. S. Pasterkamp, Delft University of Technology
- Dr.ir. C.B.M. Blom, Engineering Office of Rotterdam Public Works, Delft University of Technology

I would like to thank the engineering office of Rotterdam Public Works for providing me with a pleasant workplace at their office. Furthermore, my gratitude goes to my colleagues for the enjoyable and relaxed atmosphere during my graduation time. Finally, I would like to thank my graduation committee for their support and advice, and especially Kees Blom for his enthusiasm and personal guidance.

Rotterdam, October 2010

Ruud Kenter

Table of contents

Summary literature and preliminary study

To keep cities and metropolises accessible it is seen more and more that the infrastructure is elevated high above the ground. An elevated metro system has the advantage that it is cheaper than an underground metro system and the construction time is much shorter. The physical barrier caused by the realisation of an elevated system is also less than that of a metro system at ground level (only columns). One major disadvantage is the visual barrier of an elevated metro system. This is especially the case for a practical elevation of about 5 metres. The realisation of such elevated lines often causes resistance from residents. There is however a trend to increase the elevation even more, up to a height of about 10 to 12 metres. This is applied in some large cities/metropolises and seems to cause less visual hindrance as it creates a more open and lighter space below the structure. At the same time it can, if well designed, serve as an attractive landmark that gives the city a unique appearance.

In the future, Rotterdam wants to extent its existing metro system. An elevated metro system high above the city is one of the possible concepts. The engineering office of Rotterdam Public Works is interested in this concept and moreover in whether there can be gained profit on the elevated metro structure by applying Ultra High Performance Concrete or Fibre Reinforced Polymers instead of conventional concrete. The objective is to determine the dimensions and normative structural verifications of the elevated metro structure when this is made of conventional concrete, Ultra High Performance Concrete or Fibre Reinforced Polymers and to compare these designs with each other. The graduation thesis exists of two parts: the literature and preliminary study and the design study. The design study concerns the structural design and analysis of the elevated metro structure and results in three designs made of respectively conventional concrete, Ultra High Performance Concrete (UHPC) and Fibre Reinforced Polymers (FRP). The literature and preliminary study gives information about important aspects of elevated metro systems, UHPC and FRP and has as major objective to determine the height and span of the elevated railway for the application of an elevated metro system in Rotterdam.

Reference projects show that the alignment of an elevated metro system within a city follows the street pattern as much as possible. From a social point of view, the stations are made very transparent. The stations often consist of three levels: ground level with the access points; first level with the stations concourse; and the second level with the station platform(s). Furthermore, reference projects show that it is possible to create elevated metro systems that have a small environmental impact. The span-to-height ratio of elevated metro lines ranges between 2 to 4. For the determination of the bridge type, it is important to take into account the material and construction prices, which can differ from country to country.

The possible means for vertical transportation inside an elevated metro station are stairs, escalators and elevators. The use of moving walkways is not efficient enough. The stations will always have stairs, as this is required in emergencies. Also at least one elevator is necessary to make the station accessible for disabled persons. The choice between stairs, escalators or elevators as major means of vertical transportation depends on the height of the elevated metro station. For very small elevations stairs are chosen. When the height becomes larger and terraces for the stairs are necessary (rise of more than 4 metres), escalators are the best option. Elevators are chosen as major means of transportation if the elevation exceeds 30 metres.

The structure of an elevated railway is similar to that of a bridge. There are many types of bridges all with their own characteristics, span range and possible construction methods. Important for a metro line is the ability to follow a curved alignment. A curved alignment can be created by building several shorter straight spans or by using horizontally curved girders. The latter creates a far more uniform and aesthetical structure. The curvature however limits the maximum span length. Furthermore, it is important to take into account the maintenance and replacement of the bridge in the design phase.

A suitable height of an elevated metro system in Rotterdam ranges between 9 and 15 metres. The height of 9 metres is chosen, as people within an average building of 9 metres high can look straight out of the window without seeing the elevated railway. The height of 15 metres follows from a maximum span of 45 metres and a span-to-height ratio of 3 to create a more aesthetical appearance.

The reason for a maximum span of 45 metres is twofold: Firstly, with this span length it is expected that the metro alignment can follow the cities street pattern and fits into the proportions of the city. Secondly, this is seen as the most economical span as it can be built with in-situ concrete, precast concrete and steel girders. Rotterdam is however not just a city but wants to distinguish itself from other cities and as an elevation of 12 metres becomes more common an elevated metro system in Rotterdam should have an elevation of 15 metres. A higher elevation creates also a more open and lighter area underneath the structure. Moreover, this is more challenging for further elaboration in the design study of the graduation thesis. If the elaboration of the elevated railway with a span of 45 metres turns out to be an appropriate structural design it is still possible to diminish the height.

Ultra High Performance Concrete (UHPC) is a result of the search for a concrete with a higher strength. The strength classes of UHPC range between C90/105 and C200/230. The creation of UHPC is made possible by changing the design of the concrete mix by: improving the homogeneity and the microstructure, increasing the package density, adding steel fibres and reducing the water-cement ratio. The material has a high durability and can result in more slender structures. The costs are however high compared with conventional concrete. Furthermore, the mix design of UHPC is complex and deserves special attention. It is assumed to be the best to utilize precast UHPC elements instead of in-situ UHPC. For the design of the elevated railway made from UHPC in the design study a thesis is used [1].

Fibre Reinforced Polymers (FRP) is a composite material. FRP consists of load-bearing fibres and a polymer resin matrix in which they are embedded. Whereas the fibres exercise the actual load-bearing function, the polymer matrix essentially has four functions:

- Fixing the fibres in the desired geometrical arrangement
- Transferring the forces to the fibres
- Preventing buckling of the fibres under compression actions
- Protecting the fibres from humidity etc.

There is a wide range of FRP producible, which has resulted in few standard composites and standard codes. FRP has a very high strength at low weight and by adding additives it can be mixed for many suitable applications. And as there is a wide range of FRP producible there are also many manufacturing processes. Points of interest are the possibility of delamination and the stiffness of the bridge. The cost for FRP is relatively high. Sandwich construction is commonly used with composites to increase structural efficiency, with the FRP forming the outer skins and bonded to a variety of core materials. For the design of the elevated railway made from FRP in the design study a thesis is used[17].

Summary design study

To keep cities and metropolises accessible it is seen more and more that the infrastructure is elevated high above the ground. An elevated metro system has the advantage that it is cheaper than an underground metro system and the construction time is much shorter. The physical barrier caused by the realisation of an elevated system is also less than that of a metro system at ground level (only columns). One major disadvantage is the visual barrier of an elevated metro system. This is especially the case for a practical elevation of about 5 metres. The realisation of such elevated lines often causes resistance from residents. There is however a trend to increase the elevation even more, up to a height of about 10 to 12 metres. This is applied in some large cities/metropolises and seems to cause less visual hindrance as it creates a more open and lighter space below the structure. At the same time it can, if well designed, serve as an attractive landmark that gives the city a unique appearance.

In the future, Rotterdam wants to extent its existing metro system. An elevated metro system high above the city is one of the possible concepts. The engineering office of Rotterdam Public Works is interested in this concept and moreover in whether there can be gained profit on the elevated metro structure by applying Ultra High Performance Concrete or Fibre Reinforced Polymers instead of conventional concrete. The objective is to determine the dimensions and normative structural verifications of the elevated metro structure when this is made of conventional concrete, Ultra High Performance Concrete or Fibre Reinforced Polymers and to compare these designs with each other. The graduation thesis exists of two parts: the literature and preliminary study and the design study. The design study concerns the structural design and analysis of the elevated metro structure and results in three designs made of respectively conventional concrete, Ultra High Performance Concrete (UHPC) and Fibre Reinforced Polymers (FRP). The literature and preliminary study gives information about important aspects of elevated metro systems, UHPC and FRP and has as major objective to determine the height and span of the elevated railway for the application of an elevated metro system in Rotterdam.

Out of the literature and preliminary study followed that the railway should have an elevation of 15 metres and a span of 45 metres. The metro structure consists of four elements: railway girder, column, foundation slab and piles. Because the length of the column is large, the stiffness and stability of the whole structure are important issues. Besides, it is desired to design a slender structure from an aesthetical point of view. By minimizing the dead load of the girder, the stability of the structure becomes less critical. This can result in more slender columns and/or less piles and will save costs. It is however possible that the girder with the smallest depth is not the lightest girder. In this study the accent is more on the optimal structural design in relation to the costs and less on the aesthetical design. For the designs of the elevated metro structure made of conventional concrete, UHPC or FRP the focus is therefore on the lightest railway girder and not on the minimum depth of the girder.

The best concept for the concrete and UHPC railway girder is the precast segmental box girder with external prestressing tendons. This concept results in the lightest railway girder made of (UHP) concrete and is very practical. The best construction method for the precast segmental box girder is the span-by-span construction. The span-by-span construction method is an economic and rapid method for constructing viaducts. With this method the required construction site is small and there is little hindrance for the surrounding area.

The optimal concrete box girder, which results in the lightest railway girder, has 6 prestressing tendons with dimensions as shown in Section 4.3. This optimal design is found by means of an optimisation process where the behaviour of the box girder is examined by changing different parameters. The dead load of the optimal concrete box girder is 102.02 kN/m. The normative structural verification of the optimal concrete box girder is fatigue of the concrete at the deviation blocks at the bottom side. The best way to satisfy this verification is to increase the bottom flange thickness. The lightest box girder arises when the minimum top flange thickness and the minimum width of the webs are chosen and the bottom flange thickness is just enough to satisfy the verification of fatigue of the concrete. The minimum deck thickness is set by the verifications of the ultimate resistance moment and the rotation capacity of the deck. Buckling of the webs determines the

minimum width of the webs of the optimal design. Furthermore, the verification of the ultimate resistance moment of the box girder at t=∞ is normative for the minimum depth of the webs.

The optimal UHPC box girder has also 6 prestressing tendons. The dimensions of the box girder, which are shown in Section 6.3, are found by means of the optimisation process. The optimal UHPC box girder has a dead load of 69.4 kN/m. The normative structural verification of the optimal UHPC box girder is the ultimate resistance moment of the box girder at t=0. Increasing the bottom flange thickness is the most effective way to satisfy this verification. The lightest box girder thus arises when the minimum top flange thickness and the minimum width of the webs are chosen and the bottom flange thickness is just enough to satisfy the verification of the ultimate resistance moment at t=0. The minimum deck thickness is set by the verifications of the ultimate resistance moment and the rotation capacity of the deck. Normative for the minimum width of the webs is the verification of buckling of the webs. The minimum depth of the webs is set by the verification of the ultimate resistance moment of the box girder at t=∞.

The design of the railway girder made of FRP is a sandwich girder and is based on the InfraCore® concept. This design is a global design for a FRP railway girder. Carbon fibre epoxy is chosen for the FRP, as this is the best FRP material for the railway girder from a structural point of view. The normative structural verifications of the FRP sandwich girder are deflection of the girder and buckling of the core triangles. The dimensions of the FRP girder, which satisfies the verifications, are shown in Section 8.3. The dead load of the FRP sandwich girder is 34.48 kN/m. In order to design a fail-safe FRP structure large conversion factors are applied.

The difference in dead load between the three designed railway girders is quite large. The application of a lighter railway girder does however not result in a large reduction of the number of piles. This is due to the small weight contribution of the railway girder to the total vertical load at the piles and the large contribution of the moments at the foundation to the pile forces. The normative structural verification of the columns is stiffness of the viaduct. Stiffness is normative over stability due to the large horizontal force at the top of the column in transversal direction of the viaduct. Especially the wind load is determining for the magnitude of this horizontal force. Because the difference between the depths of the girders is relative small the difference in size between the columns of the three designs is also small. Applying UHPC or FRP instead of conventional concrete for the railway girder thus has a small impact on the substructure. The choice between the three designs will therefore probably be based on the construction/fabrication, costs and aesthetics of the railway girder.

The direct construction costs for the elevated metro structure with a concrete box girder are about €450,000 per span of 45 metres. When the unit price of UHPC is lower than € 450/m^3, the UHPC box girder becomes a serious competitor of the conventional concrete box girder from a financial point of view. Whether the UHPC box girder design is cheaper than the concrete box girder design is thus dependent on the market price of UHPC. It should be noticed that the application of UHPC results in a more slender railway girder. This can also be a reason to choose for the UHPC box girder instead of the concrete box girder. For the FRP railway girder holds that FRP is currently far too expensive to compete with the (UHP) concrete box girder.

The recommendations concerning a further detailing of the designs are:

- Execute an accurate calculation of the prestressing losses in the concrete box girder to check whether the verification of fatigue of the concrete is still satisfied.
- Examine the fatigue behaviour of UHPC and determine the fatigue verification of UHPC.
- Execute a dynamic analysis of the FRP sandwich girder to check whether the structure is determined against the dynamic effects.
- Take into account the micromechanics of the FRP sandwich girder.
- Take into account the manufacturing process of the FRP sandwich girder.

1. Introduction

1.1 Metro systems

A metro system is an electric passenger railway in an urban area. Characteristics of a metro system are the high capacity and frequency at which it transports people and the grade separation from other traffic. The grade separation allows the metro to move freely, with fewer interruptions and at higher overall speeds. Furthermore, there are fewer conflicts between traffic movements, which reduce the number of accidents, making it a safer way to travel. Grade separation for metro systems is realised by placing it in underground tunnels, elevated above street level or grade separated at ground level. Often a metro system is a combination of these three options.

Beside the traditional metro using electric multiple units on rails, nowadays one can find also some systems using magnetic levitation or monorails. By changing the capacity of the trains, the frequency and the distance between the stations, variations on traditional metros like people movers and light metros have appeared. At the same time, technological improvements have allowed new driverless lines and systems. With all these variations in metro systems it is sometimes difficult to determine to what type a system belongs. Despite all these variations, they have in common that they are executed more and more as elevated railways in dense urban areas.

1.2 Problem description

Building underground metro systems is very expensive and takes a lot of time to realise. Besides, it is often a risky operation in urban areas. In areas with high land prices and dense land use, this option may however be the only economic route for mass transportation. The construction of ground level metro lines is the cheapest of the three options, as long as the land values are low. Since ground level metro lines create a physical barrier that hinders the flow of people and vehicles it is mostly used outside dense urban areas. Elevated railways are a cheap and easy way to build an exclusive metro line without digging expensive tunnels or creating physical barriers. Considering this from a practical and economical point of view, an elevated metro system is often the most suitable solution of the three options.

In some metropolises the infrastructure is elevated up to a large height above the city. In the Netherlands this concept can also be found, but often concerns a practical elevation of about 5 metres. This elevation allows car traffic to pass underneath. Due to the limited height, this is however often seen as a psychological barrier between two areas. By increasing the elevation as is applied in some metropolises, this psychological barrier decreases. This makes the concept more attractive as alternative for the extension of the public transport. Moreover, as mentioned above an elevated metro system has the advantages that it costs less and takes less time to construct compared with an underground metro system and does not create a physical barrier. With a higher elevated metro system it is thus possible to create an even more attractive alternative as it is also accepted more from a social point of view. This all makes this concept truly worth to take into consideration as option for mass transportation by metros.

In the future, Rotterdam wants to extent its existing metro system. An elevated metro system high above the city is one of the possible concepts. The engineering office of Rotterdam Public Works is interested in this concept and moreover in whether there can be gained profit on the elevated metro structure by applying Ultra High Performance Concrete or Fibre Reinforced Polymers instead of conventional concrete. More specific, they would like to know if an elevated metro structure made of Ultra High Performance Concrete or Fibre Reinforced Polymers results in different structural dimensions. Besides, the question is what the normative structural verifications are when these materials are applied to an elevated metro structure.

Notice that the title of this thesis contains the term “composite”. The term “composite” covers a wide range of material combinations. However, in this thesis “Fibre Reinforced Polymers” is meant with the term “composite”.

1.3 Problem definition

What are the dimensions of the elevated metro structure made of conventional concrete, Ultra High Performance Concrete or Fibre Reinforced Polymers and what are the normative structural verifications in these cases?

1.4 Objective

Determine the dimensions and normative structural verifications of the elevated metro structure made of conventional concrete, Ultra High Performance Concrete or Fibre Reinforced Polymers and compare these designs with each other. The height and span of the structure should fit in the city of Rotterdam.

1.5 Work approach

The graduation thesis exists of two parts: the literature and preliminary study and the design study. The literature and preliminary study concerns the first part of the thesis and treats among other things: already existing elevated metro systems and the functional design of an elevated metro system in Rotterdam. This study gives information about important aspects of elevated metro systems and has as major objective to determine the height and span of the elevated railway for the application of an elevated metro system in Rotterdam. These dimensions together with the other information of the literature and preliminary study are taken into account in the design study. The design study concerns the final and major part of this thesis and treats the structural design of the elevated metro structure. Different concepts are analysed for the elevated railway structure made of conventional concrete and Ultra High Performance Concrete (UHPC) and the best concept is further elaborated. Besides, a global design for the elevated railway structure made of Fibre Reinforced Polymers (FRP) is presented. The three designs are finally compared with each other, which gives a clear view on the differences in dimensions and normative structural verifications between the application of conventional concrete, Ultra High Performance Concrete and Fibre Reinforced Polymers.

This report concerns the design study and treats the structural designs of the elevated metro structure. First of all, the structural schematisation of the elevated metro structure together with the boundary conditions is given in chapter 2. The possible concepts for a (UHP) concrete superstructure are described in chapter 3. In this chapter the best concept is chosen for the concrete as well as the UHPC design. Chapter 4 presents the optimal design for a railway girder made of conventional concrete. Why this design is the optimal design is explained in the next chapter. For the UHPC railway girder the same order is applied: first the optimal design is presented in chapter 6 and then the optimisation process is described in chapter 7. The FRP railway girder design according the InfraCore® concept is presented in chapter 8. Now the superstructures are known the matching substructures are determined for the three designs. This is treated in chapter 9 where also a clear comparison between the three designs is given. To make the comparison between the three designs more complete there is made an indication of the construction costs of the three designs in chapter 10. The design study ends with the conclusions and recommendations considering the designs of an elevated metro structure.

References to literature in the text are indicated with [X], where X is a number which refers to the reference list at the end of this report. References to internet pages are indicated with [iX].

2. Designing an elevated metro structure

2.1 Schematisation elevated metro structure

The functional design of an elevated metro system in Rotterdam was done in the literature and preliminary study. Out of this study followed that the railway should have an elevation of 15 metres and a span of 45 metres. The schematisation of the elevated metro structure for the design study is shown in Figure 1. The structure consists of four elements: railway girder, column, foundation slab and piles. Except for the elevation and span of the railway, the dimensions of the elements in Figure 1 are not representative for the design. The railway girder supports double track and is hatched in Figure 1. With this hatch it is signified that the shape of the girder does not represent the real geometry of the railway girder. It just shows that the girder has some kind of geometry that spans 45 metres and is supported by columns. Because the length of the column is large, the stiffness and stability of the whole structure are important issues. Therefore, it is expected that the columns become quite massive. More columns at the supports of the railway girder will require more space at ground level and will create a larger visual barrier than just one column. For this reason it is chosen that the railway is supported by just one column each 45 metres. Also the most reference projects from the literature and preliminary study show that this is the best solution and creates a more slender structure. The columns on their turn are supported by a pile foundation, which is common in Rotterdam.

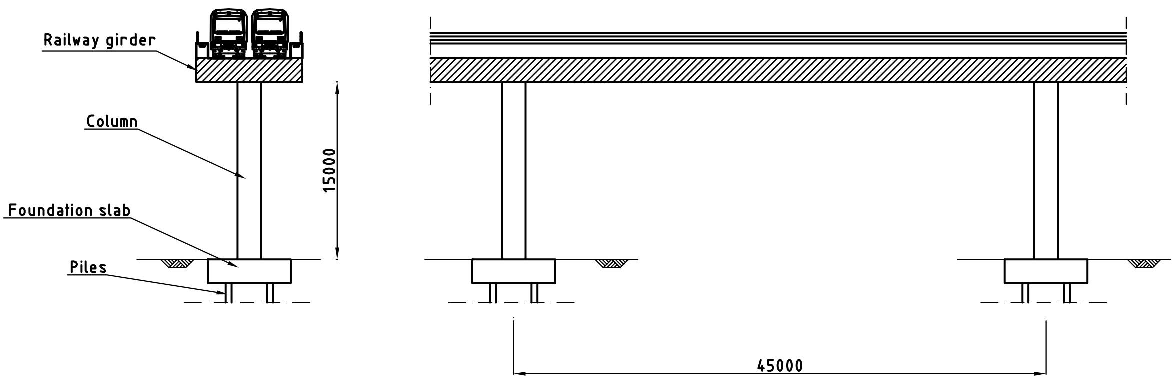

Figure 1: Schematisation elevated metro structure, cross-section and side-view of the structure

2.2 Boundary conditions

The operator of the current metro system in Rotterdam is the public transport company RET. When an elevated metro system is built in Rotterdam, it will most likely become part of this current metro network. The elevated metro structure will therefore be designed for metros of the RET. The cross-section of the top part of the superstructure for a double track metro viaduct with the clearance gauge according “Gegevens Metrobouw” [22] is shown in Figure 2. It is chosen to place the emergency walkways on the outside of the railway instead of in the middle as this creates less eccentric loading on the whole structure due to the heavy metro cars. Notice that the railway girder, which carries the construction and metros depicted in Figure 2, should have a width of at least 8.96 metres. The maximum velocity of the metros is 100 km/h. During the construction of the elevated metro system the hindrance for the surrounding area must be limited. The structural lifespan of the elevated metro structure is 100 years.

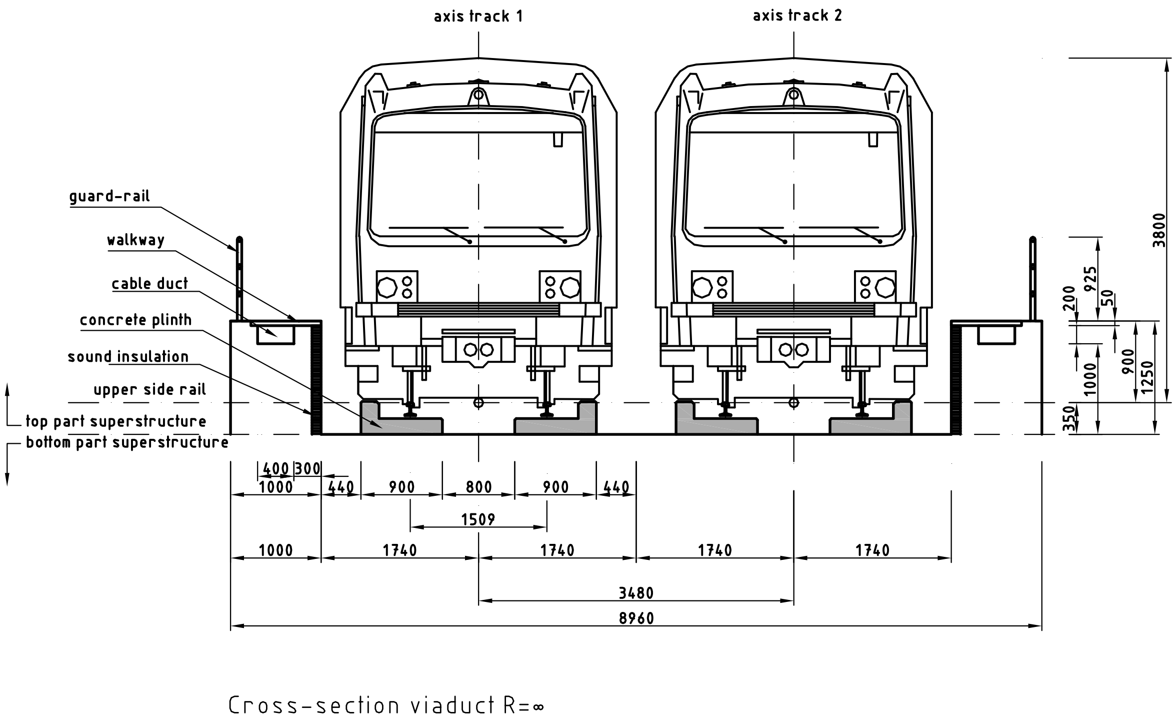

Figure 2: Cross-section top part superstructure for a double track metro viaduct

In this design study, three materials are considered for the railway girder. These materials are: conventional concrete, Ultra High Performance Concrete and Fibre Reinforced Polymers. The girders are supported by concrete columns. Whether the columns should be made of conventional or Ultra High Performance concrete results from this design study. Columns made of FRP are not taken into account. A column made of FRP would probably result in a kind of sandwich column because a massive FRP column will cost far too much. The stiffness as well as the connection with the concrete foundation are critical issues for constructing an elevated metro structure with FRP columns. Therefore, it is expected that a concrete column is more practical and cheaper. The foundation slab of the structure is made of conventional concrete as for in-situ UHPC it is hard to control the curing/quality of the concrete. For constructing in UHPC, it is better to utilize precast UHPC elements as this ensures a better quality. For the foundation slab it is however more practical to use in-situ concrete and it is even the question if applying UHPC will result in a better and/or cheaper design. Also the piles are made of conventional concrete as the soil characteristics are normative and not the concrete strength of the piles.

In the literature and preliminary study the most common bridge types are described. For an elevated metro system in Rotterdam with spans of 45 metres some bridge types are however not the best option. The suspension bridge and cable-stayed bridge for instance are usually applied for large spans. As the span in this case is just 45 metres these bridge types are not taken into consideration. The cost for such metro structures will be enormous and in addition, it will have a huge visual impact with all its cables. The question is, if this is seen as a visual barrier or as an attractive landmark? An arch bridge will also result in quite a large structure and introduces large horizontal forces in the foundation. Because the soil in the Netherlands is relative weak this bridge type will require a large foundation. Arch bridges are often the most economical choice for bridges that cross over inaccessible landscape. As the construction site concerns Rotterdam it is expected that an arch bridge will not outweigh the girder bridge and the truss bridge. The two best options left are thus the girder bridge and truss bridge which are both common for spans of 45 metres.

Truss bridges are often made from steel, but wooden trusses can also be found. In this case, a steel truss will probably be the best choice as a wooden truss results in a more massive truss. This is because the material stiffness is smaller and the required edge distance for the connections is larger. Considering the current techniques, durability of both materials is nowadays not a reason to reject these materials. Also the noise nuisance of steel bridges can be reduced to an acceptable level by application of noise reducing techniques and solutions. Although an elevated metro structure made of wood or steel could both result in a very suitable design this is not examined in this design study. This study concerns designing an elevated metro structure made of conventional concrete, UHPC or FRP. This thesis thus not examines the best overall design for an elevated metro structure. For such an examination more materials should be taken into account. In this study just three materials/designs are analysed and compared. Because a truss bridge cannot be made of concrete and, as mentioned in the literature and preliminary study, the FRP viaduct concerns a sandwich girder, the only bridge type left is the girder bridge.

2.3 Designing the utmost

For the elevated metro structure as schematised in Figure 1 the stiffness and stability of the whole structure are important issues. Besides, it is desired to design a slender structure from an aesthetical point of view. The railway girder should thus have a small depth with a small dead load. By minimizing the dead load of the girder, the stability of the structure becomes less critical. This can result in more slender columns and/or less piles and will save costs. It is however possible that the girder with the smallest depth is not the lightest girder. In this study the accent is more on the optimal structural design in relation to the costs and less on the aesthetical design. For the designs of the elevated metro structure made of conventional concrete, UHPC or FRP the focus is therefore on the lightest railway girder and subsequently on the minimum depth of the girder. The designs in this study can be classified as global designs and with the term “optimal design” is meant the optimal design according the boundary conditions and schematisations in this study. For the “real optimal designs” of an elevated metro structure made of the three materials more detailed designs are necessary. This study however considers the global designs, which are detailed enough to determine the dimensions and normative structural verifications for an elevated metro structure made of conventional concrete, UHPC or FRP.

3. Concrete concepts

3.1 Concrete concepts

The previous chapter showed that the girder bridge is the best bridge type for the elevated metro structure made of concrete. To span 45 metres it is necessary to use prestressed concrete, as reinforced concrete girder bridges are not capable to cover such a span. In general there are five appropriate concepts for a prestressed concrete railway girder which spans 45 metres.
These concepts are:

- The inverted T-beam bridge
- The box beam bridge
- The cast in-situ box girder bridge
- The precast segmental box girder bridge
- The trough bridge

Appendix A: Concrete concepts, shows the cross-section of these concepts for conventional concrete. The dimensions are determined according rule of thumbs and reference projects for a span of 45 metres.

3.1.1 Inverted T-beam bridge

The railway girder consists of prefabricated inverted T-beams with a cast in-situ topping, see Appendix A.1. The total structural depth of the girder is 1.93 metres, which means a span-to-depth ratio of 23. The total visual depth of the railway girder including the emergency walkways is 3.18 metres. The prestressed inverted T-beams are straight and supported by columns with cross-girders. A visual appealing structure in curves is created with a variable corbel attached to the topping.

3.1.2 Box beam bridge

The railway girder consists of prefabricated box beams, see Appendix A.2. The total structural depth of the girder is 1.6 metres, which means a span-to-depth ratio of 28. The total visual depth of the railway girder including the emergency walkways is 2.85 metres. The prestressed box beams can be straight or curved and are supported by columns with cross-girders. By transverse prestressing, all the box beams are coupled.

3.1.3 Cast in-situ box girder bridge

The railway girder consists of a cast in-situ box girder with internal prestressing tendons in the webs, see Appendix A.3. The total structural depth of the girder is 1.8 metres, which means a span-to-depth ratio of 25. The total visual depth of the railway girder including the emergency walkways is 3.05 metres. The prestressed box girder can be curved and is supported by columns without the need for cross-girders.

3.1.4 Precast segmental box girder bridge

The railway girder consists of a precast segmental box girder with external prestressing tendons, see Appendix A.4. The total structural depth of the girder is 2.5 metres, which means a span-to-depth ratio of 18. The total visual depth of the railway girder including the emergency walkways is 3.75 metres.
The prestressed box girder can be curved and is supported by the columns.

3.1.5 Trough bridge

The railway girder consists of two prefabricated parallel beams with a cast in-situ floor in between, see Appendix A.5. The total structural depth of the girder is 2.8 metres, which means a span-to-depth ratio of 16. The emergency walkways are integrated in the railway girder such that the total visual depth equals the total structural depth of the girder. The prestressed beams can be straight or curved and are hollow, except near the supports. The two beams are supported by columns with cross-girders.

3.2 Chosen concept

The five concepts described above show that the trough bridge results in the most slender superstructure. Together with the box beam bridge, these two concepts will result in the most suitable railway girder from a visual slender point of view. The disadvantage of these concepts is that a cross-girder is needed to support the beams. Cross-girders are often quite determining for the visual appearance of the viaduct and considered as unwanted. Also the inverted T-beam bridge requires cross-girders to support the 45 metres long beams. As mentioned before the goal is however to design the lightest railway girder instead of the most slender and visual appealing girder. Besides, the constructability should be taken into account in order to design a feasible elevated metro structure. The most slender railway girder concept (in this case the through bridge), is therefore not obviously the best concept for the design.

The construction of an elevated metro system in Rotterdam will have a huge impact on the surrounding area. To minimize the hindrance during constructing the structure, a smart construction method should be chosen. For the concepts with 45 metres long prefabricated beams (inverted T-beam bridge, box beam bridge and trough bridge) the accent for the construction will be on the transportation of the beams. The limits of a self-propelled implement, such as mobile cranes, for which no granting exemption is necessary, are [i2]:

Width:	3 metres
Length:	20 metres
Total height:	4 metres
Axle load:	12,000 kg
Total weight:	60,000 kg

This means that the transport of the beams requires exceptional transport. Not only because of the length of the beams, but probably also the total weight of a transport of one beam will exceed the prescribed limit. For exceptional transport in Rotterdam it holds in general that the maximum velocity is 10 km/h for transports heavier than 100,000 kg and 30 km/h for a total weight below 100,000 kg. The construction of an elevated metro structure consisting of beams can hereby become quite problematic. As not every location is well accessible and considering the low velocity of the transport it can be expected that there will be much hindrance for the surrounding area. To minimize the hindrance it can be considered to transport the beams only at night.

In this design study not only a railway girder made of conventional concrete is examined, but also one made of UHPC. For UHPC special attention should be paid to the curing process of the concrete. In factories a better controllability of this process is possible, which ensures a better quality. It is therefore recommended to utilize prefabricated UHPC elements instead of cast in-situ elements. In order to compare the designs made with the two materials (conventional concrete and UHPC) it is chosen to consider one concept for both materials. The chosen concept will be the most favourable one for a railway girder made of UHPC. This is chosen in order to show the ultimate possibilities for constructing with UHPC.

The inverted T-beam bridge has, as mentioned before, the disadvantage that it requires exceptional transport to transport the beams. Besides, it has a cast in-situ topping which connects the beams together. The casting of the topping at a height of 15 metres will bring a lot of construction activities to the construction site. In order to minimize the hindrance for the surrounding area it is however better to minimize the number of construction activities at the construction site. Moreover, it is more difficult to cast such a topping made of UHPC. It can be chosen to combine UHPC beams with a topping of conventional concrete. This will however weaken the benefit of using UHPC in the girder and is therefore not taken into consideration. Also the through bridge has the same disadvantages as the inverted T-beam bridge. The through bridge even has a thicker deck, which means more construction activities at the site and a more difficult curing process for UHPC. During constructing a trough bridge there acts a large eccentric load on the structure when the first prefabricated beam is placed on the cross-girder. This will probably have its influence on the dimensions of the column and the foundation. It would be pity if this construction phase is normative for the whole structure. The concept which also has difficulties with controlling the curing process of the UHPC is the cast in-situ box girder bridge. Casting the whole girder on site needs a very sophisticated falsework and formwork in order to create a fluent curved box girder. Due to internal prestressing, the webs of this cast in-situ box girder are relative thick. This concept will therefore probably not result in the lightest railway girder.

So far, the analysis shows that the inverted T-beam bridge, the trough bridge and the cast in-situ box girder are not the most practical concepts to apply. Casting on site is not very suitable for the application of UHPC. Besides, it is recommended to limit the number of construction activities in order to minimize the hindrance for the surrounding area. The two concepts left, which offer better opportunities with respect to the execution process, are the box beam bridge and the precast segmental box girder. These concepts minimize the number of construction activities at the site by prefabricating the whole railway girder. Disadvantages for the box beam bridge are the need for cross-girders and exceptional transport for the precast beams. The box girder consists of segments which can be transported without a granting exemption. This will reduce the hindrance for the surrounding area and requires a less restrictive delivery schedule as it concerns ordinary transport. Despite the box beam bridge results in a more slender railway girder, the precast segmental box girder is considered as the best concept for UHPC. Beside the aforementioned disadvantages of a box beam bridge it is namely expected that the minimum thickness of the webs is restricted by the required concrete cover on the prestressing tendons and not fully benefits the material characteristics of UHPC. The precast segmental box girder does not have this problem as it utilizes external prestressing tendons. The box girder will therefore result in the lightest railway girder. Moreover, the shape of a box girder is considered as visual appealing and the objection of a larger structural depth is weakened by the large elevation of the railway. The large elevation creates an open and enlightened area underneath the structure what makes the larger structural depth of the box girder less salient. The overall conclusion is that the precast segmental box girder is the best concept to apply in Rotterdam for an elevated metro structure made of (UHP) concrete.

3.3 Construction method

For constructing a precast segmental box girder there are in general three construction methods available: balanced cantilever, incremental launching and span-by-span construction [6]. The incremental launching method is however not a very suitable construction method for the elevated metro structure. With this method the box girder is built in sections by pushing the structure outwards. This results in large horizontal forces on the starting column/structure. As the soil in Rotterdam is relative weak a large foundation will therefore be required. The construction phase will even be normative for the dimensions of the column and the foundation. Besides, this method is used in combination with internal prestressing tendons and not with external prestressing tendons. The application of external prestressing for the incremental launching method will result in a very complicated web of prestressing tendons inside the box girder as all the segments need to be stressed together. Furthermore, the box girder needs to have a constant curvature. As the alignment will not have a constant curvature this construction method is rejected. For the balanced cantilever method holds that it is a relative slow building method. Besides, this method is also used in combination with internal prestressing tendons just as the incremental launching method. The application of external prestressing for the balanced cantilever method will thus also result in a very complicated web of prestressing tendons inside the box girder as all the segments need to be stressed together. Considering the aforementioned it is quite obvious that the span-by-span construction is the best construction method. Also the analysed reference projects base the choice for this construction method [6].

The span-by-span construction method for the elevated metro structure in Rotterdam is an economic and rapid method for constructing viaducts. This system makes use of precast segments, which are continuously placed from one column to the other. The box girder segments are positioned by a temporary staying mast or by a launching truss. As the elevation of the box girder is 15 metres, a launching truss is preferred. The launching truss with trolleys is braced over two columns. The box girder segments are transported by truck to the span under construction, see Figure 3. The length of the box girder segments is 3 metres so that exceptional transport is not required. A span of 45 metres thus includes 45 / 3 = 15 segments. The maximum weight of the segments should be about 30,000 kg so that the total weight of transport including the truck stays below 60,000 kg. Each segment is then lifted through the underslung hoist and discharged in the above mount trolley of the truss. Once all the segments are in position longitudinal prestressing connects the segments. Finally, deck joints are cast and closed. When the span is completed the launching truss moves to the next span where the construction cycle starts again until the bridge is completed. With this method the required construction site is small and there is little hindrance for the surrounding area, see Figure 4.


Figure 3: Transport of the concrete box girder segments [i8]


Figure 4: Traffic is able to pass during construction [i1]

4. Design concrete box girder C50/60

4.1 General

This chapter describes the design of the precast concrete segmental box girder with external prestressing tendons and the method of calculation. For the extensive calculation of the box girder reference is made to Appendix B: Calculations concrete box girder C50/60. This design represents the optimal design for a precast segmental box girder made of concrete C50/60 with external prestressing tendons. Why this design with its geometry and its prestressing characteristics is the optimal design is explained in the next chapter. In order to understand the optimisation process in the next chapter it is important to know the boundary conditions, the schematisation of the box girder with tendons and the structural verifications which have to be satisfied. For the design of the concrete box girder C50/60 there is mainly made use of the Eurocode 2: Design of concrete structures [11]. References to the specific codes and literature used for the design are also given in the Appendix.

4.2 Material characteristics

One speaks of conventional concrete for concrete with strength classes up to C53/65 [6]. As the dimensions of the elevated metro structure are quite large and so will be the forces, it is supposed that the application of conventional concrete should have a high strength class. Furthermore, application of conventional concrete with a high strength class results in a design which shows the ultimate possibilities for conventional concrete. This result can, when compared with the UHPC design, clearly show the differences between what is possible with conventional concrete and what is possible with UHPC. The maximum strength class for conventional concrete is C53/65. From a practical point of view, it is decided that conventional concrete in this design study has the strength class C50/60. Furthermore, reinforcing steel FeB 500 and prestressing steel FeP 1860 are chosen for the design of the box girder. For the material characteristics of these three materials reference is made to Appendix B.2. From now on in this design study, concrete C50/60 is meant with (conventional) concrete.

4.3 Geometry box girder

4.3.1 General

The structural model of the precast segmental box girder is statically determinate, see Figure 5. It can be schematised as a beam on two supports. There are some other options for the structural model like:

- A continuous box girder supported by the columns (statically indeterminate)
- A continuous box girder fixed to the columns (statically indeterminate)
- A cantilever bridge (statically determinate)

There is however chosen for a statically determinate girder bridge as the box girder is subjected to thermal expansions. The linear coefficient for thermal expansion for concrete is $\alpha = 10 * 10^{-6} K^{-1}$. The thermal expansion for a span of 45 metres and a temperature difference of lets say 30 degrees, gives an elongation of the girder of: $\Delta L = L * \alpha * \Delta T = 13.5mm$. This expansion should be made possible without the occurrence of large unwanted stresses. Therefore the metro viaduct needs expansion joints. With a continuous box girder the elongation is even larger and this results in larger forces on the columns than for a simply supported girder bridge. When the continuous box girder is fixed to the columns the stresses become even larger and still expansion joints are needed. A continuous box girder is therefore feasible for just a few spans. The anchorage of the tendons for a continuous box girder is also more difficult than for a simply supported girder bridge as there are tendons from two spans anchored at the supports in one segment. This could give some troubles during tensioning the tendons. A cantilever bridge needs a difficult connection somewhere in the middle of the span which probably needs quite a solid cross-section for the tendon anchorage and the connection with the suspended span. This gives a huge extra downward force at a very unpleasant location. Considering the arguments mentioned above the best structural model for the precast concrete segmental box girder is the statically determinate girder bridge. Besides this is the most appropriate structural model for the application of the span-by-span construction method.

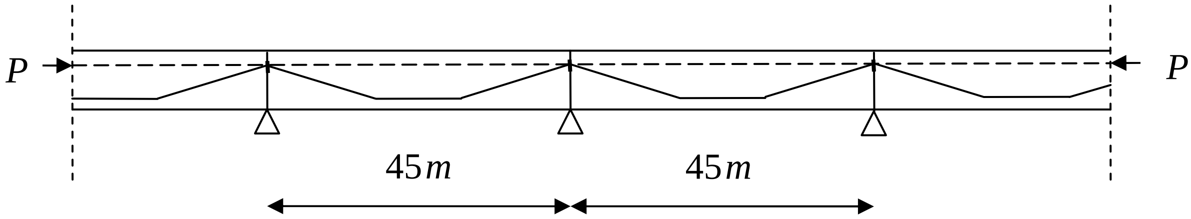

Figure 5: Statically determinate box girders supported by columns

The cross-section of the box girder is shown in Figure 6, where:

Length span	L	45	m
Depth box girder	H	2.8	m
Width top flange	b_{tf}	8.96	m
Thickness top flange	t_{tf}	0.25	m
Width web	b_w	0.16	m
Width bottom flange	b_{bf}	4	m
Thickness bottom flange	t_{bf}	0.3	m
Width box top side	b_{boxts}	5	m
Cantilever length top flange	L_{cant}	1.98	m
Depth webs	H_{box}	2.25	m

Angle of webs with vertical axis $\alpha_w = \tan^{-1}\left(\dfrac{(b_{boxts} - b_{bf})/2}{H_{box} + t_{bf}}\right) = 11.1°$

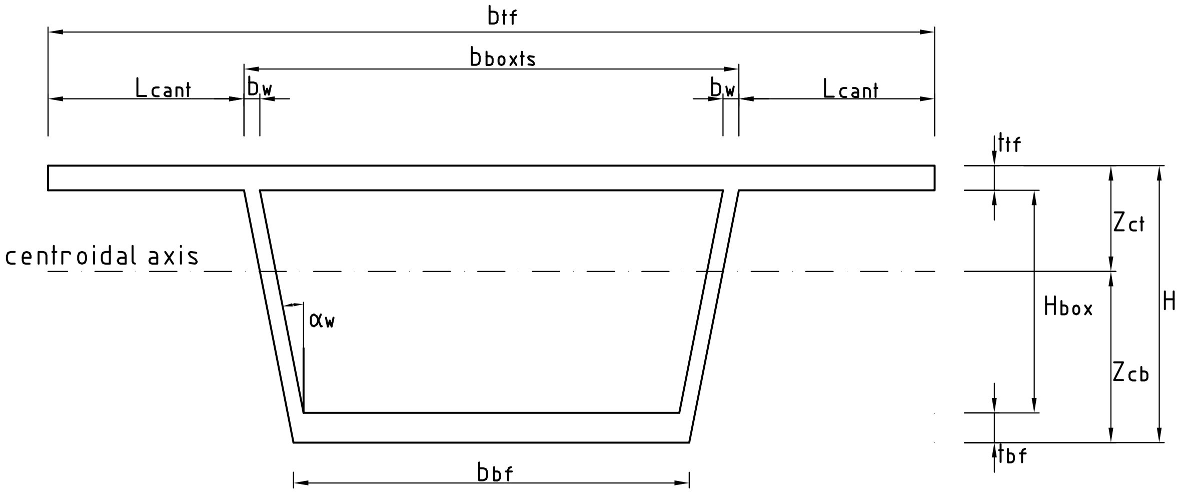

Figure 6: Cross-section of the box girder

The width of the bottom flange b_{bf} is chosen smaller than the width of the box top side b_{boxts}. This way the box girder requires a smaller support and the angle α_w is still small enough for the webs to transfer the vertical loads mainly by normal forces than by bending. The dimensions b_{bf} and b_{boxts} are deduced from reference projects, see Figure 18 [6].

The cross-section shown in Figure 6 is the constant cross-section along the span, except at the two supports and at the two deviation blocks in the middle of the span, see Figure 7. At these places the cross-section is more solid in order to anchorage and deviate the tendons. The detailing of these anchorage and deviation blocks is not treated in this design as this is too specific and goes far beyond the purpose to determine the general differences between a concrete and an UHPC segmental box girder prestressed with external tendons.

For the same reason it is chosen to design a straight girder bridge instead of a curved girder bridge which can fluently follow the alignment of the metro system. Of course in reality the metro system should consists of curved box girders for aesthetical reasons. This design with a straight span is however well able to point out the differences between the two materials without the need for extensive calculations of a curved box girder.

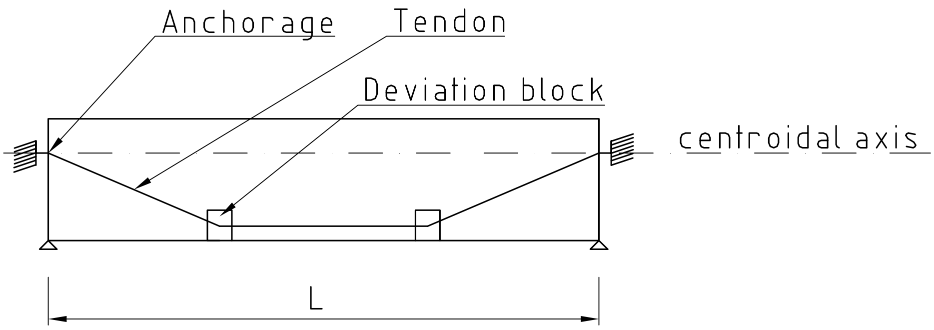

Figure 7: Schematisation of the tendons with the anchorage at the supports and the deviation blocks

4.3.2 Concrete cover

The viaduct is designed for a lifetime of minimum 100 years and is placed in exposure class XF3: Horizontal concrete surfaces exposed to rain and freezing. The concrete cover for the box girder made of C50/60 hereby becomes: $c_{nom} = 40mm$. For the calculation of the minimum concrete cover reference is made to Appendix B.3.3.

4.3.3 Effective width of flanges

The effective width of the flanges is based on the distance l_0 between points of zero moment. With a structural schematisation as given in Figure 5 the distance l_0 is 45 metres. The total effective flange width hereby becomes the same as the actual flange widths, see Table 1. For the calculation of the effective width of the flanges reference is made to Appendix B.3.4.

		Value	
Effective width top flange	$b_{eff,t}$	8.96	m
Effective width bottom flange	$b_{eff,b}$	4	m

Table 1: Total effective flange width

4.3.4 Cross-sectional properties

The cross-sectional properties of the box girder are given in Table 2. For the calculation reference is made to Appendix B.3.5.

		Value	
Cross-sectional area of concrete	A_c	4.16	m^2
Distance from bottom to centroidal axis	Z_{cb}	1.730	m
Distance from top to centroidal axis	Z_{ct}	1.070	m
Second moment of area of the concrete section	I_c	5.387	m^4
Section modulus bottom	W_b	3.114	m^3
Section modulus top	W_t	5.036	m^3
Perimeter concrete box girder	u	22.617	m

Table 2: Cross-sectional properties box girder

4.4 Loads

In Figure 8 the cross-section of the superstructure without the box girder is shown. The box girder supports a double-track metro system with emergency walkways at the cantilevers of the box girder.

The vertical loads in longitudinal direction of the box girder are:

- Dead load of the concrete box girder: $g_{dead} = 102.02 kN/m$
- Permanent load of the permanent construction shown in Figure 8: $g_{perm} = 34.42 kN/m$
- Variable load of the metros and snow loading: $q_{var} = 58.29 kN/m$

Furthermore the box girder is subjected to the horizontal loads:

- Wind load: $q_{wind} = 1.5 kN/m^2$
- Sideward force due to the metro: $Q_{sidewf} = 30 kN \; per\, track$

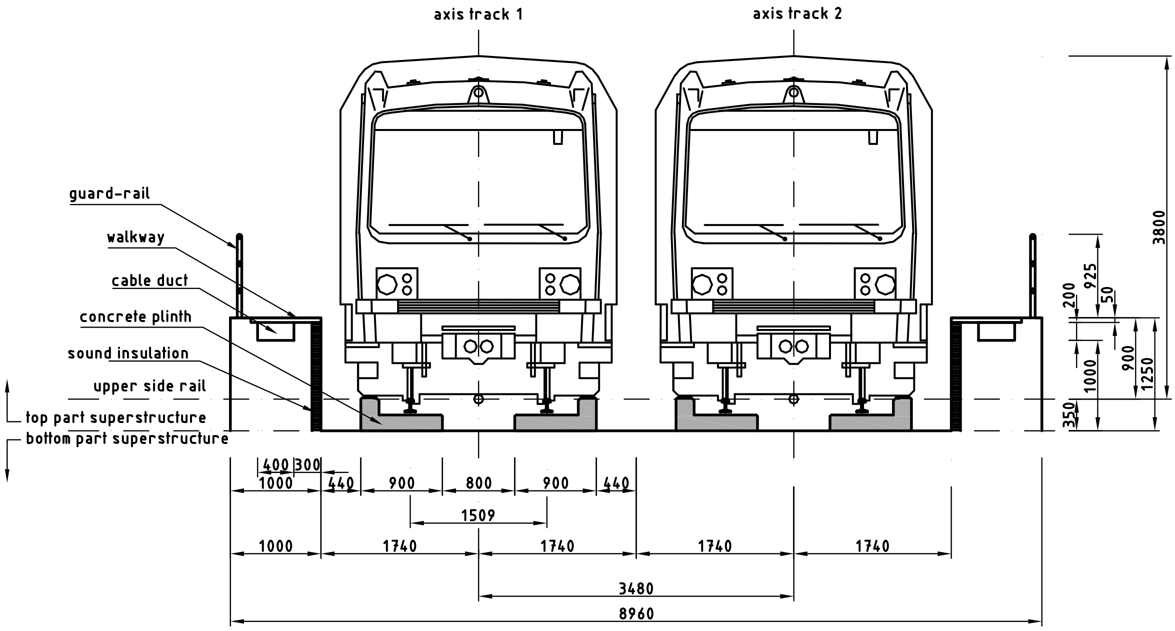

Figure 8: Cross-section top part superstructure without the box girder

The dynamic loading of the metro is taken into account by multiplying the vertical metro load with a dynamic factor: $\phi = 1 + 4/(10 + L) = 1.07$. For the exact calculation of the loads in the serviceability and ultimate limit state with the use of partial factors as well as the load schematisation in transversal direction of the box girder reference is made to Appendix B.4.

4.5 Prestressing tendons

4.5.1 Layout prestressing tendons

The layout of the external prestressing tendons inside the box girder is shown Figure 9. The tendon eccentricity at the support is 0 metre as the tendon anchorage coincides with the centroidal axis.

Furthermore:
Distance between the centre of the tendons and the bottom side at mid-span

	h_t	0.5	m
Tendon eccentricity at mid-span	$f = Z_{cb} - h_t$	1.230	m
Distance of deviation blocks to supports	a	15	m

Angle between prestressing tendon and the centroidal axis $\alpha_t = \tan^{-1}(f/a) = 4.69°$

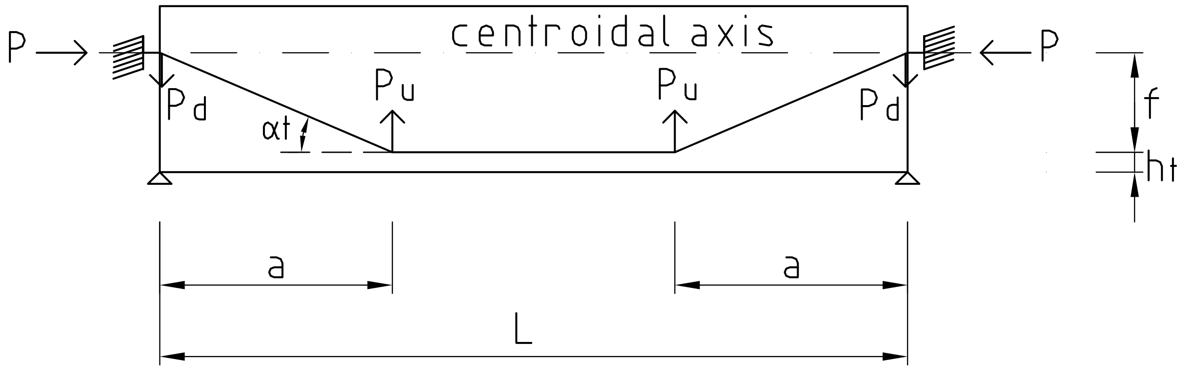

Figure 9: Layout external prestressing tendons

The resulting prestressing force $P_r = 2 * P * \sin(\alpha_t / 2)$ has a small angle with the vertical axis, see Figure 10. As the angle is very small the horizontal force of P_r is small. For simplification reasons it is chosen to take into account only the vertical upward prestressing force. The upward prestressing force P_u is dependent of the prestressing force P and the angle a_t:

$$P_u = P * \sin\alpha_t$$

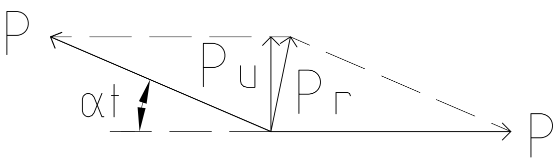

Figure 10: Polygon of prestressing forces

4.5.2 Bending moments due to prestressing

The bending moment diagram and structural schematisation due to prestressing is shown in Figure 11. Due to symmetry of loading the downward prestressing force at the supports is equal to the upward prestressing force at the deviation blocks.

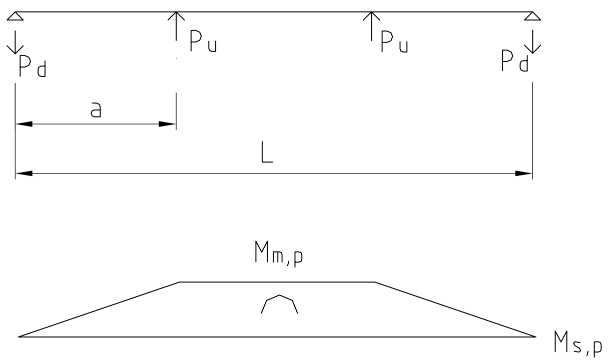

Figure 11: Structural schematisation of the box girder subjected to prestressing forces

Where:

$$P_d = P_u$$

$$M_{s,p} = 0kNm$$

$$M_{m,p} = P_d * a = P_u * a$$

The box girder has 6 tendons externally placed inside the girder according the layout shown in Figure 9. One tendon consists of 37 strands with a diameter of 15.7 mm and a cross-sectional area of 150 mm^2 per strand. The cross-sectional area of one tendon is:

$$A_p = 37 * 150 = 5550 mm^2$$

The number of tendons is:

$$n = 6 \ \ tendons$$

For prestressing in this design two phases are taken into account, namely:

- The construction phase at t = 0, no prestressing losses
- The end phase at t = ∞, assumed prestressing loss of 20%

For the calculation of the prestressing forces and bending moments reference is made to Appendix B.5.2.

4.5.3 Bending moments due to loads

The bending moments due to the loads are determined according the structural load schematisation shown in Figure 12. The dead, permanent and variable loads are schematised as a uniform distributed load in longitudinal direction of the box girder. The bending moments are calculated for two places which are: at mid-span and at the deviation blocks. In combination with the bending moments due to prestressing this will give the normative resultant bending moments for this design. Why these two places are normative for this design is explained in Section 4.8.2.

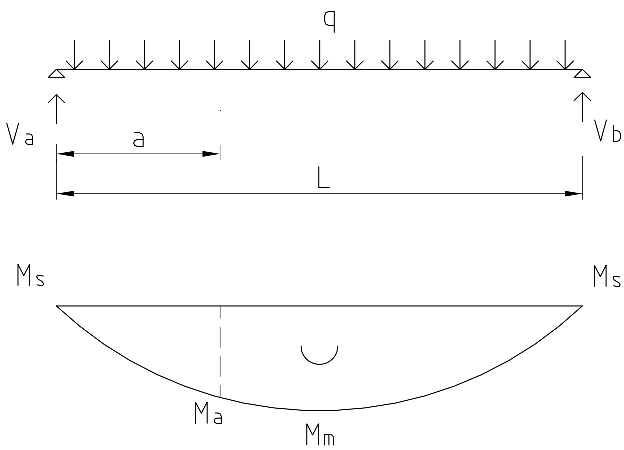

Figure 12: Structural schematisation of the box girder subjected to loads

Where:

$$V_a = V_b = \frac{1}{2} qL$$

$$M_s = 0kNm$$

$$M_m = \frac{1}{8} qL^2$$

$$M_a = \frac{1}{2} qL * a - 0.5 * q * a^2$$

For the calculation of the bending moments due to different load combinations reference is made to Appendix B.5.3.

4.5.4 Stresses due to loading

As the railway girder is a prefabricated segmental box girder, the joints between the segments cannot resist tensile stresses without opening of the joints. Opening of the joints is however not allowed so the concrete cannot resist tensile stresses: $\sigma_c \leq 0N/mm^2$. Furthermore the concrete stress may not become too large. In order to rule out the non-linearity of creep, the concrete compressive stress should not exceed $\sigma_c \geq -0.45 * f_{ck} = -22.5N/mm^2$. The stresses at the top and bottom side of the box girder in the serviceability limit state are calculated for different phases:

- The construction phase at t = 0, dead load and prestressing load only
- The end phase at t = ∞, fully loaded
- The end phase at t = ∞, without variable load

The maximum stress arises at the deviation blocks at the bottom side of the box girder during the construction phase. This maximum stress is:

$$\sigma_{cb} = -\frac{P_0}{A_c} - \frac{M_{m,p0}}{W_b} + \frac{M_{a,0}}{W_b} = -21.35N/mm^2$$

For the calculation of the other compressive stresses in the cross-section of the box girder at different phases reference is made to Appendix B.5.4.

4.5.5 Prestressing losses

Losses due to the instantaneous deformation of concrete

During tensioning the box girder will shorten. As the tendons are prestressed successively there arises an immediate prestressing loss which can be calculated for each tendon with the following formula:

$$\Delta P_{el} = A_p * E_p * \sum \left[\frac{j * \Delta\sigma_c(t)}{E_{cm}} \right]$$

This prestressing loss taking into account the order in which the tendons are stressed can be compensated by slightly overstressing the tendons. The maximum overstress is needed in the first prestressed tendon as this tendon has the largest loss due the instantaneous deformation of concrete. The required overstress $\sigma_{overstr}$ in the first prestressed tendon to compensate the losses due to instantaneous deformation of concrete is:

$$\sigma_{overstr} = 1364.07N/mm^2$$

The maximum allowed tensile stress of the tendons during tensioning is $\sigma_{p,\max} = 1440N/mm^2$. The stress caused by overstressing is far below this value and as also the concrete compressive stress during tensioning is limited to $\sigma_c \leq 0.6 * f_{ck} = 30N/mm^2$ this small overstressing will not cause any problems for the structure. It can be concluded that the losses due to the instantaneous deformation of concrete can be compensated by overstressing the tendons. By overstressing the tendons the initial tensile stress in all the tendons after tensioning can be the maximum tensile stress $\sigma_{pm0} = 1360 N/mm^2$.

Losses due to friction

The formula to calculate the loss due to friction in post-tensioned tendons is:

$$\Delta P_{\mu}(x) = P_{\max}(1 - e^{-\mu(\theta + kx)})$$

There are four places where tendon deviation takes place, namely: at the two supports and at the two deviation blocks at a distance a from the supports. At these places losses due to friction in post-tensioned tendons takes place. The loss due to friction per deviation is:

$$\Delta P_{\mu}(x) = P_{\max}(1 - e^{-\mu * \theta}) = 369.11 kN$$

Time dependent losses of prestress for post-tensioning

The time dependent losses of prestress for post-tensioning at a location x is calculated according the formula below:

$$\Delta P_{c+s+r} = A_p \Delta\sigma_{p,c+s+r} = A_p \frac{\varepsilon_{cs} E_p + 0.8 \Delta\sigma_{pr} + \frac{E_p}{E_{cm}} \varphi(\infty, t_0) * \sigma_{c,QP}}{1 + \frac{E_p}{E_{cm}} \frac{n * A_p}{A_c} (1 + \frac{A_c}{I_c} z_{cp}^2)[1 + 0.8 \varphi(t, t_0)]}$$

The time dependent loss of prestress for post-tensioning at the support is:

$$\Delta P_{c+s+r,s} = 4664 kN$$

The time dependent loss of prestress for post-tensioning at mid-span is:

$$\Delta P_{c+s+r,m} = 4276 kN$$

Total prestressing losses

The box girder segments are tensioned from one side from a practical point of view. This is because the construction of the metro system concerns a continuous placement of the segments from one column to the next column. This means that there is only one end well accessible to tension the tendons. The total prestressing losses hereby become, see Table 3:

Place	*Prestressing loss*	*Value*		*Percentage of loss*	*Value*	
At the first support	$\Delta P_{c+s+r,s} + \Delta P_{\mu}$	5033	kN	$\frac{\Delta P_{c+s+r,s} + \Delta P_{\mu}}{n * A_p * \sigma_{pm0}}$	11.11	%
After the first deviation block (at mid-span)	$\Delta P_{c+s+r,m} + 2 * \Delta P_{\mu}$	5014	kN	$\frac{\Delta P_{c+s+r,m} + 2 * \Delta P_{\mu}}{n * A_p * \sigma_{pm0}}$	11.07	%
After the second deviation block (at mid-span)	$\Delta P_{c+s+r,m} + 3 * \Delta P_{\mu}$	5384	kN	$\frac{\Delta P_{c+s+r,m} + 3 * \Delta P_{\mu}}{n * A_p * \sigma_{pm0}}$	11.89	%
At the second support	$\Delta P_{c+s+r,s} + 4 * \Delta P_{\mu}$	6141	kN	$\frac{\Delta P_{c+s+r,s} + 4 * \Delta P_{\mu}}{n * A_p * \sigma_{pm0}}$	13.56	%

Table 3: Total prestressing losses

The maximum prestressing loss arises at the end of the span, at the other end where the tensioning takes place. This loss = 13.56 % which is smaller than the assumed prestressing loss of 20 %. This assumption is thus a safe value for the prestressing losses and has not to be taken any larger. To take into account other unexpected losses and other expected losses like for instance thermal losses and slip of the anchorage it is decided to keep the expected final prestressing loss of 20 %. In the continuation of this design the prestressing loss in the end phase at t = ∞ is thus 20 %.

For the calculation of all the prestressing losses reference is made to Appendix B.5.5.

4.6 Deflection

The bending moments due to the loads are determined according the structural load schematisation shown in Figure 13. This schematisation gives a deflection at mid-span of: $w = \frac{5}{384}\frac{qL^4}{EI}$.

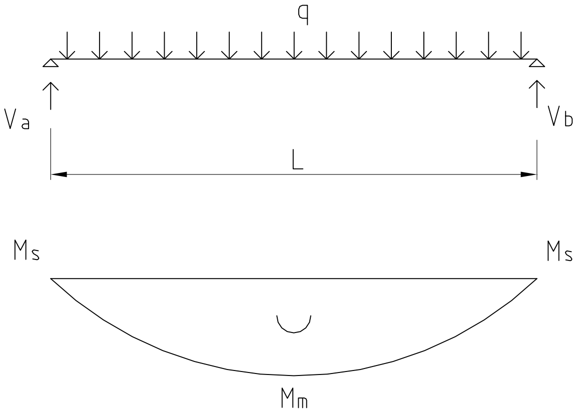

Figure 13: Structural schematisation of the box girder subjected to loads

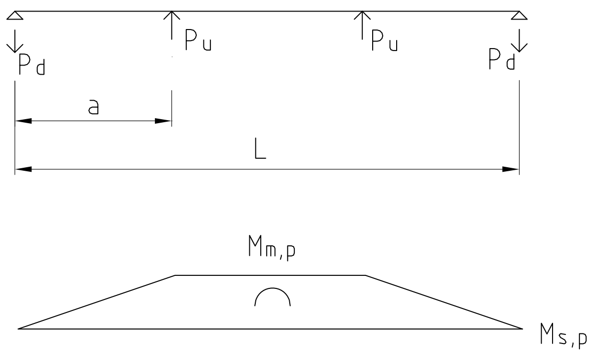

Figure 14: Structural schematisation of the box girder subjected to prestressing forces

The moment diagram and structural schematisation due to prestressing is given in Figure 14. The exact upward deflection of this schematisation is more difficult to determine. Therefore it is chosen to re-schematise the schematisation into a more easy and conservative schematisation to calculate the deflection. It can be seen that the moment diagram due to prestressing looks like the one due to the loads but then upside-down and angular. It is therefore chosen to change the structural schematisation of the box girder subjected to prestressing forces into a schematisation with a uniform distributed load like in Figure 13, but then with an upward uniform distributed load.

The uniform distributed load for prestressing is determined by equalizing the bending moments for both structural schematisations:

$$M_m = M_{m,p} \rightarrow \frac{1}{8}qL^2 = P_u * a \rightarrow q$$

Notice that this new schematisation causes a smaller upward deflection than in the real schematisation. With the requirement of a limited downward deflection this verification thus becomes more conservative.

The deflections and unity checks at mid-span for different phases are:

Time	*Load q*	*Deflection w*	*value*	*Maximum allowed deflection $w_{\max}$*	*Unity check $w/w_{\max}$*
At t=0	$g_{dead} - q_{pt0}$	-68.6	mm	$L/250 = -180mm$	0.38
At t=∞ without variable load	$g_{dead} + g_{perm} - q_{pt\infty}$	-22.8	mm	$L/500 = 90mm$	-0.25
Additional deflection under mobile load	q_{var}	15.5	mm	$L/1500 = 30mm$	0.52
At t=∞ fully loaded	$g_{dead} + g_{perm} + q_{\text{var}} - q_{pt\infty}$	-22.8 + 15.5 = -7.3	mm	$L/500 = 90mm$	-0.08

Table 4: The deflections and unity checks at mid-span for different phases

An upward deflection has a negative sign and a downward deflection has a positive sign. As the unity checks show, the construction satisfies with respect to deflection for all phases and always has a camber. The normative deflection is the additional deflection under mobile load.

For the calculation of the deflections reference is made to Appendix B.6.

4.7 Shear + torsion

4.7.1 Shear + torsion in webs

The webs have to resist the vertical shear and torsion. As it concerns a segmental box girder the joints between the segments consists of shear keys, see Figure 15 and Figure 16. These shear keys are normative over a cross-section of a segment with respect to shear and torsion of the box girder.

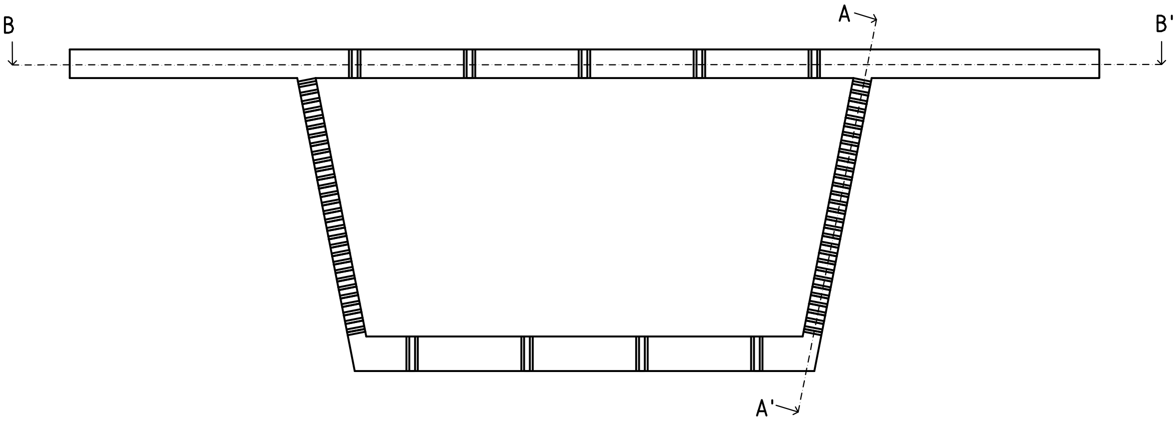

Figure 15: Shear keys in the flanges and in the webs

Each web has 15 shear keys with a height H_s of 150 mm per shear key, see Figure 17. The shear force is taken by compression in the sloped part of the shear key, see Figure 18. Friction of the remaining parts of the shear keys and flanges is not taken into account.

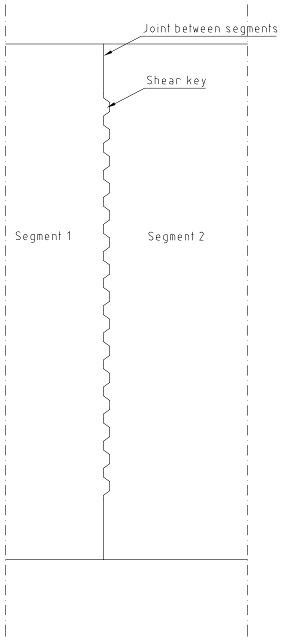

Figure 16: Section A-A'

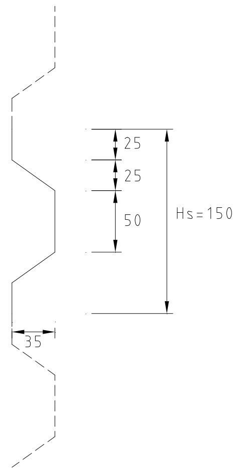

Figure 17: Dimensions shear key in mm

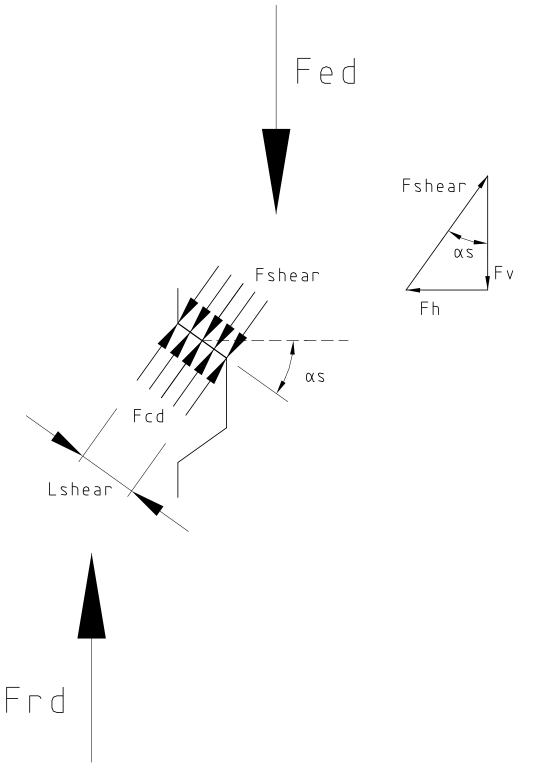

Figure 18: Schematisation of the shear resistance in a shear key by compression in the sloped part L_{shear}

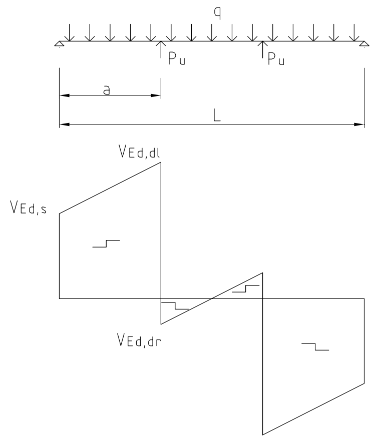

Figure 19: Shear force diagram at t=0

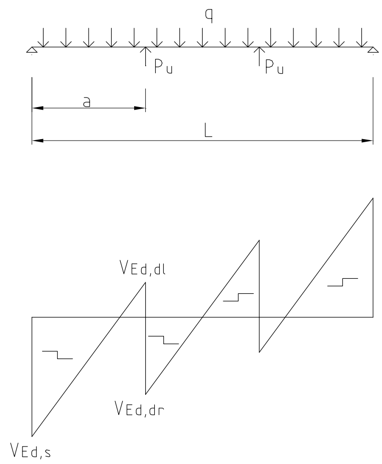

Figure 20: Shear force diagram at t=∞

The vertical shear strength of one web is:

$$V_{Rd,1} = f_{cd} * L_{shear} * \cos\alpha_s * \cos\alpha_w * t_w * n_s = 2292kN$$

The vertical shear strength of two webs is:

$$V_{Rd,2} = 2 * V_{Rd,1} = 4584kN$$

The maximum vertical shear force at t=0 is: See Figure 19

$$V_{Ed,dl0} = 4047kN$$

Unity check

The unity check for shear in the webs at t=0 is:

$$\boxed{V_{Ed,dl0} / V_{Rd,2} = 0.88 \leq 1.0 \rightarrow Ok}$$

The maximum vertical shear force at t=∞ is: See Figure 20

$$V_{Ed,s\infty} = 3150kN$$

The extra shear force in the webs due to torsion is:

$$V_{Ed+w} = T_{ed} / z_{webs} = 491kN$$

Unity checks

The unity check for shear in the webs at t=∞ is:

$$V_{Ed,s\infty} / V_{Rd,2} = 0.69 \leq 1.0 \rightarrow Ok$$

The unity check for shear + torsion in the webs at t=∞ is:

$$V_{Ed,s\infty} / V_{Rd,2} + V_{ed+w} / V_{Rd,1} = 0.90 \leq 1.0 \rightarrow Ok$$

The webs satisfy with respect to shear and torsion. The shear and torsion resistance is more than what is required and friction of the remaining parts of the shear keys and flanges is not even taken along. When this verification is not satisfied, the depth of the webs H_{box} should be increased to place more shear keys in the webs. Also increasing the web thickness is an option. For this design this is however not necessary as the verification is satisfied.

For the calculation of the shear strength of the webs and shear forces in the webs reference is made to Appendix B.7.1.

4.7.2 Shear + torsion in flanges

The flanges have to resist the horizontal shear and torsion. As it concerns a segmental box girder the joints between the segments consists of shear keys see, Figure 15 and Figure 21. These shear keys are normative over a cross-section of a segment with respect to shear and torsion of the box girder.

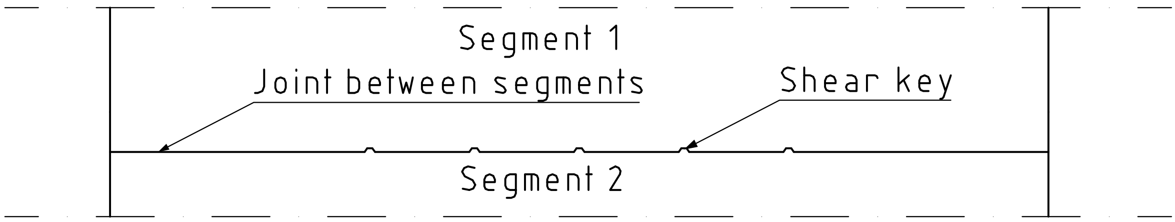

Figure 21: Section B-B'

The top flange has 5 shear keys and the bottom flange has 4 shear keys with a thickness which is the same as the flange thickness, see Figure 15. The shear force is taken by compression in the sloped part of the shear key, see Figure 22. Friction of the remaining parts of the shear keys, flanges and webs is not taken into account.

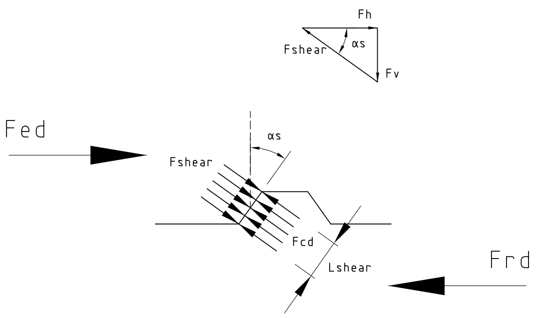

Figure 22: Schematisation of the shear resistance in a shear key by compression in the sloped part L_{shear}

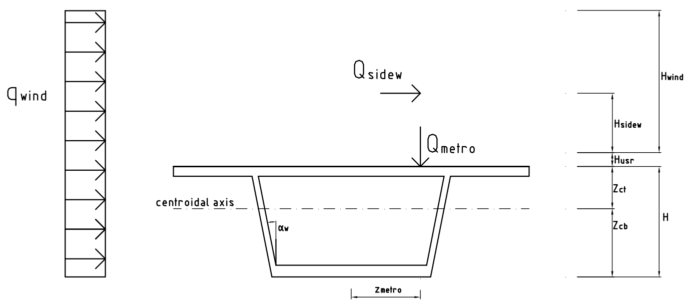

Figure 23: Load schematisation for maximum torsional moment

The horizontal shear strength of the top flange is:

$$V_{Rd,tf} = f_{cd} * L_{shear} * \cos\alpha_s * t_{tf} * n_{s,tf} = 1240kN$$

The horizontal shear strength of the bottom flange is:

$$V_{Rd,bf} = f_{cd} * L_{shear} * \cos\alpha_s * t_{bf} * n_{s,bf} = 1190kN$$

The horizontal shear force in the top flange at t=∞ is: See Figure 23

$$V_{Ed,tf\infty} = q_{wind} * L/2 * (H_{wind} + H_{usr} + H/2) + Q_{sidew} = 239kN$$

The horizontal shear force in the bottom flange at t=∞ is: See Figure 23

$$V_{Ed,bf\infty} = q_{wind} * L/2 * H/2 = 53kN$$

The extra shear force in the flanges due to torsion is:

$$V_{Ed+f} = T_{ed} / z_f = 845kN$$

Unity checks

Top flange

The unity check for shear in the top flange at t=∞ is:

$$\boxed{V_{Ed,tf\infty} / V_{Rd,tf} = 0.19 \leq 1.0 \rightarrow Ok}$$

The unity check for shear + torsion in the top flange at t=∞ is:

$$\boxed{V_{Ed,tf\infty} / V_{Rd,tf} + V_{Ed+f} / V_{Rd,tf} = 0{,}87 \leq 1.0 \rightarrow Ok}$$

Bottom flange

The unity check for shear in the bottom flange at t=∞ is:

$$\boxed{V_{Ed,bf\infty} / V_{Rd,bf} = 0.04 \leq 1.0 \rightarrow Ok}$$

The unity check for shear + torsion in the bottom flange at t=∞ is:

$$\boxed{V_{Ed,bf\infty} / V_{Rd,bf} + V_{Ed+f} / V_{Rd,bf} = 0{,}75 \leq 1.0 \rightarrow Ok}$$

The flanges satisfy with respect to shear and torsion. The shear and torsion resistance is not much more than what is required. Friction of the remaining parts of the shear keys and flanges is however not even taken along. When this verification is not satisfied, more shear keys should be placed in the flanges. As the flanges offer enough space for additional shear keys this verification will never be normative for the design and will easily satisfy.

For the calculation of the shear strength of the flanges and shear forces in the flanges reference is made to Appendix B.7.2.

4.8 Ultimate resistance moment

4.8.1 General

In all phases during the lifetime of the box girder the concrete force N_c due to the compressive stresses in the concrete should balance the prestressing force P, see Figure 24.

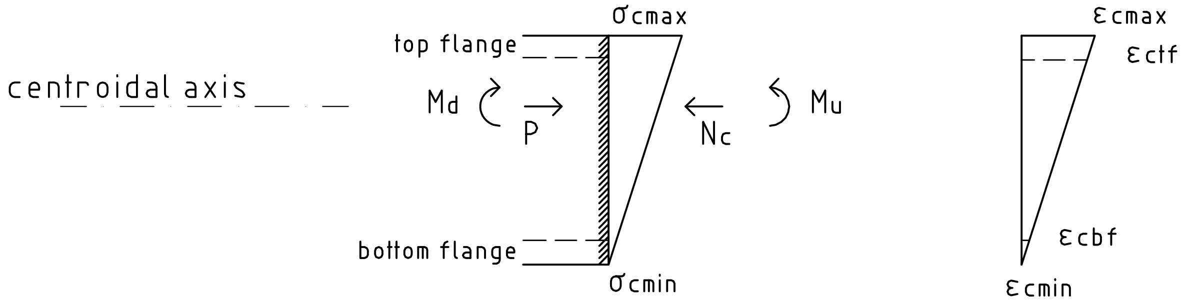

Figure 24: Equilibrium between axial forces P and N_c in the cross-section of the box girder

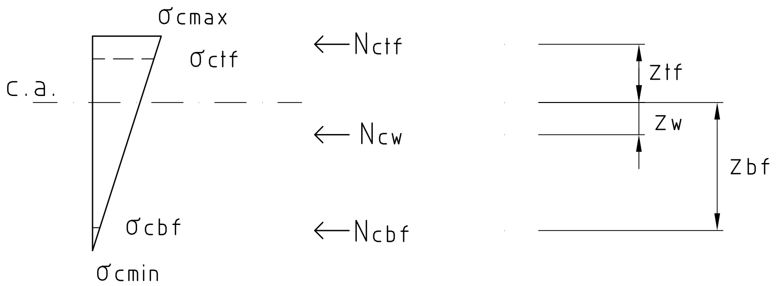

Figure 25: Overview for the calculation of the ultimate resistance moment

At the same time the bending moment M_d due to loading should be resisted by the ultimate resistance moment M_u of the box girder. The ultimate resistance moment arises when the strain difference between the top and bottom flange is as large as possible taking into account that tensile stresses are not allowed. This means that $\sigma_{c\min} = 0N/mm^2$. In which flange the maximum strain arises depends on the stage of loading. For the example given above it would mean that:
The concrete force $N_c = N_{ctf} + N_{cw} + N_{cbf}$ and should be equal to P, see Figure 25.

The ultimate resistance moment $M_u = N_{ctf} * z_{tf} + N_{cw} * z_w + N_{cbf} * z_{bf}$ and should be larger than the bending moment M_d. Where $z_{tf}, z_w \; and \; z_{bf}$ are positive or negative values considering the location of the force with regard to the centroidal axis.

For this calculation there is made use of the Bi-linear stress-strain relation, see Figure 26.

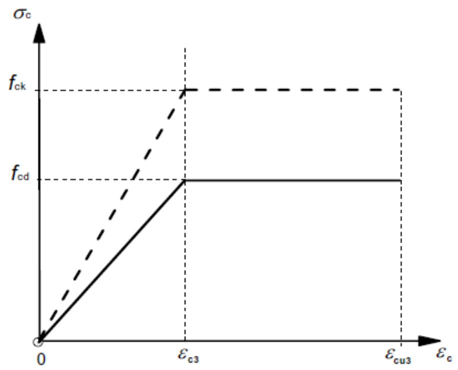

Figure 26: Bi-linear stress-strain relation

Where:

$\varepsilon_{c3} = 1.75‰$	Is the maximum elastic compressive strain in the concrete
$\varepsilon_{cu3} = 3.5‰$	Is the ultimate compressive strain in the concrete

4.8.2 Bending moments due to loads and prestressing

Bending moment M_d at t=0

In the construction phase at t=0 the loads on the box girder are the dead load and the prestressing force. As the permanent and variable loads are missing and the initial prestressing force is large the box girder has a camber. The normative hogging moment in this phase arises at the deviation blocks, see Figure 27. The maximum strain arises in the bottom flange.

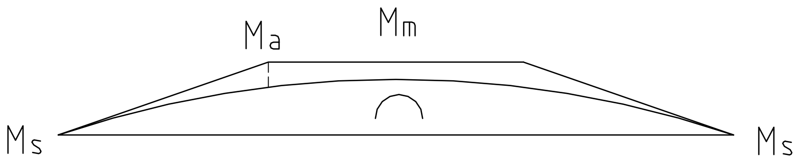

Figure 27: The bending moments due to prestressing minus the bending moments due to dead load results in the largest bending moment M_a at the deviation blocks

Hogging moment at the deviation blocks is:

$$M_{da,0} = \gamma_{P,unfav} * P_{u0} * a - \frac{1}{2} * \gamma_{G,fav} * g_{dead} * L * a - 0.5 * \gamma_{G,fav} * g_{dead} * a^2 = 49235 kNm (\frown)$$

Bending moment M_d at t=∞

In the end phase at t=∞ the box girder is fully loaded by the dead, permanent and variable load and is partly resisted by the prestressing force. This load case causes a downward deflection, which means that the normative sagging moment arises at mid-span, see Figure 28. The maximum strain arises in the top flange.

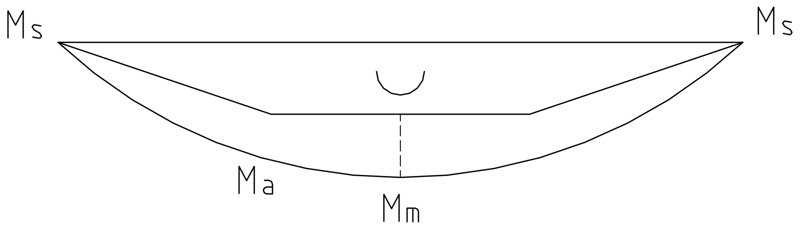

Figure 28: The bending moments due to dead, permanent and variable load minus the bending moments due to prestressing results in the largest bending moment M_m at mid-span

Sagging moment at mid-span is:

$$M_{dm,\infty} = \frac{1}{8} * (\gamma_{G,unfav} * g_{dead} + \gamma_{G,unfav} * g_{perm} + \gamma_{Q,unfav} * q_{var}) * L^2 - \gamma_{P,fav} * P_{u\infty} * a$$
$$= 24334 kNm (\smile)$$

4.8.3 Ultimate resistance moment at t=0

Ultimate resistance moment at deviation blocks

$M_{da,0} = 49235 kNm (\frown)$ means that the maximum compressive strain arises in the bottom flange. To determine the maximum strain for which holds that $N_c = P_0$ everything is filled in a spreadsheet program (Microsoft Excel) and solved with the function “goal seek”. With the function “goal seek” the concrete force N_c is set to be equal to the prestressing force P_0 by changing the maximum compressive strain in the cross-section $\varepsilon_{c\max}$.

The maximum strain in the cross-section which causes equilibrium between N_c and P_0 is:

$\varepsilon_{c\max} = 1.760‰$

This means that the compressive strain in the concrete is just beyond the linear-elastic phase and is in the plastic phase.

The ultimate resistance moment of the box girder at t=0 is:

$$M_u = N_{ctf} * z_{tf} + N_{cw} * z_w + N_{cbf} * z_{bf} = 54826 kNm$$

Unity check for the ultimate resistance moment:

$$M_{da,0} / M_u = 0.90 \leq 1.0 \rightarrow Ok$$

The ultimate resistance moment of the box girder is thus large enough to resist the bending moments in the construction phase at t=0. The unity check however approaches the limit 1.0, so this verification needs attention. When this verification is not satisfied the depth of the webs H_{box} should be decreased, see Figure 6. This way the upward prestressing force becomes smaller, see Figure 9, and thus the hogging moment due to prestressing decreases. Another option is to make the box girder heavier such that the hogging moment M_d becomes smaller.

For the calculation of the ultimate resistance moment of the box girder at t=0 reference is made to Appendix B.8.3.

4.8.4 Ultimate resistance moment at t=∞

Ultimate resistance moment at mid-span

$M_{dm,\infty} = 24334 kNm (\cup)$ means that the maximum compressive strain arises in the top flange. To determine the maximum strain for which holds that $N_c = P_\infty$ everything is filled in a spreadsheet program (Microsoft Excel) and solved with the function "goal seek". With the function "goal seek" the concrete force N_c is set to be equal to the prestressing force P_∞ by changing the maximum compressive strain in the cross-section $\varepsilon_{c\max}$.

The maximum strain in the cross-section which causes equilibrium between N_c and P_∞ is:

$\varepsilon_{c\max} = 0.870‰$

This means that the compressive strain in the concrete is in the linear-elastic phase.

The ultimate resistance moment of the box girder at t=∞ is:

$$M_u = N_{ctf} * z_{tf} + N_{cw} * z_w + N_{cbf} * z_{bf} = 27117 kNm$$

Unity check for the ultimate resistance moment:

$$M_{dm,\infty} / M_u = 0.90 \leq 1.0 \rightarrow Ok$$

The ultimate resistance moment of the box girder is thus enough to resist the bending moments in the end phase at t=∞. The unity check however approaches the limit 1.0, so this verification needs attention. When this verification is not satisfied the depth of the webs H_{box} should be increased, see Figure 6. This way the lever arms z become larger which has a positive effect on the ultimate resistance moment. Also the upward prestressing force then becomes larger, see Figure 9. The bending moment M_d should be kept as small as possible by having a light as possible box girder.

For the calculation of the ultimate resistance moment of the box girder at t=∞ reference is made to Appendix B.8.4.

4.9 Deck

4.9.1 General

To determine if the thickness of the top flange / deck meet the requirements of shear and bending moments, the local schematisation is considered. The deck is schematised in the transversal direction as a floor of 1 metre wide with two fixed supports (the webs). The width of 1 metre in longitudinal direction comes from [8], which says that for the calculation of the deck the wheel pressure in longitudinal direction of the track may be spread to two sides over a distance of 1 metre + twice the height of the concrete plinth. For a more conservative calculation only the width of 1 metre is taken. To calculate the shear and bending moments in the deck there is made use of the program Scia Engineer. For the geometry of the deck the assumption was made that the web width should be 0.2 metres. With this width the geometry in Figure 29 becomes:

$$L_{cant,centre} = L_{cant} + b_w / 2 = 2.08m$$

$$L_{span} = b_{tf} - 2 * L_{cant,centre} = 4.8m$$

With the shear force and bending moments due to loading as result from the input in Scia Engineer next the verification of shear and ultimate resistance moment of the deck is made.

For the load schematisation and results of the input reference is made to Appendix B.9.1.

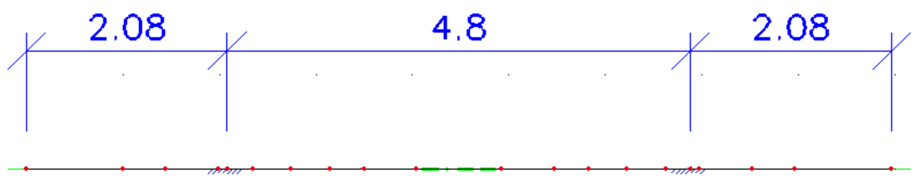

Figure 29: Structural schematisation deck box girder

4.9.2 Shear resistance

The maximum total shear force in the deck is:

$$\boxed{V_{Ed} = V_{Ed,perm+\text{var}} + V_{Ed,dead} = 134.89kN}$$

The maximum total bending moment in the deck is:

$$\boxed{M_d = M_{d,dead} + M_{d,perm+\text{var}} = 129.82kNm}$$

The shear strength of the deck with longitudinal reinforcement is:

$$\boxed{V_{Rd,c2} = [C_{Rd,c} k (100 \rho_l f_{ck})^{1/3} + k_1 \sigma_{cp}] b_{deck} d = 167.59kN}$$

The longitudinal reinforcement in the deck near the webs, as is shown in Figure 30 to resist the shear force and bending moment, consists of bars with a diameter of $\phi_{\text{reinf}} = 16mm$ and a spacing of $S_{\text{reinf}} = 110mm$.

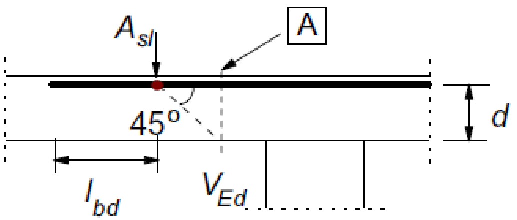

Figure 30: Definition of A_{sl}

Unity check for shear in the deck near the webs is:

$$\boxed{V_{Ed} / V_{Rd,c2} = 0.80 \leq 1.0 \rightarrow Ok}$$

Furthermore, in case of concrete cracked in shear the shear force in the deck should always satisfy the condition:

$$V_{Ed} \leq 0.5 * b_{deck} * d * \nu * f_{cd}$$

Filling in the formula gives:
$V_{Ed} = 134.89kN \leq 0.5 * b_{deck} * d * \nu * f_{cd} = 1319kN \rightarrow Ok$

It can be noticed that with longitudinal reinforcement the deck easily satisfies with respect to local shear.

For the calculation of the shear force and shear strength of the deck reference is made to Appendix B.9.2.

4.9.3 Ultimate resistance moment

The ultimate resistance moment of the deck is calculated according to the schematisation in Figure 31. In this case however the schematisation should be mirrored along the centre line as the tension arises at the top side and the compression zone is at the bottom side of the deck, see Figure 30.

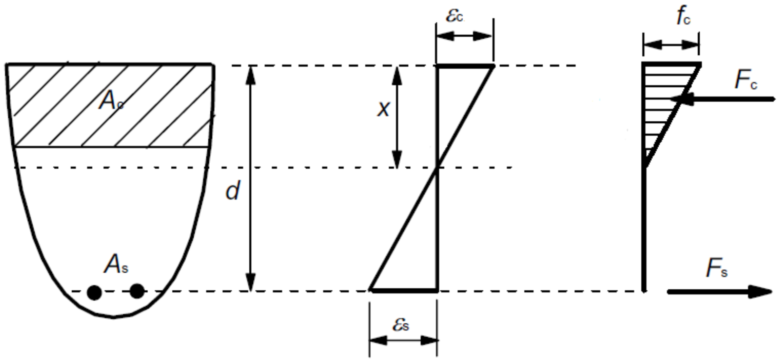

Figure 31: Rectangular stress distribution

The two horizontal forces F_c and F_s should be in equilibrium:

$$F_c - F_s = 0$$

This can be written as:

$$0.5 * x * b_{deck} * \frac{\varepsilon_c}{\varepsilon_{c3}} * f_{cd} - \varepsilon_s * E_s * A_{sl} = 0$$

Where:

$$x = \frac{\varepsilon_c}{\varepsilon_{tot}} * t_{tf}$$

The tensile strain in the reinforcement is the stain at the end of the linear elastic phase of steel:

$$\varepsilon_s = \frac{f_{yd}}{E_s} = 2.174‰$$

Solving the formula gives the compressive strain in the concrete:

$$F_c - F_s = 0 \rightarrow \varepsilon_c = 1.134‰$$

The concrete compressive zone is:

$$x = \frac{\varepsilon_c}{\varepsilon_{tot}} * t_{tf} = 85.7mm$$

The ultimate resistance moment of the deck is:

$$\boxed{M_u = \varepsilon_s * E_s * A_{sl} * (d - \frac{1}{3}x) = 130.16kNm}$$

TUDelft Delft University of Technology

Unity check for the ultimate resistance moment of the deck:

$$M_d / M_u = 0.9974 \leq 1.0 \rightarrow Ok$$

The ultimate resistance moment of the deck is thus just enough to resist the bending moments. If this verification is not satisfied the lever arm between the two forces F_c and F_s should be increased. This means that the deck becomes thicker. Another option is to add more reinforcement bars. This however has a strong influence on the rotation capacity, see hereunder.

The cracking moment is:

$$M_r = f_{ctm,fl} * \frac{1}{6} * b_{deck} * t_{tf}^2 = 57.26 kNm$$

Because $M_r \leq M_u$, the deck satisfies with respect to the minimum required percentage of reinforcement.

Rotation capacity
The height of the compression zone may not become too large as this limits the rotation capacity of the deck.
The verification of the rotation capacity of the deck is:

$$x / d = 0.44 \leq 0.45 \rightarrow Ok$$

This verification considers the rotation capacity of the deck at the supports (the webs). It shows that the rotation capacity of the deck is sufficient, but is very close to the limit so attention is needed. If this verification is not satisfied the thickness of the deck should be increased. Another option is to diminish the number of reinforcement bars which will result in a smaller compressive zone x. This will however also reduce the ultimate resistance moment.

For the calculation of the ultimate resistance moment and cracking moment of the deck reference is made to Appendix B.9.2.

4.10 Fatigue + vibration

4.10.1 Fatigue prestressing steel

The fatigue verification for prestressing steel is:

$$\gamma_{F,fat} * \Delta\sigma_{S,equ}(N^*) \leq \frac{\Delta\sigma_{Rsk}(N^*)}{\gamma_{s,fat}} \rightarrow \frac{\gamma_{F,fat} * \Delta\sigma_{S,equ}(N^*) * \gamma_{s,fat}}{\Delta\sigma_{Rsk}(N^*)} = 0.137 \leq 1.0 \rightarrow Ok$$

The fatigue verification for prestressing steel is easily satisfied and as the standard [12] (6.8.4) says: “Fatigue verification for external and unbonded tendons, lying within the depth of the concrete section, is not necessary” this could also be expected. This calculation with a rough estimation of the elongation of the tendons is however done to confirm the assumption. Fatigue of the prestressing tendons is not an issue for the design.

For the fatigue verification for prestressing steel reference is made to Appendix B.10.1.

4.10.2 Fatigue concrete

For concrete subjected to compression, adequate fatigue resistance may be assumed if the following expression is satisfied:

$$14 * \frac{1 - E_{cd,\max,equ}}{\sqrt{1 - R_{equ}}} \geq 6$$

The fluctuations of the concrete compressive stresses used in the verifications are the stresses in the end phase at t=∞ with and without variable load. The fatigue verification of concrete is determined at the four possible normative locations, which are:

Fatigue at mid-span, at the top side

$$14 * \frac{1-E_{cd,\max,equ}}{\sqrt{1-R_{equ}}} \geq 6 \rightarrow \frac{6}{14} * \sqrt{1-R_{equ}} + E_{cd,\max,equ} = 0.74 \leq 1.0 \rightarrow Ok$$

Fatigue at mid-span, at the bottom side

$$14 * \frac{1-E_{cd,\max,equ}}{\sqrt{1-R_{equ}}} \geq 6 \rightarrow \frac{6}{14} * \sqrt{1-R_{equ}} + E_{cd,\max,equ} = 0.95 \leq 1.0 \rightarrow Ok$$

Fatigue at the deviation blocks, at the top side

$$14 * \frac{1-E_{cd,\max,equ}}{\sqrt{1-R_{equ}}} \geq 6 \rightarrow \frac{6}{14} * \sqrt{1-R_{equ}} + E_{cd,\max,equ} = 0.68 \leq 1.0 \rightarrow Ok$$

Fatigue at the deviation blocks, at the bottom side

$$14 * \frac{1-E_{cd,\max,equ}}{\sqrt{1-R_{equ}}} \geq 6 \rightarrow \frac{6}{14} * \sqrt{1-R_{equ}} + E_{cd,\max,equ} = 0.998 \leq 1.0 \rightarrow Ok$$

Conclusion

These are the normative locations as here the largest bending moments arises in the box girder, see Section 4.8.2. In Section 4.8 where the ultimate resistance moment is verified, the bending moment due to loads and prestressing at t=∞ is a sagging moment ($\cup$) due to the calculation in the ultimate limit state. For the fatigue verification of concrete the calculation of the stresses is in the serviceability limit state and result in a hogging moment ($\cap$). The maximum compressive strain arises in the bottom flange. This can be seen in the fatigue verifications as the fatigue of concrete at the bottom side of the box girder is normative, especially at the deviation blocks. That the bending moment is hogging ($\cap$) is also confirmed by the calculations of the deflections which show that the girder has a camber at all times, see Table 4.

The fatigue verification for concrete is satisfied but it is a very important issue in the design of the box girder as some unity checks are very near the limit 1.0. When this verification is not satisfied the best way is to increase the thickness of the bottom flange which decreases the compressive stress in the concrete at the bottom and also brings down the centroidal axis of the box girder and thus reduces the upward prestressing force, see Figure 9.

For the fatigue verification of the concrete reference is made to Appendix B.10.2.

4.10.3 Vibration

For the box girder only the static analysis is considered. The dynamic metro load is multiplied by the dynamic factor ϕ to take into account the dynamic loading. This method of calculation holds when the first natural frequency of the box girder stays within the prescribed limits [10]. When the limits are exceeded a dynamic analysis is required. A dynamic analysis can prove that the box girder is still determined against the dynamic effects. Such an analysis is however extensive and more difficult and is therefore left out of the design of the box girder. For this design the first natural frequency of the box girder should stay within the limits such that a static analysis is sufficient and a dynamic analysis is not necessary. The check for determining whether a dynamic analysis is required is done according two verifications which hold for railway bridges:

Verification according Annex F [10]
The first natural bending frequency of the box girder is:

$$n_0 = \frac{C_{end}}{2\pi}\sqrt{\frac{E_{cm}I_c}{A_c\rho_c L^4}} = 3.43Hz$$

The velocity of the metros is:
$v = 100km/h = 27.78m/s$

The maximum value of the velocity divided by the first natural frequency is:
$(v/n_0)_{\lim} = 14.73m$

Verification of the ratio of the velocity over the first natural frequency is:

$$\boxed{v/n_0 = 8.09m \le 14.73m \rightarrow Ok}$$

Verification according to Figure 6.10 [10]
Limits of natural frequency n_0 (Hz) as a function of L (m)

The upper limit of natural frequency is governed by dynamic enhancements due to track irregularities and is given by:
$n_{0\max} = 94.76 * L^{-0.748} = 5.5Hz$
The lower limit of natural frequency is governed by dynamic impact criteria and is given by:
$n_{0\min} = 23.58 * L^{-0.592} = 2.48Hz$

The first natural frequency of the box girder is:

$$\boxed{n_0 = \frac{C_{end}}{2\pi}\sqrt{\frac{E_{cm}I_c}{A_c\rho_c L^4}} = 3.43Hz \rightarrow Ok}$$

Conclusion
Both verifications show that the box girder does not require a dynamic analysis and a static analysis is sufficient. As the first natural frequency of the girder easily stays within the limits, the box girder is well determined against the dynamic effects. The increasing and decreasing of static stresses and deformations under the effects of moving traffic should, considering the calculations, not give any problems for this box girder.

For the vibration verifications reference is made to Appendix B.10.3.

4.11 Buckling webs

Verification of buckling is needed for the webs of the box girder. As the webs are fixed to the flanges, this would mean that buckling mode d, see Figure 32, can be considered to determine the effective buckling length. But as the webs and flanges are relatively slender, full rotation stiffness is not likely to occur. In reality buckling mode f should be taken to calculate the effective buckling length of the webs. The rotation stiffness is dependent on the stiffness of the flanges. To determine this rotation stiffness a more extensive calculation is necessary. To be able to make a simple verification of buckling it is therefore chosen to schematise the webs as buckling mode a, see Figure 32. This is the most conservative buckling mode for the webs, where the effective buckling length equals the length of the webs.

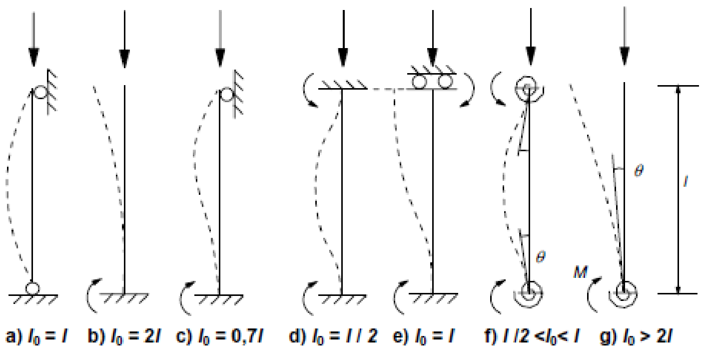

Figure 32: Examples of different buckling modes and corresponding effective lengths for isolated members

The effective length of the webs in longitudinal direction of the box girder which can be taken for the buckling resistance is hard to determine, especially for a segmental box girder with its joints between the segments creating discontinuities in the webs. For this calculation it is chosen to take the effective length of the webs as 1 metre. This is chosen as in the local schematisation of the deck, see Section 4.9.1, the local metro point load is distributed over 1 metre in the longitudinal direction of the box girder. In the deck schematisation it is therefore chosen to take a deck width of 1 metre. This local deck load should be taken by the webs. For this reason an effective length of the webs of 1 metre is chosen with respect to buckling of the webs. Besides, this assumption is considered as quite conservative as buckling of the webs will probably concern more than 1 metre. Most likely the effective length of the webs equals the length of a segmental box girder, which means a length of 3 metres. However, in this buckling verification a safe assumption of the effective length is taken of 1 metre.

Verification of buckling of the webs:

$$b_w = 160mm \geq b_{w,req} = 157mm \rightarrow Ok$$

The webs thus satisfy with respect to buckling. The thickness of the webs is however just enough to resist buckling. When this verification is not satisfied the thickness of the webs should be increased.

For the calculation of the minimum required width of the webs with respect to buckling reference is made to Appendix B.11.

4.12 Conclusions

The design concerns a segmental box girder and therefore mainly the verifications of the global effects are considered. The steel reinforcement in the box girder segments is only of interest for the local effects as there is no continuation of the reinforcement along the span. In this design the reinforcement is only considered for the deck. This is an important verification as the deck must be able to carry all the loads, also in the local schematisation. For the rest, the reinforcement in the segments is not taken into account because it will not be normative for the design. The reinforcement needed in the flanges and webs will easily fit within the required thickness of the elements according the verifications which are taken into account in this design. Shear reinforcement in the webs of a segment for instance is not normative as the depth of the webs is quite large. This way the shear force crosses many stirrups in the webs and can easily be transferred within the segment. Interesting is however how the shear force is transferred between two segments. This is therefore taken along in this design. Besides, detailing of the reinforcement in the segments is too specific and goes far beyond the purpose to determine the general differences between a concrete and a UHPC segmental box girder prestressed with external tendons. This design is thus a global design without a specific detailing of the reinforcement as this is not normative for a segmental box girder.

The precast concrete segmental box girder with six external prestressing tendons which is schematised in this chapter satisfies all the structural verifications. A critical verification for the design is the fatigue verification of the concrete at the deviation blocks at the bottom side. This unity check is very close to the limit of 1.0. Interesting point is that when the prestressing losses at the end phase at t=∞ are less than the assumed 20 % this verification will probably not fulfil, as the compressive stress in the bottom flange then becomes even larger. In first instance it was assumed that taking the largest prestressing loss in the end phase would result in the most conservative design. This is however not the case as due to the slender cross-section of the box girder the compressive stresses are large which makes the fatigue verification of the concrete normative. For this design it would mean that the prestressing losses in the end phase should be at least 20 % and hopefully a little bit larger so that the compressive stress at the bottom becomes smaller and thus easier satisfies the fatigue verification of the concrete. Of course the prestressing losses may not become too large as then in the end phase the deflection, the ultimate resistance moment of the box girder and fatigue of the concrete at the top side may become a problem. An accurate calculation of the prestressing losses for this design is thus advisable.

Another important verification for the design is the minimum required width of the webs with respect to buckling. The width of the webs is just enough to resist buckling and cannot be taken any smaller. The width of the webs also influences the vertical shear + torsion strength of the webs with its shear keys. The unity checks for shear + torsion in the webs are however easier satisfied than the unity check for buckling of the webs. The width of the webs for this design is thus determined by buckling and not by shear + torsion. Furthermore, the verifications of the ultimate resistance moment of the box girder and the local effects on the deck are important, as these checks are near the limits. Especially the local verifications of the ultimate resistance moment and rotation capacity of the deck showed that the deck thickness with its reinforcement was just enough to satisfy. Structural verifications which are of less importance for this design are the verifications of deflection, shear + torsion in the flanges, fatigue of the prestressing steel and vibration of the box girder. The reason that deflection is not problematic is due to the depth of the box girder and the relative thin webs creating a large moment of inertia of the box girder versus a small dead load. The flanges offer enough space to place extra shear keys when this is necessary and does not influences the design. Fatigue of the external prestressing tendons is also not of importance as the unity check showed that it easily satisfies and also the codes even say that this verification is not needed. The verifications of vibration of the box girder showed that the box girder does not require a dynamic analysis and a static analysis is sufficient. The increasing and decreasing of static stresses and deformations under the effects of moving traffic should therefore not give any problems for this box girder.

Concluded can be that this slender design for a precast concrete segmental box girder with external prestressing tendons is close to its limits. The important structural verifications for the design are:

- Fatigue of the concrete
- Buckling of the webs
- Ultimate resistance moment of the box girder
- Ultimate resistance moment of the deck
- Rotation capacity of the deck
- Shear + torsion in the webs

5. Optimisation process concrete box girder C50/60

5.1 General

The design of the concrete segmental box girder with six external prestressing tendons, as described in the previous chapter, is the optimal design. This optimal design is the result of an optimisation process. The most important point is that the dead weight of the railway girder, which is supported by the columns, is as small as possible. This is of importance as the verification of stiffness and stability of the whole elevated metro structure should be satisfied. When the weight of the railway girder is reduced, the stiffness and stability of the structure becomes less critical. Furthermore, a reduced weight of the box girder can result in more slender columns and/or less piles which saves costs. Other important points for the design are the desire for a small depth of the box girder for aesthetical reasons and the preference for a small number of prestressing tendons used in the design as this also saves money.

In this optimisation process there is searched for the optimal design by changing six parameters:

- Thickness of the top flange t_{tf} , steps of 10 mm
- Thickness of the bottom flange t_{bf} , steps of 10 mm
- Width of the webs b_w , steps of 10 mm
- Depth of the webs H_{box} , steps of 150 mm (height of a shear key)
- Distance of the deviation blocks to the supports a , steps of 1 m
- Number of prestressing tendons n

The optimisation process in this chapter is done for a box girder with 4, 6 and 8 tendons. In Section 5.6 it will be made clear why the application of more or less tendons is not interesting for the design. An odd number of tendons is not wanted as the tendons are mostly anchored to the sides of a box girder, which then results in a non-symmetrical prestressed box girder. A solution is to place the odd tendon in the middle of the cross-section. This is however from a practical point of view not desirable because at this place the box girder's manhole is situated. This chapter contains three sections in which the optimisation process for the design with respectively 6, 8 and 4 tendons is described. First however the minimum thickness of the deck / top flange is determined out of the local schematisation which holds for all the possible designs. The conclusions of the optimisation process are described in the last section.

5.2 Minimum deck thickness

In Section 4.9 the top flange / deck was verified for shear and ultimate resistance moment for the local schematisation. This local schematisation is the same for all the designs irrespective of the number of tendons. The calculation showed that a deck thickness of 250 mm and longitudinal reinforcement in the deck near the webs of bars with a diameter of $\phi_{reinf} = 16mm$ and a spacing of $S_{reinf} = 110mm$ was enough to resist the shear and bending moments. Shear was not normative for the minimum deck thickness. The ultimate resistance moment and the rotation capacity of the deck were however just enough to satisfy the verification. To increase the ultimate resistance moment of the deck the lever arm between the two forces F_c and F_s should be increased. This means that the deck becomes thicker. Another option is to add more reinforcement bars. This however has a strong influence on the rotation capacity of the deck. More reinforcement bars means that the compression zone of the concrete increases. The height of the compression zone may however not become too large as this limits the rotation capacity of the deck. The verification of the rotation capacity is: $x/d \leq 0.45$. When this verification is not satisfied the thickness of the deck should be increased. Another option is to diminish the number of reinforcement bars which results in a smaller compressive zone (x). This will however also reduce the ultimate resistance moment of the deck.

The number of reinforcement bars in the deck is thus an important factor for the determination of the minimum deck thickness. There is a minimum number of reinforcement bars needed for the ultimate resistance moment to resist the bending moments. But the number of bars may not become too large as then the verification of the rotation capacity is not satisfied anymore. To find the minimum deck thickness, the ultimate resistance moment and the rotation capacity are calculated for a specific deck thickness and different spacings of the reinforcement bars. The chosen diameter of the reinforcement bars is $\phi_{reinf} = 16mm$. The results for a deck thickness of 250 mm and different spacings of the reinforcement bars are shown in Graph 1. The graph shows that the deck will satisfy when the spacing of the bars is between 105 and 110 mm. For the design of the deck the largest spacing which satisfies should be chosen as this requires fewer bars and thus saves money. For a deck thickness of 250 mm it is therefore chosen that the reinforcement bars in the deck have a spacing of 110 mm. The horizontal parts in the graph are the result of rounding off the number of bars within one metre width of the deck. Notice that this deck thickness already is very thin as the number of possible spacings is very small.

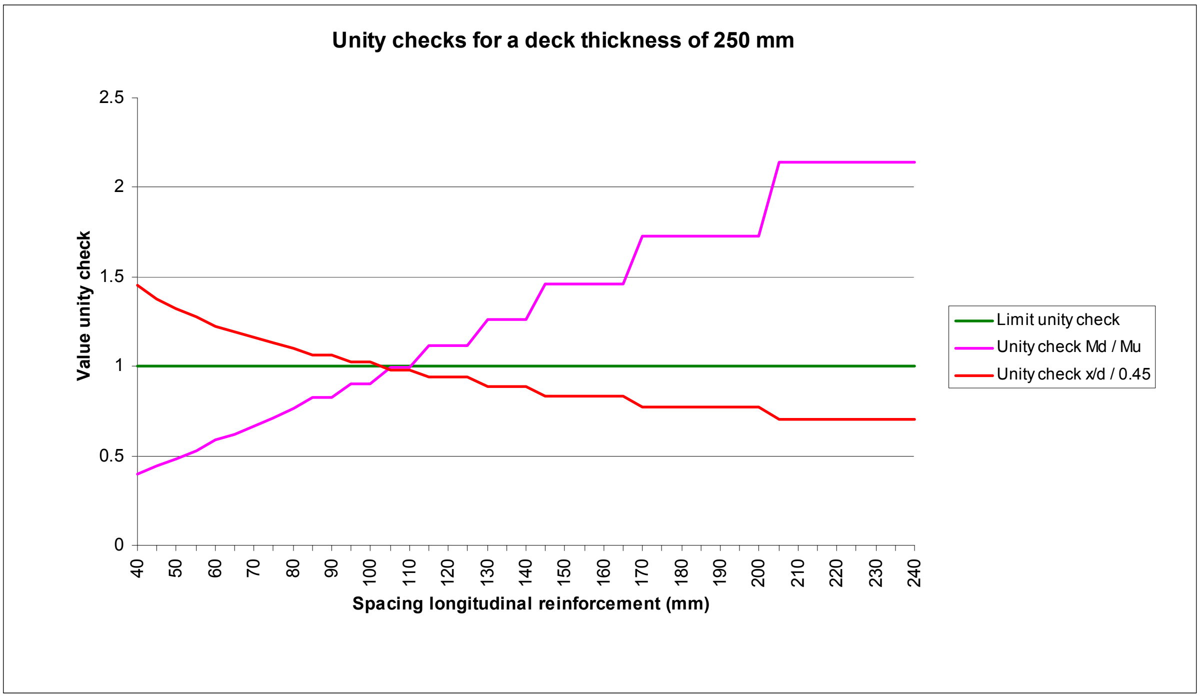

Graph 1: Unity checks for a deck thickness of 250 mm

To verify if the deck thickness can be taken smaller, the deck thickness is decreased with 10 mm to a thickness of 240 mm. The results of the calculations for a deck thickness of 240 mm are shown in Graph 2. The graph shows that this deck thickness is too thin as there are no results where both unity checks satisfy. The steps taken for the different spacings of the bars are 5 mm. The lines of the two checks cross each other between a spacing of 100 and 105 mm. At a spacing of 100 mm the verification of the rotation capacity is however not satisfied. At a spacing of 115 mm the verification of the rotation capacity is satisfied but now the ultimate resistance moment of the deck is not enough anymore. Concluded can be that the minimum deck thickness is 250 mm with reinforcement bars $\phi_{reinf} = 16mm$ and a spacing of $S_{reinf} = 110mm$. Notice that this is exactly the same as what is chosen for the optimal design described in the previous chapter.

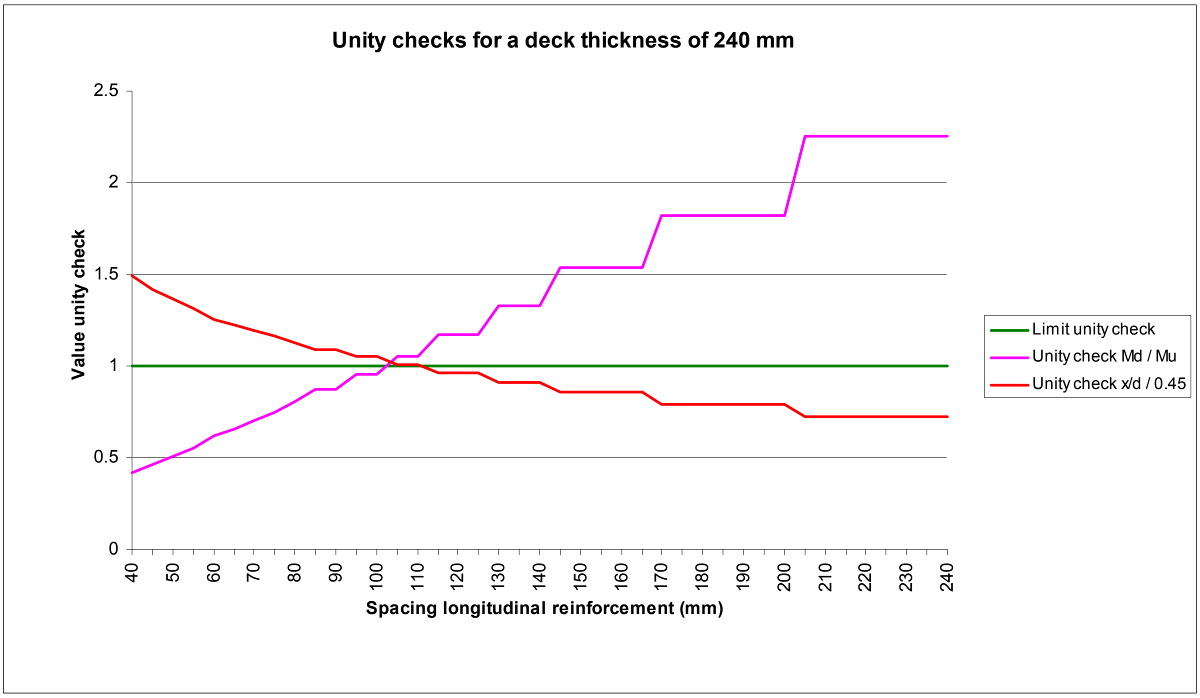

Graph 2: Unity checks for a deck thickness of 240 mm

5.3 Box girder with 6 prestressing tendons

The previous chapter, where the precast concrete segmental box girder with six external prestressing tendons was described, showed the important structural verifications for the design: fatigue of the concrete, the ultimate resistance moment and rotation capacity of the deck, buckling of the webs, the ultimate resistance moment of the box girder and shear + torsion in the webs. For a box girder with 6 tendons the minimum dead load of the girder is determined for different depths of the webs (H_{box}). The depth of the webs is changed in steps of 150 mm (height of a shear key). For each depth of the webs the geometry of the cross-section and the distance of the deviation blocks to the supports are adjusted in such a way that the minimum dead load of the box girder arises which still satisfies all the verifications. The result of this iterative optimisation process is shown in Table 5. Table 5 shows in each column the optimal design for a certain depth of the webs and the normative structural verifications. For the results of all the structural verifications of the different designs reference is made to Appendix D.1.1.

In Table 5 nine designs are shown. Notice that only eight designs are feasible as design 1 does not satisfy the verification of the ultimate resistance moment at t=∞, see the red cell. The green cells represent the normative verification to which the bottom flange has to be adjusted and the pink cells represent the normative verification to which the width of the webs has to be adjusted. Design 2, which is the same as the design in Chapter 4, is the design with the smallest dead load and has also the smallest depth of the box girder. This is thus the optimal design for a box girder with 6 tendons. For design 2 the normative verification is fatigue of the concrete at the deviation blocks at the bottom side. The bottom side is normative over the top side of the box girder. This is due to a resultant hogging moments in the serviceability limit state causing a camber in the box girder, see Section 4.10.2. To satisfy this verification there are three options: change the thickness of the top flange, change the width of the webs and change the thickness of the bottom flange. Graph 4, Graph 5 and Graph 6 show the impact on fatigue of the concrete for design 2 for changing respectively the thickness of the top flange, the width of the webs and the thickness of the bottom flange. The graphs show that increasing the thickness of the bottom flange has the most effect. This is logic as increasing the thickness of the bottom flange decreases the compressive stress in the concrete at the bottom side. At the same time, increasing the bottom flange thickness brings down the centroidal axis of the box girder which reduces the upward prestressing force and the compressive stress in the bottom flange. Increasing the thickness of the bottom flange has also the most favourable effect on the weight of the box girder. Because the width of the bottom flange is just 4 metres which is smaller than the width of the top flange (8.96 metres) and twice the depth of the webs (2* H_{box}). The lightest box girder thus arises when the minimum top flange thickness and the minimum width of the webs are chosen and the bottom flange thickness is just enough to satisfy the verification of fatigue of the concrete. This can be noticed for design 2, where the minimum top flange thickness is 0.25 m (see Section 5.2) and the minimum width of the webs is 0.16 m, which is determined by buckling of the webs (see pink cell in Table 5). A bottom flange thickness of 0.3 m is just enough to satisfy the verification of fatigue of the concrete at the deviation blocks at the bottom side, see Graph 6. Notice that increasing the top flange thickness has the least effect on the verification of fatigue of the concrete at the bottom side. Unless this adds more weight and thus results in a smaller hogging moment it also brings the centroidal axis of the box girder upwards which reduces the effect of adding weight.

Table 5 shows that for designs with a larger depth of the webs than design 2 at a certain depth the verification of the ultimate resistance moment at t=0 becomes normative instead of fatigue of the concrete. This can be explained as for a design with larger web depths the upward prestressing force at the deviation blocks is larger. The hogging moment at the deviation blocks then becomes larger. Graph 7, Graph 8 and Graph 9 show the impact on the ultimate resistance moment at t=0 for design 2 for changing respectively the thickness of the top flange, the width of the webs and the thickness of the bottom flange. To satisfy this verification it is, considering the graphs, the best way to increase the thickness of the bottom flange. This adds weight to the box girder and brings down the centroidal axis of the box girder which both results in a smaller hogging moment. For the designs 6 up to 9 it thus also holds that the lightest box girder arises when the minimum top flange thickness and the minimum width of the webs are chosen and the bottom flange thickness is just enough to satisfy the verification of the ultimate resistance moment at t=0. Notice in Graph 8 that for a small width of the webs the line suddenly rises very fast. This is because the compressive strain in the webs then becomes larger than the maximum elastic compressive strain ($\varepsilon_{c3} = 1.75‰$). The flat line in Graph 8 implies that the compressive strain in the bottom flange is larger than the elastic compressive strain. The strong curvature for a small top or bottom flange thickness as shown in Graph 7 and Graph 9 also implies that the compressive strain in the bottom flange then becomes larger than the elastic compressive strain.

Table 5 shows that the dead load of the box girder is smaller for box girders with a smaller depth. The lightest design is thus also the most slender design. There is however a limit to the slenderness of the prestressed box girder and thus to the minimum dead load. This limit is set by the verification of the ultimate resistance moment at t=∞. When the depth of the webs decreases, the upward prestressing force becomes smaller and also the lever arms (z) of the concrete forces within the cross-section of the box girder become smaller, see Graph 10 (for design 2). The ultimate resistance moment thus becomes smaller. The only option left to let the box girder satisfy the verification of to the ultimate resistance moment is to decrease the dead load of the box girder. For design 1 this is however not possible as the box girder needs its minimum bottom flange thickness to satisfy the verification of fatigue of the concrete. Box girder designs with a smaller depth than design 2 are thus not feasible. Designs with a larger depth than design 9 are possible but are in the end determined by the first natural bending frequency of the box girder as this frequency then becomes too large, see Table 5. The stiffness of the box girder increases namely faster than the weight of the girder. This verification can be satisfied by adding more weight. The designs with a larger depth than design 9 are however not interesting and are left out of the optimisation process as these design are less slender and have also a larger dead load.

The distance of the deviation blocks to the supports (a), is placed at the distance from the supports where the minimum shear force in the box girder arises for t=0 and for t=∞. In Graph 11 the influence of the distance of the deviation blocks to the supports on the vertical shear + torsion in the webs is shown for design 2. As the distance a only influences the shear force and not the shear resistance, Graph 11 shows that the box girder has the minimal shear force for a distance of the deviation blocks to the supports of 15 metres. Graph 11 shows for the vertical shear at t=∞ a line with two kinks which implicates the change of the normative section of the box girder with respect to the shear force, see Figure 20. For the vertical shear at t=0 the normative section of the box girder with respect to the shear force stays the same which results in a smooth line. Notice that the unity checks for vertical shear at t=0 and at t=∞ are close to each other for all the designs in Table 5. For the designs with a larger web depth the upward prestressing force becomes larger. To compensate this, the distance of the deviation blocks to the supports is made larger as this creates a smaller angle between the prestressing tendon and the centroidal axis and thus results in a smaller upward prestressing force. The placement of the deviation blocks farther away from the supports results in a smaller hogging moment at the deviation blocks in the serviceability limit state. This can be seen in Graph 12 (for design 2) as, unless the increasing of the lever arm (a) of the upward prestressing force, the unity check for fatigue of the concrete at the deviation blocks at the bottom side decreases. Because fatigue of the concrete is normative for the bottom flange thickness, see Table 5, it is thus the best to place the deviation blocks in the middle of the span at 22.5 metres from the supports, see Graph 12. This will however cause a too large shear force in the box girder in the end phase which cannot be taken by the webs, see Graph 11. At the same time the maximum bending moment in the box girder in the ultimate limit state t=∞ will not arise at mid-span but somewhere between the support and the middle of the span, see Figure 33. The place where this maximum moment arises is variable when the cross-section of the box girder is changed. For simplification reason it is therefore chosen to place the deviation blocks at a distance to the supports where the minimum shear force arises, such that the maximum bending moment for the verification of the ultimate resistance moment at t=∞ always arises at mid-span. Notice that the maximum bending moment at the deviation blocks arises at a distance of the deviation blocks to the supports of 3 metres, see Graph 12.

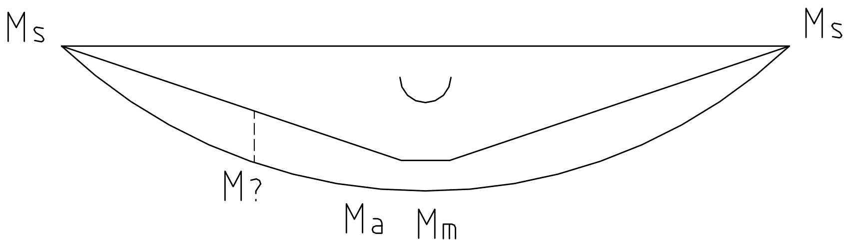

Figure 33: The bending moments due to dead, permanent and variable load minus the bending moments due to prestressing results in the largest bending moment $M_?$ somewhere between the supports and mid-span

The optimal design for a concrete box girder with 6 tendons is thus design 2 from Table 5. This design is also the one that is described in Chapter 4. In Graph 3 the dead load is shown for the 8 feasible designs of Table 5. Notice the kink in the line where the normative verification for the box girder changes (green cells in Table 5).

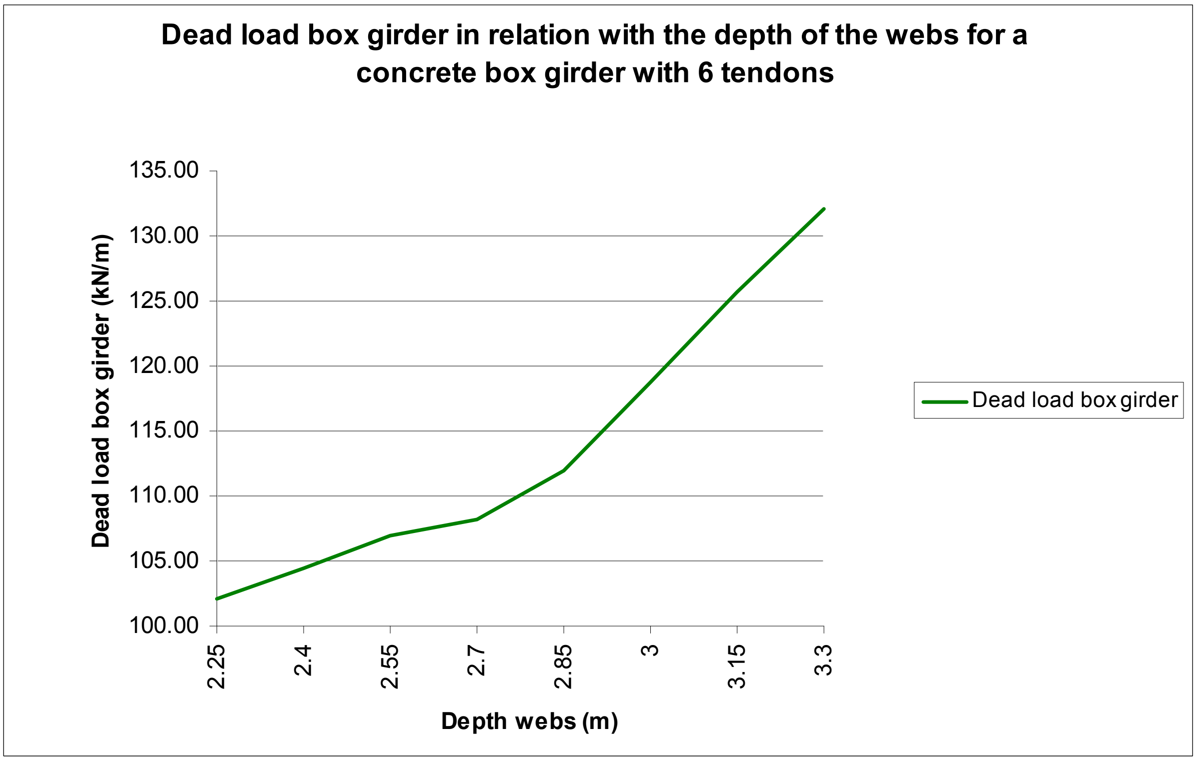

Graph 3: Dead load box girder in relation with the depth of the webs for a concrete box girder with 6 tendons

Design number	1	2	3	4	5	6	7	8	9	Unity
Depth webs	2.1	2.25	2.4	2.55	2.7	2.85	3	3.15	3.3	m
Depth box girder	2.65	2.8	2.95	3.1	3.25	3.41	3.6	3.79	3.99	m
Thickness top flange	0.25	0.25	0.25	0.25	0.25	0.25	0.25	0.25	0.25	m
Width webs	0.16	0.16	0.17	0.18	0.18	0.19	0.2	0.21	0.21	m
Thickness bottom flange	0.3	0.3	0.3	0.3	0.3	0.31	0.35	0.39	0.44	m
Distance of deviation blocks to supports	14	15	16	17	18	19	19	19	19	m
Dead load box girder	100.85	102.02	104.38	106.88	108.20	111.91	118.70	125.64	132.09	kN/m
Ultimate resistance moment at t=0, bottom side	0.870853	0.898022	0.925355	0.952394	0.978226	0.996586	0.996742	0.998938	0.994933	Unity check
Ultimate resistance moment at t=∞, top side	1.067195	0.897363	0.769691	0.658194	0.538472	0.464228	0.436005	0.414428	0.390166	Unity check
Additional deflection under mobile load	0.586826	0.516595	0.455878	0.404604	0.362771	0.318792	0.267035	0.226779	0.192968	Unity check
Vertical shear in the webs at t=0	0.920781	0.883005	0.795721	0.722152	0.699394	0.636519	0.59001	0.549604	0.537309	Unity check
Vertical shear + torsion in the webs at t=∞	0.966541	0.901702	0.805451	0.726368	0.689049	0.636085	0.588759	0.547896	0.53545	Unity check
Fatigue concrete, deviation block top side	0.703712	0.681884	0.659761	0.638493	0.618683	0.59845	0.574681	0.553056	0.534609	Unity check
Fatigue concrete, deviation block bottom side	0.990855	0.998424	0.991537	0.983196	0.987956	0.958542	0.885371	0.823682	0.769402	Unity check
Fatigue concrete, mid-span top side	0.787934	0.743081	0.702748	0.666959	0.636664	0.608771	0.584513	0.562448	0.543598	Unity check
Fatigue concrete, mid-span bottom side	0.92299	0.948056	0.955623	0.958755	0.972329	0.949759	0.87773	0.816947	0.763511	Unity check
First natural bending frequency n0	3.239833	3.433065	3.613091	3.790051	3.978044	4.172774	4.426872	4.669173	4.936596	Hz
Minimum required width of the webs (buckling)	150.4414	156.8861	163.9233	171.0415	178.4204	185.4541	193.2599	201.1085	208.808	mm

Table 5: Optimal designs of the concrete box girder for different depths of the webs and 6 prestressing tendons

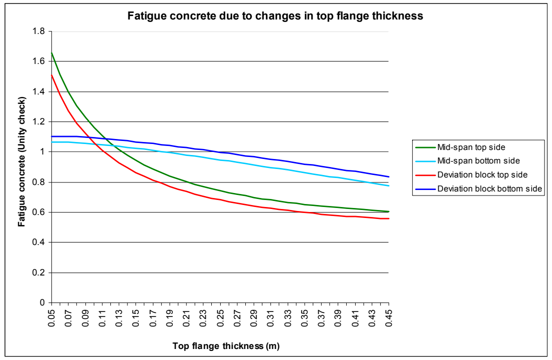

Graph 4

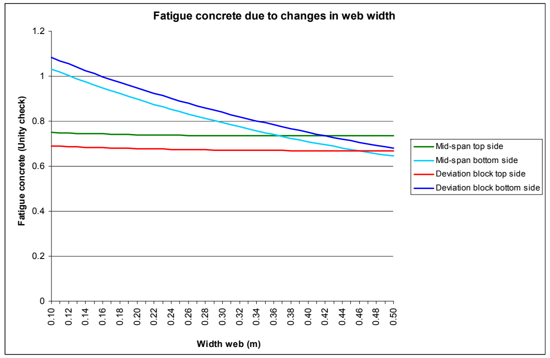

Graph 5

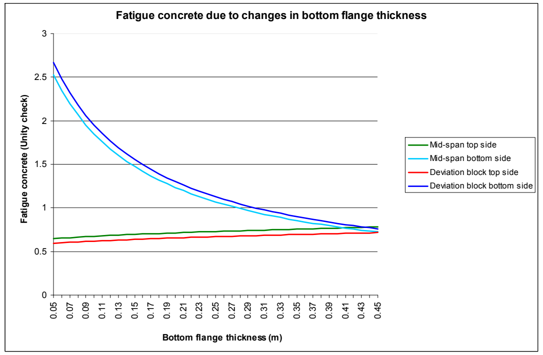

Graph 6

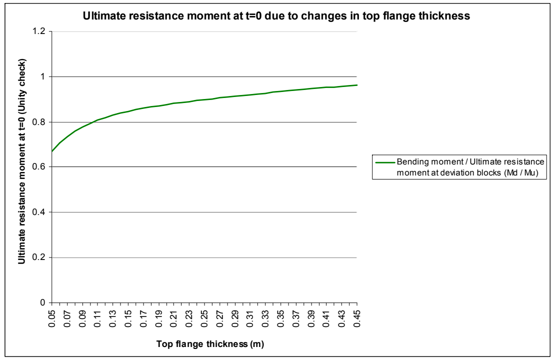

Graph 7

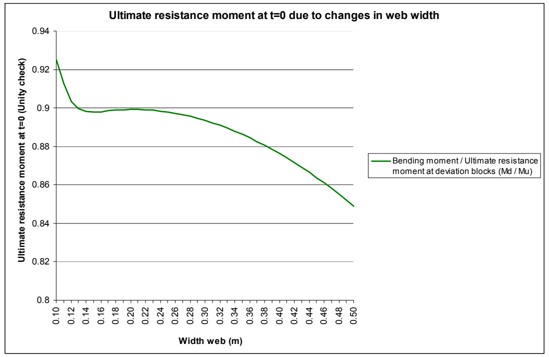

Graph 8

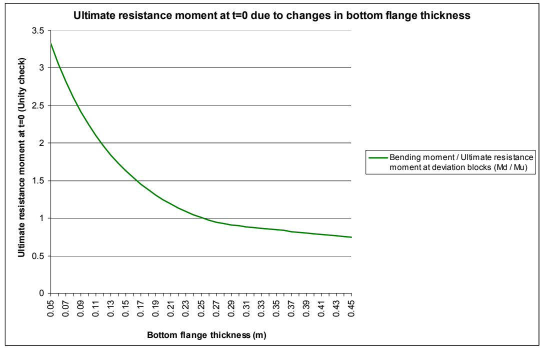

Graph 9

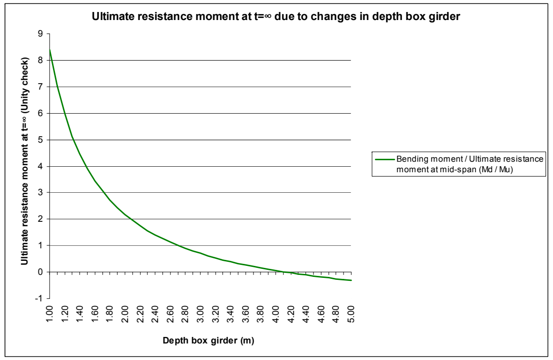

Graph 10

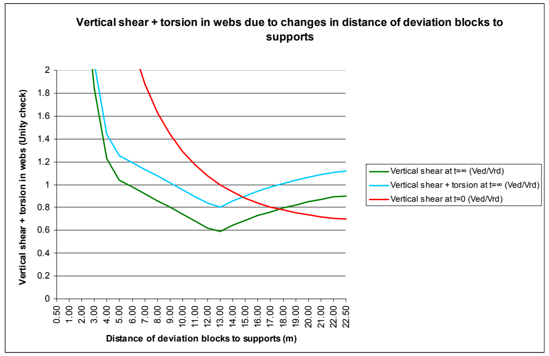

Graph 11

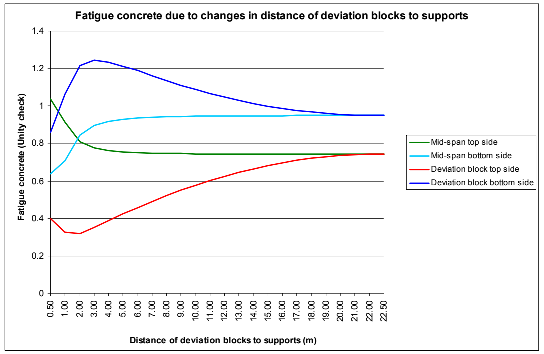

Graph 12

5.4 Box girder with 8 prestressing tendons

For a box girder with 8 tendons the minimum dead load of the box girder for different depths of the webs (H_{box}) is shown in Table 6. The depth of the webs is changed in steps of 150 mm (height of a shear key). Table 6 shows in each column the optimal design for a certain depth of the webs and the normative structural verification. For the results of all the structural verifications of the different designs reference is made to Appendix D.1.2.

In Table 6 nine designs are shown. Notice that only eight designs are feasible as design 1 does not satisfy the verification of the ultimate resistance moment at t=∞, see the red cell. The green cells represent the normative verification to which the bottom flange has to be adjusted and the pink cells represent the normative verification to which the width of the webs has to be adjusted. Design 2 is the design with the smallest dead load and depth of the box girder. This is thus the optimal design for a box girder with 8 tendons.

The difference with a box girder with 6 tendons is the smaller depth of the designs; compare Table 5 with Table 6. Due to the larger prestressing force the verification of the ultimate resistance moment at t=∞ is easier satisfied. It is therefore possible to decrease the depth of the webs. For design 2 the verification of fatigue of the concrete at the deviation blocks at the bottom side is normative. This is also the case for the optimal design of a box girder with 6 tendons. The best way to satisfy this verification is to increase the thickness of the bottom flange, see Section 5.3. The lightest box girder thus arises when the minimum top flange thickness and the minimum width of the webs are chosen and the bottom flange thickness is just enough to satisfy the fatigue verification. This can be noticed for design 2, where the minimum top flange thickness is 0.25 m (see Section 5.2) and the minimum width of the webs is 0.2 m, which is determined by vertical shear + torsion in the webs (see pink cell in Table 6). Due to the larger prestressing force (8 instead of 6 tendons) and the smaller depth of the webs (less shear keys) the minimum width of the webs is determined by vertical shear + torsion in the webs instead of buckling. For designs with a larger depth of the webs than design 4, Table 6 shows that buckling becomes normative over vertical shear + torsion in the webs. This is because the required width of the webs to satisfy the verification of vertical shear + torsion in the webs becomes smaller for designs with a larger depth of the webs (more shear keys). For buckling however the required width of the webs increases for designs with a larger depth as the depth of the webs is raised to a square in the Euler buckling force. Table 6 shows that for designs with a larger depth the unity check of the ultimate resistance moment at t=0 increases. For design 9 the verification of the ultimate resistance moment at t=0 even becomes normative instead of fatigue of the concrete. Notice that the change of normative verification arises between a depth of the webs of 2.7 and 2.85 metres. This is also the case for a box girder with 6 tendons, see Table 5.

The optimal design for a concrete box girder with 8 tendons is thus design 2 from Table 6. In Graph 13 the dead load is shown for the 8 feasible designs of Table 6. Notice that it looks like there is some kind of optimal design with a minimum dead load as the slope decreases for designs with a smaller depth.
A design with a specific depth of the webs and 8 prestressing tendons results in a larger dead load than for the same depth of the webs and 6 prestressing tendons. This is due to the larger prestressing force. The resulting hogging moment (SLS) becomes larger and increases the compressive stress in the bottom flange. To satisfy the verification of fatigue of the concrete at this place the minimum required thickness of the bottom flange becomes larger. This is the main difference between the application of 6 and 8 prestressing tendons. Concluded can be that a concrete box girder with 8 tendons is not recommended as the weight of the box girder becomes larger than for a box girder with 6 prestressing tendons. Besides, the application of two extra tendons will increase the costs considerably. Worth to notice is that with 8 prestressing tendons a more slender railway girder can be created; compare Table 5 with Table 6. In this optimisation process it is however the objective to find the optimal structural design in relation to the costs and not to find the most slender design.

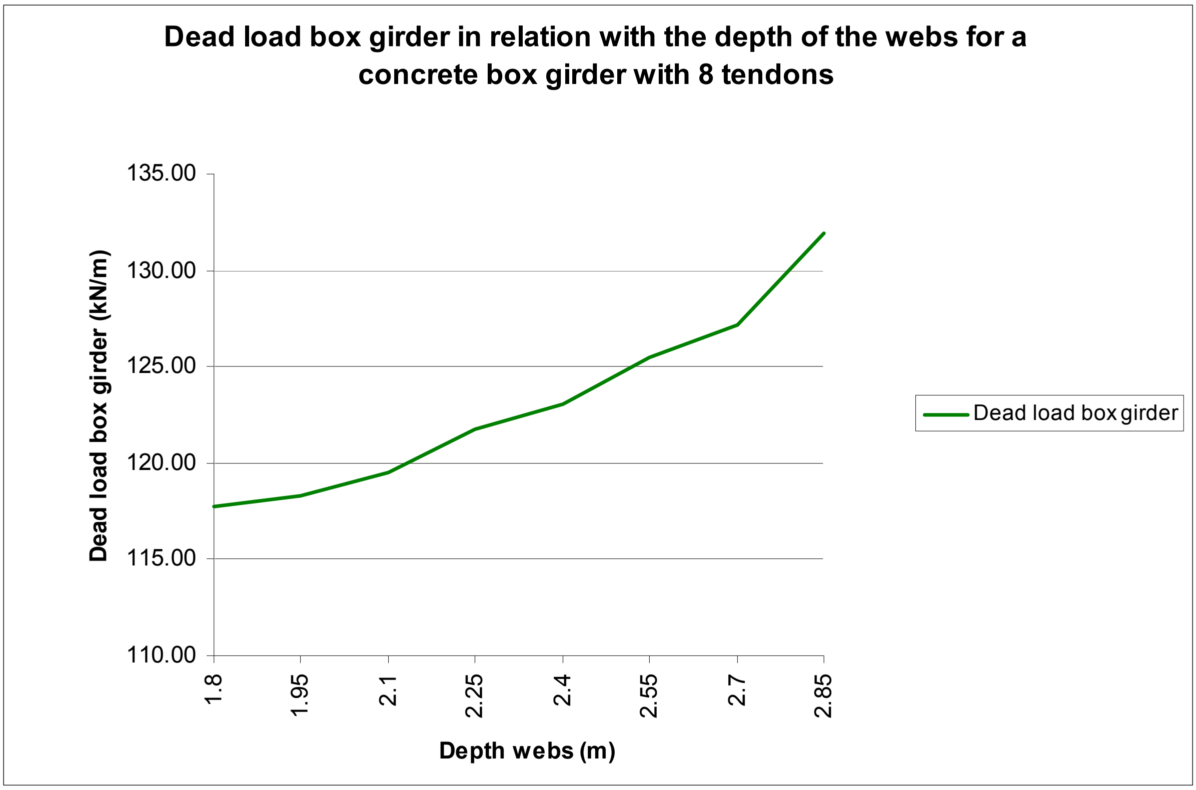

Graph 13: Dead load box girder in relation with the depth of the webs for a concrete box girder with 8 tendons

										Unity
Design number	1	2	3	4	5	6	7	8	9	
Depth webs	1.65	1.8	1.95	2.1	2.25	2.4	2.55	2.7	2.85	m
Depth box girder	2.35	2.51	2.67	2.83	2.99	3.14	3.29	3.43	3.6	m
Thickness top flange	0.25	0.25	0.25	0.25	0.25	0.25	0.25	0.25	0.25	m
Width webs	0.21	0.2	0.18	0.17	0.17	0.17	0.18	0.19	0.2	m
Thickness bottom flange	0.45	0.46	0.47	0.48	0.49	0.49	0.49	0.48	0.5	m
Distance of deviation blocks to supports	12	13	15	16	17	19	20	22	22.5	m
Dead load box girder	116.08	117.72	118.26	119.53	121.77	123.02	125.52	127.19	131.94	kN/m
Ultimate resistance moment at t=0, bottom side	0.798788	0.826345	0.835166	0.860645	0.88578	0.907148	0.938517	0.972639	0.99691	Unity check
Ultimate resistance moment at t=∞, top side	1.046222	0.863562	0.695275	0.563076	0.46048	0.363565	0.288101	0.211599	0.168796	Unity check
Additional deflection under mobile load	0.663693	0.564345	0.486204	0.422092	0.368642	0.328819	0.294128	0.267943	0.235558	Unity check
Vertical shear in the webs at t=0	0.961124	0.955118	0.955469	0.971807	0.934503	0.875838	0.805681	0.731982	0.68367	Unity check
Vertical shear + torsion in the webs at t=∞	0.974449	0.933925	0.999524	0.979478	0.919985	0.894481	0.801177	0.739222	0.67392	Unity check
Fatigue concrete, deviation block top side	0.787301	0.759789	0.75601	0.728737	0.701276	0.683655	0.654289	0.628255	0.599675	Unity check
Fatigue concrete, deviation block bottom side	0.996299	0.997226	0.992307	0.995352	0.989273	0.990801	0.98923	0.999006	0.969763	Unity check
Fatigue concrete, mid-span top side	0.949277	0.881823	0.826333	0.777906	0.734253	0.69621	0.660336	0.628478	0.599675	Unity check
Fatigue concrete, mid-span bottom side	0.888571	0.915542	0.945345	0.962608	0.967428	0.982423	0.985157	0.998848	0.969763	Unity check
First natural bending frequency n0	2.839565	3.057814	3.286859	3.50879	3.719991	3.91874	4.101903	4.269392	4.470579	Hz
Minimum required width of the webs (buckling)	131.7484	139.4915	147.3084	153.9059	161.7387	169.5143	176.8395	184.8665	193.0263	mm

Table 6: Optimal designs of the concrete box girder for different depths of the webs and 8 prestressing tendons

5.5 Box girder with 4 prestressing tendons

For a box girder with 4 tendons the minimum dead load of the box girder for different depths of the webs (H_{box}) is shown in Table 7. The depth of the webs is changed in steps of 150 mm (height of a shear key). Table 7 shows in each column the optimal design for a certain depth of the webs and the normative structural verification. For the result of all the structural verifications of the different designs reference is made to Appendix D.1.3.

In Table 7 nine designs are shown. Notice that only eight designs are feasible as design 1 does not satisfy the verification of the ultimate resistance moment at t=∞, see the red cell. The green cells represent the normative verification to which the bottom flange has to be adjusted and the pink cells represent the normative verification to which the width of the webs has to be adjusted. Design 2 is the design with the smallest dead load and depth of the box girder. This is thus the optimal design for a box girder with 4 tendons.

The difference with a box girder with 6 tendons is the much larger depth of the designs; compare Table 5 with Table 7. Due to the smaller prestressing force a larger depth of the webs is required in order to satisfy the verification of the ultimate resistance moment at t=∞. For design 2 the verification of the ultimate resistance moment at t=0 is normative. Due to the large angle α_t the upward prestressing force becomes very large. The hogging moment at t=0 is thus quite large, despite of the application of just 4 tendons. The best way to satisfy this verification is to increase the thickness of the bottom flange, see Section 5.3. The lightest box girder thus arises when the minimum top flange thickness and the minimum width of the webs are chosen and the bottom flange thickness is just enough to satisfy the verification of the ultimate resistance moment at t=0. This can be noticed for design 2, where the minimum top flange thickness is 0.25 m (see Section 5.2) and the minimum width of the webs is 0.23 m, which is determined by buckling of the webs (see pink cell in Table 7). Due to the large depth of the webs the verification of buckling is normative for the width of the webs. Fatigue of the concrete is not the normative verification anymore as a result of the smaller prestressing force and the large section modulus (W).

The optimal design for a concrete box girder with 4 tendons is thus design 2 from Table 7. In Graph 14 the dead load is shown for the 8 feasible designs of Table 7. The designs of the box girders with 4 prestressing tendons result in a much larger dead load than for box girders with 6 prestressing tendons. This is mainly due to the large webs of the box girder. Besides the larger dead load, the application of 4 tendons also results in an unacceptable large depth of the box girder. Concluded can be that a concrete box girder with 4 tendons not outweighs the optimal design of a box girder with 6 prestressing tendons. Worth to notice is that for some designs the first natural frequency of the box girder exceeds the upper limit of 5.5 Hz, see Table 7. Due to the large stiffness of the box girder these designs require a dynamic analysis in order to verify if the box girder is well determined against the dynamic effects.

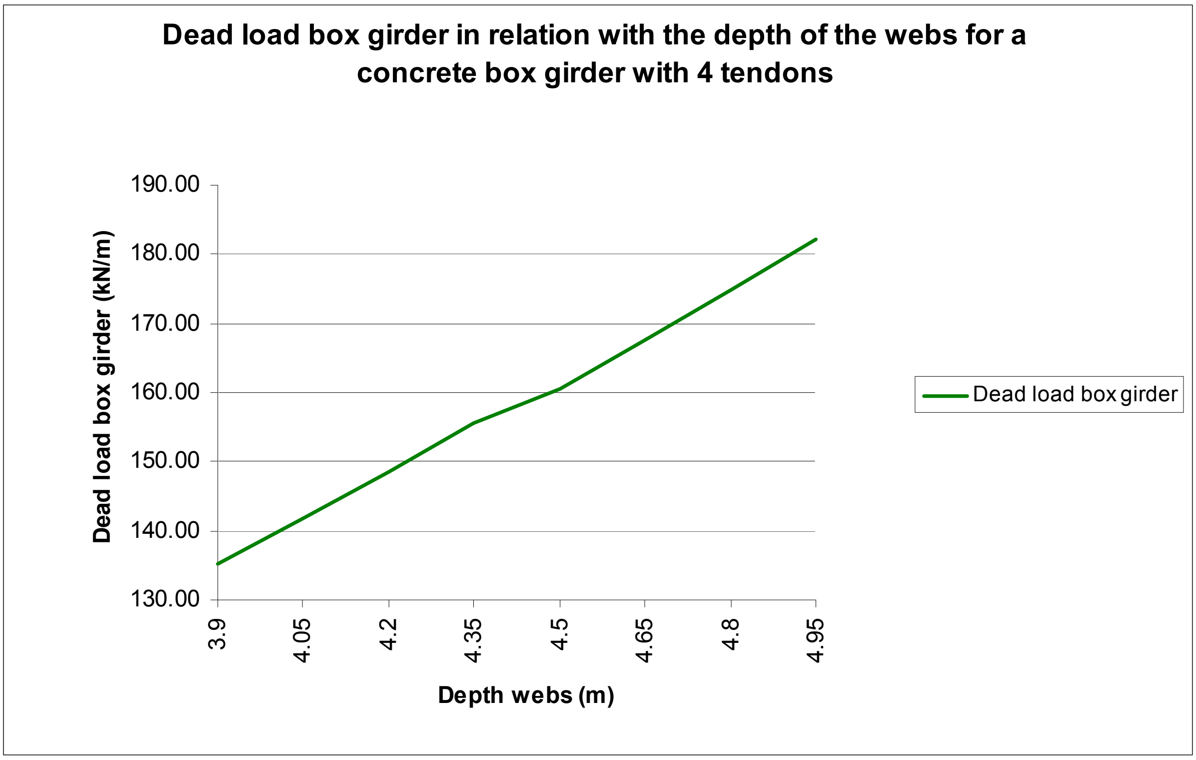

Graph 14: Dead load box girder in relation with the depth of the webs for a concrete box girder with 4 tendons

										Unity
Design number	1	2	3	4	5	6	7	8	9	
Depth webs	3.75	3.9	4.05	4.2	4.35	4.5	4.65	4.8	4.95	m
Depth box girder	4.34	4.52	4.7	4.88	5.06	5.24	5.42	5.6	5.78	m
Thickness top flange	0.25	0.25	0.25	0.25	0.25	0.25	0.25	0.25	0.25	m
Width webs	0.23	0.23	0.24	0.25	0.26	0.26	0.27	0.28	0.29	m
Thickness bottom flange	0.34	0.37	0.4	0.43	0.46	0.49	0.52	0.55	0.58	m
Distance of deviation blocks to supports	14	14	14	14	14	14	14	14	14	m
Dead load box girder	130.60	135.23	141.85	148.62	155.54	160.39	167.53	174.81	182.25	kN/m
Ultimate resistance moment at t=0, bottom side	0.999156	0.997921	0.996951	0.996519	0.996479	0.997403	0.997946	0.998605	0.999315	Unity check
Ultimate resistance moment at t=∞, top side	1.034306	0.975543	0.954693	0.938688	0.926662	0.89013	0.884705	0.881608	0.880525	Unity check
Additional deflection under mobile load	0.17231	0.152154	0.134497	0.119619	0.106962	0.096612	0.087175	0.078966	0.071783	Unity check
Vertical shear in the webs at t=0	0.403441	0.397049	0.372743	0.351027	0.331536	0.327425	0.310321	0.294821	0.280723	Unity check
Vertical shear + torsion in the webs at t=∞	0.405701	0.394738	0.374111	0.355674	0.339114	0.331985	0.317748	0.304827	0.29306	Unity check
Fatigue concrete, deviation block top side	0.461284	0.449602	0.438147	0.427423	0.417353	0.408571	0.399623	0.391153	0.383121	Unity check
Fatigue concrete, deviation block bottom side	0.593323	0.569151	0.54062	0.515495	0.492959	0.477407	0.458478	0.441212	0.425397	Unity check
Fatigue concrete, mid-span top side	0.508097	0.494595	0.481593	0.469425	0.458001	0.447863	0.43772	0.42812	0.419014	Unity check
Fatigue concrete, mid-span bottom side	0.57032	0.549113	0.523782	0.501115	0.480705	0.466554	0.449331	0.433613	0.419217	Unity check
First natural bending frequency n0	5.253979	5.494511	5.706019	5.911096	6.110502	6.33141	6.521781	6.70809	6.890781	Hz
Minimum required width of the webs (buckling)	222.131	229.1686	236.4649	244.2666	252.1273	258.8415	266.7976	274.8114	282.8829	mm

Table 7: Optimal designs of the concrete box girder for different depths of the webs and 4 prestressing tendons

5.6 Conclusions

In the abovementioned optimisation process it is concluded that the design of a precast concrete segmental box girder with 6 prestressing tendons from Chapter 4 is the optimal design. The application of 6 tendons results in the lightest box girder. The optimal design is however not the most slender railway girder. For the most slender box girder 8 prestressing tendons are required. The normative verification for the optimal design is fatigue[1] of the concrete at the deviation blocks at the bottom side. The best way to satisfy this verification is to increase the bottom flange thickness. Increasing the thickness of the bottom flange decreases the compressive stress in the concrete at the bottom side. At the same time, increasing the bottom flange thickness brings down the centroidal axis of the box girder which reduces the upward prestressing force and the compressive stress in the bottom flange. The lightest box girder thus arises when the minimum top flange thickness and the minimum width of the webs are chosen and the bottom flange thickness is just enough to satisfy the verification of fatigue of the concrete.

The application of 8 prestressing tendons results in a larger prestressing force. The verification of the ultimate resistance moment at t=∞ is hereby easier satisfied. For box girders with 8 prestressing tendons it is therefore possible to decrease the depth of the webs, resulting in a more slender design. However, due to this larger prestressing force the resulting hogging moment (SLS) becomes larger and increases the compressive stress in the bottom flange. To satisfy the verification of fatigue of the concrete at the deviation blocks at the bottom side the minimum required thickness of the bottom flange becomes large. Thereby the design of a box girder with 8 tendons results in a larger dead load than a box girder with 6 tendons, unless the smaller depth. The designs of the box girders with 4 prestressing tendons result also in a much larger dead load than box girders with 6 prestressing tendons. This is mainly due to the large webs of the box girder in order to satisfy the verification of the ultimate resistance moment at t=∞. Besides the larger dead load, the application of 4 tendons results also in an unacceptable large depth of the box girder.

For the optimisation process holds that the most slender box girders are also the lightest box girders, irrespective of the number of tendons. There is however a limit to the slenderness of the prestressed box girder and thus to the minimum dead load. This limit is set by the verification of the ultimate resistance moment at t=∞. When the depth of the webs decreases, the upward prestressing force becomes smaller. Also the lever arms (z) of the concrete forces within the cross-section of the box girder become smaller. The ultimate resistance moment thus becomes smaller as the depth of the webs decreases. The only option left to let the box girder satisfy the verification of to the ultimate resistance moment is to decrease the dead load of the box girder. At a certain depth this is however not possible anymore as the box girder needs its minimum bottom flange thickness to satisfy the verification of fatigue of the concrete.

Buckling is determined for the minimum web width of the optimal design. For more slender box girders (e.g. the optimal design of a box girder with 8 tendons) the verification of vertical shear + torsion becomes normative. This is due to the large shear force due to prestressing and the small number of shear keys. For a box girder made of concrete C50/60 it holds that the verification of deflection is not normative. Because the depth of the box girder designs is relative large, the moment of inertia is large so that the verification of additional deflection under mobile load is easily satisfied. Considering the optimisation process it can be concluded that the application of more than 8 or less than 4 tendons is not interesting for the design as the optimum is in the middle (6 tendons). The application of more tendons results in heavier box girders. This is because the stress in the bottom flange increases due to the larger prestressing force. The verification of fatigue of the concrete thereby becomes more critical, requiring a thicker bottom flange. The application of 2 tendons will not even result in a feasible

[1] The concrete box girder is verified for fatigue of the concrete according to Annex NN.3.2 NN.112 [12] (Eurocode). This is a simplified approach for railway bridges which results in a conservative fatigue verification. Other fatigue verifications show however that fatigue of the concrete is not normative for the design. When the fatigue verification is not normative for the box girder the verification of the ultimate resistance moment of the box girder at t=0 becomes normative. The change of normative structural verification for the design results however not in a radically different design of the elevated metro structure. For the comparison of the different fatigue verifications for concrete reference is made to Appendix K: Comparison fatigue verifications for concrete.

design as the verification of the ultimate resistance moment at t=∞ requires such a large depth of the webs so that the ultimate resistance moment at t=0 is not enough anymore. The optimal design for a precast concrete segmental box girder is thus the one as presented in Chapter 4.

6. Design UHPC box girder C180

6.1 General

This chapter describes the design of the precast UHPC segmental box girder with external prestressing tendons. The structural schematisation and the considered time phases of the concrete design are the same for the UHPC design. The UHPC design in general thus has the same characteristics as the concrete design. To avoid repetition reference is made to Chapter 4 for the explanation of the schematisations and boundary conditions. In this chapter only the design, structural verifications and differences with the concrete design are described. For the extensive calculation of the UHPC box girder reference is made to: Appendix C: Calculations UHPC box girder C180. This design represents the optimal design for a precast segmental box girder made of Ultra High Performance Concrete C180 with external prestressing tendons. Why this design with its geometry and its prestressing characteristics is the optimal design is explained in the next chapter. References to the specific codes and literature used for the design are given in the Appendix.

6.2 Material characteristics

One speaks of Ultra High Performance Concrete for concrete with strength classes between C90/105 and C200/230 [6]. For the UHPC box girder design the material Ductal®-AF [i5] is chosen. This material consists of concrete with metal fibres and has excellent standardized fire-resistance behaviour. This UHPC can be classified as concrete with strength class C180. As there are many different UHPC mixes with all there own characteristics, the French recommendations [18] does not prescribe the material characteristics for a sudden strength class. It is therefore chosen to take an existing UHPC product so all the material characteristics are known. Furthermore reinforcing steel FeB 500 and prestressing steel FeP 1860 are chosen for the design of the box girder. For the material characteristics of these three materials reference is made to Appendix C.2. From now on in this design study Ductal®-AF C180 is meant with UHPC.

6.3 Geometry box girder

6.3.1 General

The cross-section of the box girder is shown in Figure 34, where:

Length span	L	45	m
Depth box girder	H	2.41	m
Width top flange	b_{tf}	8.96	m
Thickness top flange	t_{tf}	0.18	m
Width web	b_w	0.14	m
Width bottom flange	b_{bf}	4	m
Thickness bottom flange	t_{bf}	0.13	m
Width box top side	b_{boxts}	5	m
Cantilever length top flange	L_{cant}	1.98	m
Depth webs	H_{box}	2.1	m

Angle of webs with vertical axis $\alpha_w = \tan^{-1}\left(\frac{(b_{boxts} - b_{bf})/2}{H_{box} + t_{bf}}\right) = 12.64°$

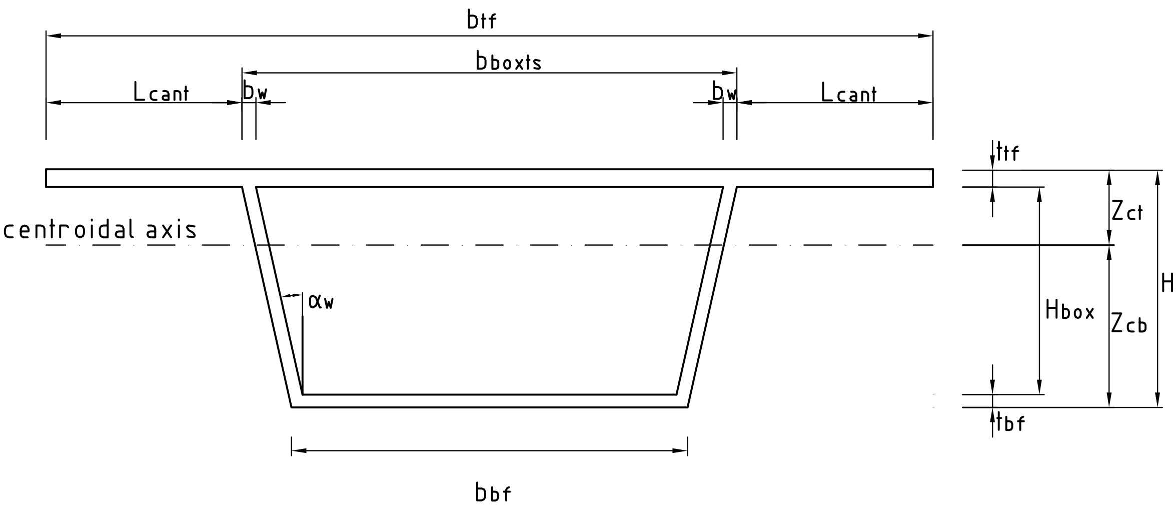

Figure 34: Cross-section of the box girder

6.3.2 Concrete cover

The very dense material structure of UHPC results in a higher durability and smaller concrete cover compared with concrete C50/60.
The concrete cover for the box girder made of C50/60 is:

$c_{nom} = c_{\min} + \Delta c_{dev} = 40mm$ See Section 4.3.2

The concrete cover for UHPC is assumed to be half of this value:

$c = 20mm$

6.3.3 Cross-sectional properties

The cross-sectional properties of the box girder are given in Table 8. For the calculation reference is made to Appendix C.3.5.

		Value	
Cross-sectional area of UHPC	A_c	2.721	m^2
Distance from bottom to centroidal axis	Z_{cb}	1.643	m
Distance from top to centroidal axis	Z_{ct}	0.767	m
Second moment of area of the UHPC section	I_c	2.381	m^4
Section modulus bottom	W_b	1.450	m^3
Section modulus top	W_t	3.103	m^3
Perimeter UHPC box girder	u	21.851	m

Table 8: Cross-sectional properties box girder

6.4 Loads

In Figure 35 the cross-section of the superstructure without the box girder is shown. The box girder supports a double-track metro system with emergency walkways at the cantilevers of the box girder.

The vertical loads in longitudinal direction of the box girder are:

- Dead load of the UHPC box girder: $g_{dead} = 69.4kN/m$
- Permanent load of the permanent construction shown in Figure 35: $g_{perm} = 34.42kN/m$
- Variable load of the metros and snow loading: $q_{var} = 58.29kN/m$

Furthermore the box girder is subjected to the horizontal loads:

- Wind load: $q_{wind} = 1.5kN/m^2$
- Sideward force due to the metro: $Q_{sidewf} = 30kN \; per\, track$

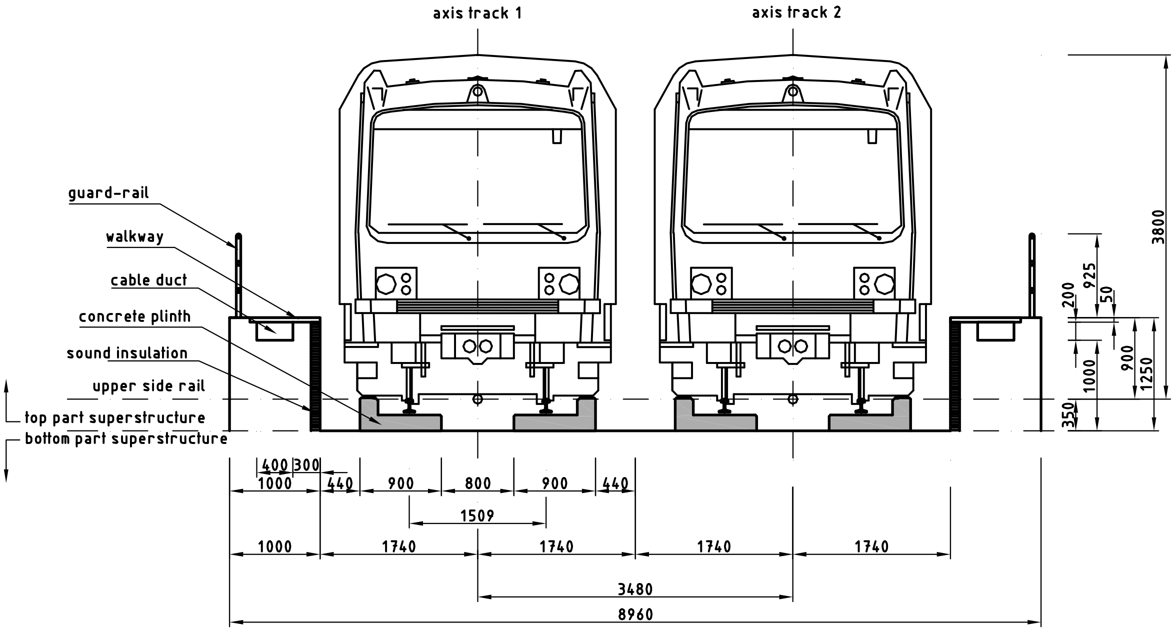

Figure 35: Cross-section top part superstructure without the box girder

The dynamic loading of the metro is taken into account by multiplying the vertical metro load with a dynamic factor: $\phi = 1 + 4/(10 + L) = 1.07$. For the exact calculation of the loads in the serviceability and ultimate limit state with the use of partial factors as well as the load schematisation in transversal direction of the box girder reference is made to Appendix C.4.

6.5 Prestressing tendons

6.5.1 Layout prestressing tendons

The layout of the external prestressing tendons inside the box girder is shown Figure 36.

Where:
Distance between the centre of the tendons and bottom side at mid-span

	h_t	0.5	m
Tendon eccentricity at mid-span	$f = Z_{cb} - h_t$	1.143	m
Distance of deviation blocks to supports	a	17	m

Angle between prestressing tendon and the centroidal axis $\alpha_t = \tan^{-1}(f/a) = 3.845°$

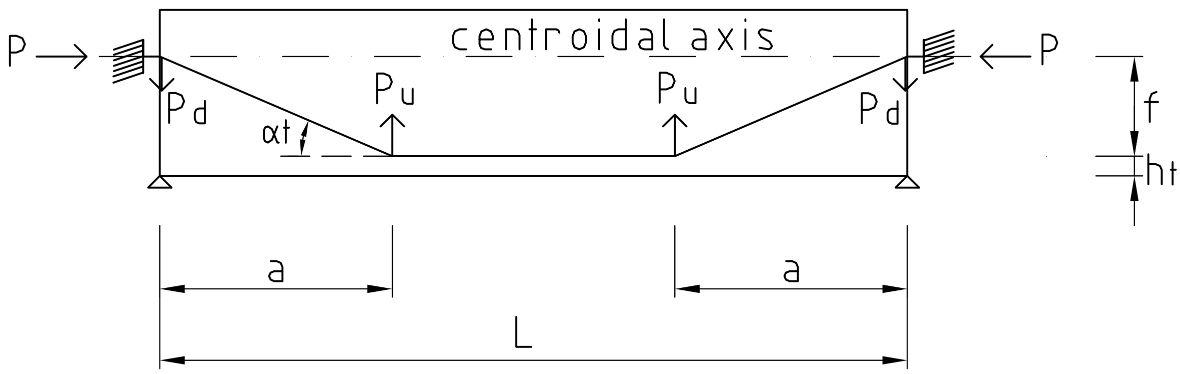

Figure 36: Layout external prestressing tendons

6.5.2 Bending moments

The UHPC box girder also has 6 tendons externally placed inside the girder according the layout shown in Figure 36. One tendon consists of 37 strands with a diameter of 15.7 mm and a cross-sectional area of 150 mm^2 per strand. The cross-sectional area of one tendon is:

$$A_p = 37 * 150 = 5550 mm^2$$

The number of tendons is:

$$n = 6 \quad tendons$$

For the calculation of the prestressing forces and bending moments reference is made to Appendix C.5.2.
For the calculation of the bending moments due to different load combinations reference is made to Appendix C.5.3.

6.5.3 Stresses due to loading

As the railway girder is a prefabricated segmental box girder, the joints between the segments cannot resist tensile stresses without opening of the joints. Opening of the joints is however not allowed so the UHPC cannot resist tensile stresses: $\sigma_c \leq 0 N / mm^2$. Furthermore the UHPC stress may not become too large. In order to rule out the non-linearity of creep it is assumed that the UHPC compressive stress should not exceed $\sigma_c \geq -0.45 * f_{ck} = -81 N / mm^2$. The stresses at the top and bottom side of the box girder in the serviceability limit state are calculated for different phases:

- The construction phase at t = 0, dead load and prestressing load only
- The end phase at t = ∞, fully loaded
- The end phase at t = ∞, without variable load

The maximum stress arises at the deviation blocks at the bottom side of the box girder during the construction phase. This maximum stress is:

$$\sigma_{cb} = -\frac{P_0}{A_c} - \frac{M_{m,p0}}{W_b} + \frac{M_{a,0}}{W_b} = -40.87 N / mm^2$$

For the calculation of the other compressive stresses in the cross-section of the box girder at different phases reference is made to Appendix C.5.4.

6.5.4 Prestressing losses

Losses due to the instantaneous deformation of concrete

The required overstress $\sigma_{overstr}$ in the first prestressed tendon to compensate the losses due to instantaneous deformation of UHPC is:

$$\sigma_{overstr} = 1364.64 N / mm^2$$

The maximum allowed tensile stress of the tendons during tensioning is $\sigma_{p,\max} = 1440 N/mm^2$. The stress caused by overstressing is far below this value and as it is also assumed that the UHPC compressive stress during tensioning is limited to $\sigma_c \leq 0.6 * f_{ck} = 108 N/mm^2$ this small overstressing will not cause any problems for the structure. It can be concluded that the losses due to the instantaneous deformation of UHPC can be compensated by overstressing the tendons. By overstressing the tendons the initial tensile stress in all the tendons after tensioning can be the maximum tensile stress $\sigma_{pm0} = 1360 N/mm^2$.

Losses due to friction

There are four places where tendon deviation takes place, namely: at the two supports and at the two deviation blocks at a distance a from the supports. At these places losses due to friction in post-tensioned tendons takes place. The loss due to friction per deviation is:

$$\Delta P_\mu(x) = P_{\max}(1 - e^{-\mu * \theta}) = 302.93 kN$$

Time dependent losses of prestress for post-tensioning

The time dependent loss of prestress for post-tensioning at the support is:

$$\Delta P_{c+s+r,s} = 2220 kN$$

The time dependent loss of prestress for post-tensioning at mid-span is:

$$\Delta P_{c+s+r,m} = 2046 kN$$

Total prestressing losses

The total prestressing losses are shown in Table 9:

Place	*Prestressing loss*	*Value*		*Percentage of loss*	*Value*	
At the first support	$\Delta P_{c+s+r,s} + \Delta P_\mu$	2523	kN	$\frac{\Delta P_{c+s+r,s} + \Delta P_\mu}{n * A_p * \sigma_{pm0}}$	5.57	%
After the first deviation block (at mid-span)	$\Delta P_{c+s+r,m} + 2 * \Delta P_\mu$	2651	kN	$\frac{\Delta P_{c+s+r,m} + 2 * \Delta P_\mu}{n * A_p * \sigma_{pm0}}$	5.85	%
After the second deviation block (at mid-span)	$\Delta P_{c+s+r,m} + 3 * \Delta P_\mu$	2954	kN	$\frac{\Delta P_{c+s+r,m} + 3 * \Delta P_\mu}{n * A_p * \sigma_{pm0}}$	6.52	%
At the second support	$\Delta P_{c+s+r,s} + 4 * \Delta P_\mu$	3432	kN	$\frac{\Delta P_{c+s+r,s} + 4 * \Delta P_\mu}{n * A_p * \sigma_{pm0}}$	7.58	%

Table 9: Total prestressing losses

The maximum prestressing loss arises at the end of the span, at the other end where the tensioning takes place. This loss = 7.58 % which is smaller than the assumed prestressing loss of 20 %. This assumption is thus a safe value for the prestressing losses and has not to be taken any larger. To take into account other unexpected losses and other expected losses like for instance thermal losses and slip of the anchorage it is decided to keep the expected final prestressing losses of 20 %. Notice that these formulas for prestressing losses are from [11] which can be used for concrete C50/60. For UHPC there are no formulas to determine the prestressing losses, but as the method should be quite similar this should give an impression of the losses. As the calculations show that the losses are far below the expected loss of 20 %, it is assumed to be on the safe side. In the continuation of this design the prestressing loss in the end phase at t = ∞ is thus 20 %.

For the calculation of all the prestressing losses reference is made to Appendix C.5.5.

6.6 Deflection

The deflections and unity checks at mid-span for different phases are:

Time	*Load* q	*Deflection* w	*value*	*Maximum allowed deflection* $w_{\max}$	*Unity check* $w / w_{\max}$
At t=0	$g_{dead} - q_{pt0}$	-78.5	mm	$L/250 = -180mm$	0.44
At t=∞ without variable load	$g_{dead} + g_{perm} - q_{pt\infty}$	-34.6	mm	$L/500 = 90mm$	-0.38
Additional deflection under mobile load	q_{var}	26.1	mm	$L/1500 = 30mm$	0.87
At t=∞ fully loaded	$g_{dead} + g_{perm} + q_{\text{var}} - q_{pt\infty}$	-34.6 + 26.1 = -8.5	mm	$L/500 = 90mm$	-0.09

Table 10: The deflections and unity checks at mid-span for different phases

An upward deflection has a negative sign and a downward deflection has a positive sign. As the unity checks show, the construction satisfies with respect to deflection for all phases and always has a camber. The normative deflection is the additional deflection under mobile load.

For the calculation of the deflections reference is made to Appendix C.6.

6.7 Shear + torsion

6.7.1 Shear + torsion in webs

The webs have to resist the vertical shear and torsion. As it concerns a segmental box girder the joints between the segments consists of shear keys, see Figure 37. These shear keys are normative over a cross-section of a segment with respect to shear and torsion of the box girder.

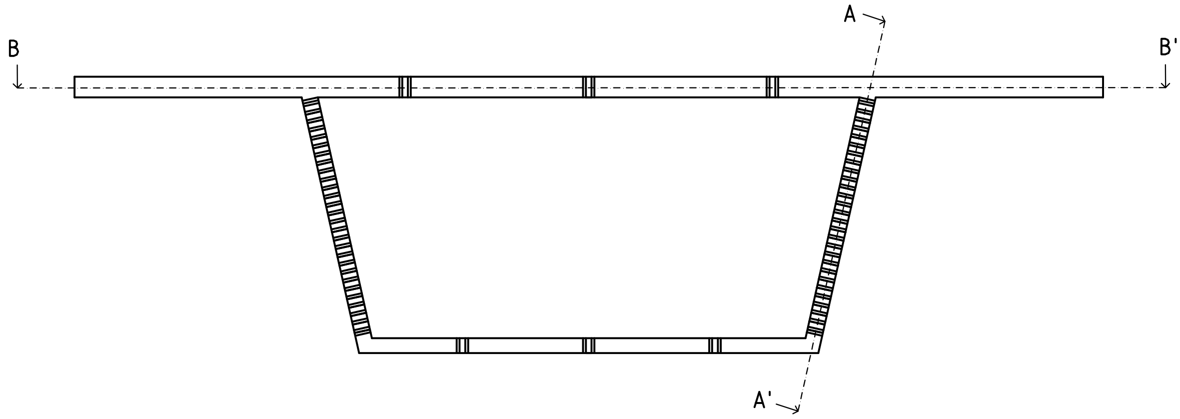

Figure 37: Shear keys in the flanges and in the webs

Each web has 14 shear keys with a height of 150 mm per shear key.

TU Delft Delft University of Technology

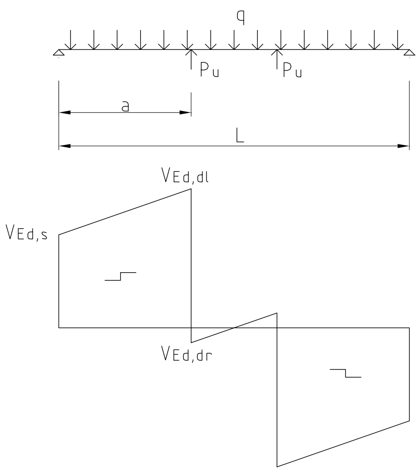

Figure 38: Shear force diagram at t=0

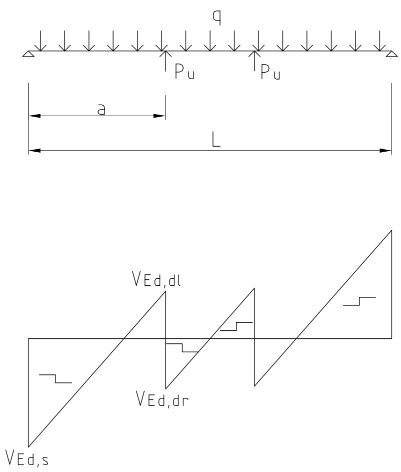

Figure 39: Shear force diagram at t=∞

The vertical shear strength of one web is:

$$V_{Rd,1} = f_{cd,uls} * L_{shear} * \cos\alpha_s * \cos\alpha_w * t_w * n_s = 5330kN$$

The vertical shear strength of two webs is:

$$V_{Rd,2} = 2 * V_{Rd,1} = 10660kN$$

The maximum vertical shear force at t=0 is: See Figure 38

$$V_{Ed,dl0} = 3567kN$$

Unity check

The unity check for shear in the webs at t=0 is:

$$V_{Ed,dl0} / V_{Rd,2} = 0.33 \leq 1.0 \rightarrow Ok$$

The maximum vertical shear force at t=∞ is: See Figure 39

$$V_{Ed,s\infty} = 2691kN$$

The extra shear force due to torsion in the webs is:

$$V_{Ed+w} = T_{ed} / z_{webs} = 475kN$$

Unity checks

The unity check for shear in the webs at t=∞ is:

$$V_{Ed,s\infty} / V_{Rd,2} = 0.25 \leq 1.0 \rightarrow Ok$$

The unity check for shear + torsion in the webs at t=∞ is:

$$V_{Ed,s\infty} / V_{Rd,2} + V_{ed+w} / V_{Rd,1} = 0.34 \leq 1.0 \rightarrow Ok$$

The webs satisfy with respect to shear and torsion. The shear and torsion resistance is much more than what is required and friction of the remaining parts of the shear keys and flanges is not even taken along. It is thus possible to have less shear keys in the webs. When this verification is not satisfied, the depth of the webs H_{box} should be increased to place more shear keys in the webs. Also increasing the web thickness is an option. For this design this is however not necessary as the verification is easily satisfied.

For the calculation of the shear strength of the webs and shear forces in the webs reference is made to Appendix C.7.1.

6.7.2 Shear + torsion in flanges

The flanges have to resist the horizontal shear and torsion. As it concerns a segmental box girder the joints between the segments consists of shear keys see, Figure 37. These shear keys are normative over a cross-section of a segment with respect to shear and torsion of the box girder. The top and bottom flange both have 3 shear keys with a thickness which is the same as the flange thickness, see Figure 37.

The horizontal shear strength of the top flange is:
$$V_{Rd,tf} = f_{cd} * L_{shear} * \cos\alpha_s * t_{tf} * n_{s,tf} = 1542kN$$

The horizontal shear strength of the bottom flange is:
$$V_{Rd,bf} = f_{cd} * L_{shear} * \cos\alpha_s * t_{bf} * n_{s,bf} = 1114kN$$

The horizontal shear force in the top flange at t=∞ is:
$$V_{Ed,tf\infty} = q_{wind} * L/2 * (H_{wind} + H_{usr} + H/2) + Q_{sidew} = 232kN$$

The horizontal shear force in the bottom flange at t=∞ is:
$$V_{Ed,bf\infty} = q_{wind} * L/2 * H/2 = 46kN$$

The extra shear force in the flanges due to torsion is:
$$V_{Ed+f} = T_{ed} / z_f = 919kN$$

Unity checks

Top flange
The unity check for shear in the top flange at t=∞ is:
$$\boxed{V_{Ed,tf\infty} / V_{Rd,tf} = 0.15 \leq 1.0 \rightarrow Ok}$$

The unity check for shear + torsion in the top flange at t=∞ is:
$$\boxed{V_{Ed,tf\infty} / V_{Rd,tf} + V_{Ed+f} / V_{Rd,tf} = 0,75 \leq 1.0 \rightarrow Ok}$$

Bottom flange
The unity check for shear in the bottom flange at t=∞ is:
$$\boxed{V_{Ed,bf\infty} / V_{Rd,bf} = 0.04 \leq 1.0 \rightarrow Ok}$$

The unity check for shear + torsion in the bottom flange at t=∞ is:
$$\boxed{V_{Ed,bf\infty} / V_{Rd,bf} + V_{Ed+f} / V_{Rd,bf} = 0,87 \leq 1.0 \rightarrow Ok}$$

The flanges satisfy with respect to shear and torsion. The shear and torsion resistance is not much more than what is required. Friction of the remaining parts of the shear keys and flanges is however not even taken along. When this verification is not satisfied, more shear keys should be placed in the flanges. As the flanges offer enough space for additional shear keys this verification will never be normative for the design and will easily satisfy.

For the calculation of the shear strength of the flanges and shear forces in the flanges reference is made to Appendix C.7.2.

6.8 Ultimate resistance moment

6.8.1 General

For this calculation there is made use of the stress-strain relation for UHPC according the strain softening law, see Figure 40.

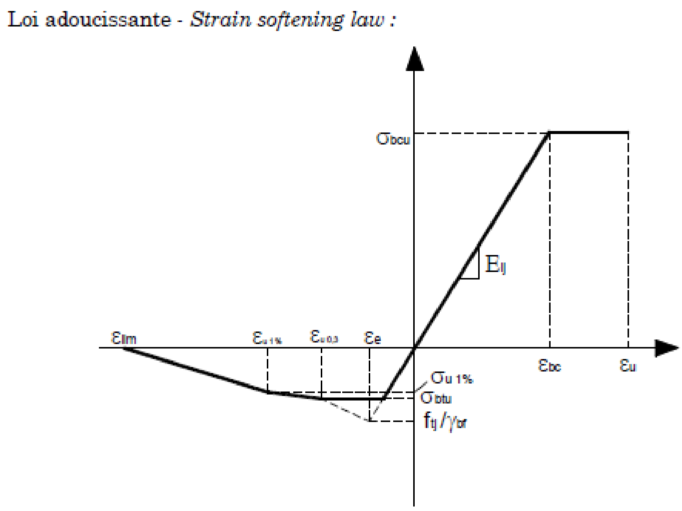

Figure 40: Stress-strain relation for UHPC [18]

Where:

$\varepsilon_{c3} = \varepsilon_{bc} = 1.632‰$	Is the maximum elastic compressive strain in the UHPC
$\varepsilon_{cu3} = \varepsilon_{u} = 3.0‰$	Is the ultimate compressive strain in the UHPC
$\sigma_{bcu} = f_{cd,uls} = 81.6 N/mm^2$	Is the design value of UHPC compressive strength, ULS

6.8.2 Ultimate resistance moment at t=0

Hogging moment at the deviation blocks is:

$$M_{da,0} = \gamma_{P,unfav} * P_{u0} * a - \frac{1}{2} * \gamma_{G,fav} * g_{dead} * L * a - 0.5 * \gamma_{G,fav} * g_{dead} * a^2 = 50605 kNm (\frown)$$

$M_{da,0} = 50605 kNm(\frown)$ means that the maximum compressive strain arises in the bottom flange.

The maximum strain in the cross-section which causes equilibrium between N_c and P_0 is:

$\varepsilon_{c\max} = 1.046‰$

This means that the compressive strain in the concrete is in the linear-elastic phase.

The ultimate resistance moment of the box girder at t=0 is:

$$M_u = N_{ctf} * z_{tf} + N_{cw} * z_w + N_{cbf} * z_{bf} = 51654 kNm$$

Unity check ultimate resistance moment:

$$M_{da,0} / M_u = 0.98 \leq 1.0 \rightarrow Ok$$

The ultimate resistance moment of the box girder is thus enough to resist the bending moments in the construction phase at t=0. The unity check however approaches the limit 1.0, so this verification needs attention. When this verification is not satisfied the depth of the webs H_{box} should be decreased, see Figure 34. This way the upward prestressing force becomes smaller, see Figure 36, and thus the hogging moment due to prestressing decreases. Another option is to make the box girder heavier such that the hogging moment M_d becomes smaller.

For the calculation of the ultimate resistance moment of the box girder at t=0 reference is made to Appendix C.8.3.

6.8.3 Ultimate resistance moment at t=∞

Sagging moment at mid-span is:

$$M_{dm,\infty} = \frac{1}{8} * (\gamma_{G,unfav} * g_{dead} + \gamma_{G,unfav} * g_{perm} + \gamma_{Q,unfav} * q_{\text{var}}) * L^2 - \gamma_{P,fav} * P_{u\infty} * a$$
$$= 16304 kNm (\cup)$$

$M_{dm,\infty} = 16304 kNm (\cup)$ means that the maximum compressive strain arises in the top flange.

The maximum strain in the cross-section which causes equilibrium between N_c and P_∞ is:

$\varepsilon_{c\max} = 0.391‰$

This means that the compressive strain in the concrete is in the linear-elastic phase.

The ultimate resistance moment of the box girder at t=∞ is:

$$M_u = N_{ctf} * z_{tf} + N_{cw} * z_w + N_{cbf} * z_{bf} = 19304 kNm$$

Unity check ultimate resistance moment:

$$M_{dm,\infty} / M_u = 0.84 \leq 1.0 \rightarrow Ok$$

The ultimate resistance moment of the box girder is thus enough to resist the bending moments in the end phase at t=∞. The unity check however approaches the limit 1.0, so this verification needs attention. When this verification is not satisfied the depth of the webs H_{box} should be increased, see Figure 34. This way the lever arms z become larger which has a positive effect on the ultimate resistance moment. Also the upward prestressing force then becomes larger, see Figure 36. The bending moment M_d should be kept as small as possible by having a light as possible box girder.

For the calculation of the ultimate resistance moment of the box girder at t=∞ reference is made to Appendix C.8.4.

6.9 Deck

6.9.1 Shear resistance

The maximum total shear force in the deck is:

$$V_{Ed} = V_{Ed,perm+\text{var}} + V_{Ed,dead} = 130.56 kN$$

The maximum total bending moment in the deck is:

$$M_d = M_{d,dead} + M_{d,perm+\text{var}} = 125.83 kNm$$

The total shear strength of the UHPC deck is:

$$V_{Rd} = V_{Rd,c} + V_{Rd,s} + V_{Rd,f} = 733.30 kN$$

Where:

$$V_{Rd,c} = \frac{1}{\gamma_E} * \frac{0.24}{\gamma_b} * \sqrt{f_{ck}} * b_{deck} * z = 278.20kN$$

Shear strength due to participation of the concrete

$$V_{Rd,s} = 0.9 * d * \frac{A_{sw}}{s} * f_{yd} * (\sin\alpha + \cos\alpha) = 0kN$$

Shear strength due to participation of the stirrup reinforcement. As there are no stirrups in the deck this does not contribute to the shear strength of the deck.

$$V_{Rd,f} = \frac{S * \sigma_p}{\gamma_{bf} * \tan\theta} = 455.10kN$$

Shear strength due to participation of the fibres

Unity check for shear in the deck near the webs is:

$$\boxed{V_{Ed} / V_{Rd} = 0.18 \leq 1.0 \rightarrow Ok}$$

Furthermore, in case of concrete cracked in shear the shear stress in the deck should always satisfy the condition:

$$\tau_u \leq 1.14 \frac{0.85}{\gamma_E * \gamma_c} f_{ck}^{\,2/3} \sin(2\theta)$$

Filling in the formula gives:

$$V_{Ed} = 130.56 \leq 1.14 \frac{0.85}{\gamma_E * \gamma_c} f_{ck}^{\,2/3} \sin(2\theta) * b_{deck} * d = 2966kN \rightarrow Ok$$

Without stirrup reinforcement the deck easily satisfies with respect to local shear.

For the calculation of the shear force and shear strength of the deck reference is made to Appendix C.9.2.

6.9.2 Ultimate resistance moment

The ultimate resistance moment of the deck is calculated according to the schematisation in Figure 41. In this case however the schematisation should be mirrored along the centre line as the tension arises at the top side and the compression zone is at the bottom side of the deck, see Figure 42.

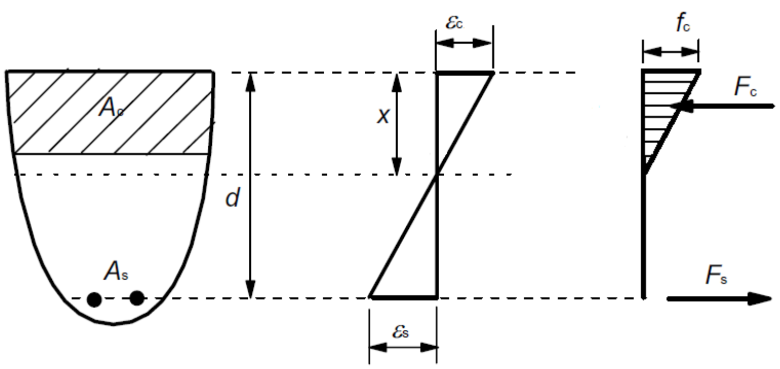

Figure 41: Rectangular stress distribution

The longitudinal reinforcement in the deck near the webs as is shown in Figure 42 to resist the bending moment consists of bars with a diameter of $\phi_{reinf} = 16mm$ and a spacing of $S_{reinf} = 80mm$.

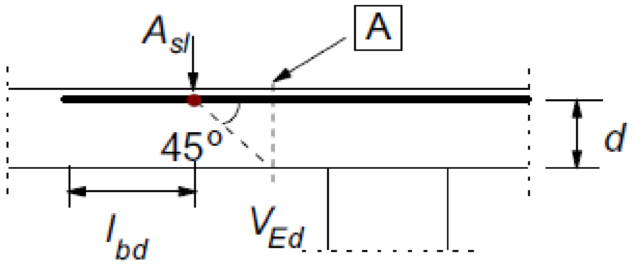

Figure 42: Definition of A_{sl}

The two horizontal forces F_c and F_s should be in equilibrium:

$$F_c - F_s = 0$$

This can be written as:

$$0.5 * x * b_{deck} * \frac{\varepsilon_c}{\varepsilon_{c3}} * f_{cd} - \varepsilon_s * E_s * A_{sl} = 0$$

Where:

$$x = \frac{\varepsilon_c}{\varepsilon_{tot}} * t_{tf}$$

The tensile strain in the reinforcement is the stain at the end of the linear elastic phase of steel:

$$\varepsilon_s = \frac{f_{yd}}{E_s} = 2.174‰$$

Solving the formula gives the compressive strain in the concrete:

$$F_c - F_s = 0 \rightarrow \varepsilon_c = 0.84‰$$

The concrete compressive zone is:

$$x = \frac{\varepsilon_c}{\varepsilon_{tot}} * t_{tf} = 50.1mm$$

The ultimate resistance moment of the deck is:

$$\boxed{M_u = \varepsilon_s * E_s * A_{sl} * (d - \frac{1}{3}x) = 133.55kNm}$$

Unity check for the ultimate resistance moment of the deck is:

$$\boxed{M_d / M_u = 0.94 \leq 1.0 \rightarrow Ok}$$

The ultimate resistance moment of the deck is thus just enough to resist the bending moments. If this verification is not satisfied the lever arm between the two forces F_c and F_s should be increased. This means that the deck becomes thicker. Another option is to add more reinforcement bars. This however has a strong influence on the rotation capacity, see hereunder.

The cracking moment is:

$$M_r = f_{ctm,fl} * \frac{1}{6} * b_{deck} * t_{tf}^2 = 162kNm$$

Because $M_r \geq M_u$ brittle failure can occur. Due to the fibres the flexural tensile strength of this material is much larger than for conventional concrete. The ultimate resisting moment M_u should therefore be larger than the bending moment M_d at all times as brittle failure caused by failure of the reinforcement should be excluded.

Rotation capacity
The height of the compression zone may not become too large as this limits the rotation capacity of the deck.
The verification of the rotation capacity of the deck is:

$$\boxed{x / d = 0.3478 \leq 0.35 \rightarrow Ok}$$

This verification considers the rotation capacity of the deck at the supports (the webs). It shows that the verification is satisfied but is very close to the limit so attention is needed. If this verification is not satisfied the thickness of the deck should be increased. Another option is to diminish the number of reinforcement bars which will result in a smaller compressive zone x. This will however also reduce the ultimate resistance moment.

For the calculation of the ultimate resistance moment and cracking moment of the deck reference is made to Appendix C.9.2.

6.10 Fatigue + vibration

6.10.1 Fatigue prestressing steel

The fatigue verification for prestressing steel is:

$$\boxed{\gamma_{F,fat} * \Delta\sigma_{S,equ}(N*) \leq \frac{\Delta\sigma_{Rsk}(N*)}{\gamma_{s,fat}} \rightarrow \frac{\gamma_{F,fat} * \Delta\sigma_{S,equ}(N*) * \gamma_{s,fat}}{\Delta\sigma_{Rsk}(N*)} = 0.167 \leq 1.0 \rightarrow Ok}$$

The fatigue verification for prestressing steel is easily satisfied and as the standard [12] (6.8.4) says: “Fatigue verification for external and unbonded tendons, lying within the depth of the concrete section, is not necessary” this could also be expected. This calculation with a rough estimation of the elongation of the tendons is however done to confirm the assumption. Fatigue of the prestressing tendons is not an issue for the design.

For the fatigue verification for prestressing steel reference is made to Appendix C.10.1.

6.10.2 Fatigue UHPC

The fatigue verification for concrete C50/60 is calculated according Equation NN.112 [12]:
For concrete C50/60 subjected to compression adequate fatigue resistance may be assumed if the following expression is satisfied:

$$14 * \frac{1 - E_{cd,\max,equ}}{\sqrt{1 - R_{equ}}} \geq 6$$

For UHPC there is no fatigue verification and the verification for concrete C50/60 given above cannot be used as the design fatigue strength of the UHPC then becomes:

$$f_{cd,fat} = k_1 \beta_{cc}(t_0) f_{cd,uls} \left(1 - \frac{f_{ck}}{250}\right) = 19.42 N / mm^2$$

Some stresses in the concrete at t=∞ are larger than this design fatigue strength. According this verification the stresses are thus too large and should be smaller in order to satisfy. But as UHPC contains steel fibres which makes the concrete more ductile it is expected that the design fatigue strength is much larger than the value calculated above. The maximum stress in the box girder at t=∞ is:

At deviation block, bottom side:

$$\sigma_{cb} = -\frac{P_\infty}{A_c} - \frac{M_{m,p\infty}}{W_b} + \frac{M_{a,\infty} - M_{s,v}}{W_b} = -24.77N/mm^2$$

The design value of UHPC compressive strength is:

$$f_{cd,uls} = 81.6N/mm^2$$

The maximum compressive stress is thus much smaller than the design compressive strength of UHPC. As the ductile UHPC contains steel fibres the design fatigue strength is assumed to be at least 30.0 N/mm^2. It is expected that the design fatigue strength is even more than this value. My assumption is that even half of the design value of the UHPC compressive strength is still a safe assumption:

$$f_{cd,fat} \approx \frac{1}{2} * f_{cd,uls} = 40.8N/mm^2$$

Considering the material UHPC with its fibres it is thus expected that the fatigue verification for UHPC is satisfied and will never become an issue for this design. This is however a very critical assumption for the design and should be validated in order to present this design as a good design.

For the fatigue verification of UHPC reference is made to Appendix C.10.2.

6.10.3 Vibration

Verification according Annex F [10]

The first natural bending frequency of the box girder is:

$$n_0 = \frac{C_{end}}{2\pi}\sqrt{\frac{E_{cm}I_c}{A_c\rho_c L^4}} = 3.21Hz$$

The velocity of the metros is:

$$v = 100km/h = 27.78m/s$$

The maximum value of the velocity divided by the first natural frequency is:

$$(v/n_0)_{\lim} = 10.0m$$

Verification of the ratio of the velocity over the first natural frequency is:

$$v/n_0 = 8.67m \le 10.0m \rightarrow Ok$$

Verification according to Figure 6.10 [10]

Limits of natural frequency n_0 (Hz) as a function of L (m)

The upper limit of natural frequency is governed by dynamic enhancements due to track irregularities and is given by:

$$n_{0\max} = 94.76 * L^{-0.748} = 5.5Hz$$

The lower limit of natural frequency is governed by dynamic impact criteria and is given by:

$$n_{0\min} = 23.58 * L^{-0.592} = 2.48Hz$$

The first natural frequency of the box girder is:

$$n_0 = \frac{C_{end}}{2\pi}\sqrt{\frac{E_{cm}I_c}{A_c\rho_c L^4}} = 3.21Hz \rightarrow Ok$$

Conclusion
Both verifications show that the box girder does not require a dynamic analysis and a static analysis is sufficient. As the first natural frequency of the girder easily stays within the limits, the box girder is well determined against the dynamic effects. The increasing and decreasing of static stresses and deformations under the effects of moving traffic should, considering the calculations, not give any problems for this box girder.

For the vibration verifications reference is made to Appendix C.10.3.

6.11 Buckling webs

Verification of buckling of the webs:
$b_w = 140mm \geq b_{w,req} = 132mm \rightarrow Ok$

The webs thus satisfy with respect to buckling. The thickness of the webs is however just enough to resist buckling. When this verification is not satisfied the thickness of the webs should be increased.

For the calculation of the minimum required width of the webs with respect to buckling reference is made to Appendix C.11.

6.12 Conclusions

The precast UHPC segmental box girder with six external prestressing tendons which is schematised in this chapter satisfies all the structural verifications. A critical verification for the design is the ultimate resistance moment of the box girder. This verification shows for the construction phase as well as the end phase a unity check which is close to the limit of 1.0. Another important verification for the design is the minimum required width of the webs with respect to buckling of the webs. The width of the webs is just enough to resist buckling and cannot be taken any smaller. The width of the webs also influences the vertical shear + torsion strength of the webs with its shear keys. The unity checks for shear + torsion in the webs are however easier satisfied and are not an issue for this design. The width of the webs for this design is thus determined by buckling and not by shear + torsion. Furthermore the verifications of the local effects on the deck are important. The ultimate resistance moment and rotation capacity of the deck are namely just enough to satisfy the verifications. The shear strength of the deck is much more than what is required. This is due to the participation of the steel fibres in the concrete.

Structural verifications which are of less importance for this design are the verifications of deflection, shear + torsion in the flanges, fatigue of the prestressing steel and vibration of the box girder. The reason that deflection is not problematic is due to the depth of the box girder and the relative thin webs creating a large moment of inertia of the box girder versus a small dead load. The flanges offer enough space to place extra shear keys when this is necessary and does not influences the design. Fatigue of the external prestressing tendons is also not of importance as the unity check showed that it easily satisfies and also the codes even say that this verification is not needed. The verification of vibration of the box girder showed that the box girder does not require a dynamic analysis and a static analysis is sufficient. The increasing and decreasing of static stresses and deformations under the effects of moving traffic should therefore not give any problems for this box girder. In this design it is also assumed that the fatigue of UHPC is not an issue for this design considering the ductile material UHPC with its fibres. This is however a very critical assumption for the design and should be validated in order to present this design as a good design.

Concluded can be that this slender design for a precast UHPC segmental box girder with external prestressing tendons is close to its limits. The important structural verifications for the design are:

- Ultimate resistance moment of the box girder
- Buckling of the webs
- Ultimate resistance moment of the deck
- Rotation capacity of the deck

7. Optimisation process UHPC box girder C180

7.1 General

The design of the UHPC segmental box girder with six external prestressing tendons, as described in the previous chapter, is the optimal design. This optimal design is, just as the optimal concrete box girder design, the result of an optimisation process. The goal of the optimisation process is to find the lightest box girder as this will result in the optimal structural design. To avoid repetition, reference is made to Chapter 5 for a more detailed description of the optimisation process. In this chapter only the specific characteristics and results of the optimisation process are described for an UHPC box girder.

The optimal design of an UHPC box girder is searched by changing six parameters:

- Thickness of the top flange t_{tf} , steps of 10 mm
- Thickness of the bottom flange t_{bf} , steps of 10 mm
- Width of the webs b_w , steps of 10 mm
- Depth of the webs H_{box} , steps of 150 mm (height of a shear key)
- Distance of the deviation blocks to the supports (a), steps of 1 m
- Number of prestressing tendons n

The optimisation process in this chapter is done for a box girder with 4, 6 and 8 tendons. In Section 7.6 it will be made clear why the application of more or less tendons is not interesting for the design. This chapter contains three sections in which the optimisation process for the design with respectively 6, 8 and 4 tendons is described. First however the minimum thickness of the deck / top flange is determined out of the local schematisation which holds for all the possible designs. The conclusions of the optimisation process are described in the last section.

7.2 Minimum deck thickness

In Section 6.9 the top flange / deck was verified for shear and ultimate resistance moment for the local schematisation. The calculation showed that a deck thickness of 180 mm and longitudinal reinforcement in the deck near the webs of bars with a diameter of $\phi_{reinf} = 16mm$ and a spacing of $S_{reinf} = 80mm$ was enough to resist the shear and bending moments. Shear was not normative for the minimum deck thickness. The ultimate resistance moment and the rotation capacity of the deck were however just enough to satisfy the verification. The verification of the rotation capacity for UHPC is: $x/d \leq 0.35$.

To find the minimum deck thickness, the ultimate resistance moment and the rotation capacity are calculated for a specific deck thickness and different spacings of the reinforcement bars. The chosen diameter of the reinforcement bars is $\phi_{reinf} = 16mm$. The results for a deck thickness of 180 mm and different spacings of the reinforcement bars are shown in Graph 15. The graph shows that the deck will satisfy when the spacing of the bars is exactly 80 mm. The horizontal parts in the graph are the result of rounding off the number of bars within one metre width of the deck.

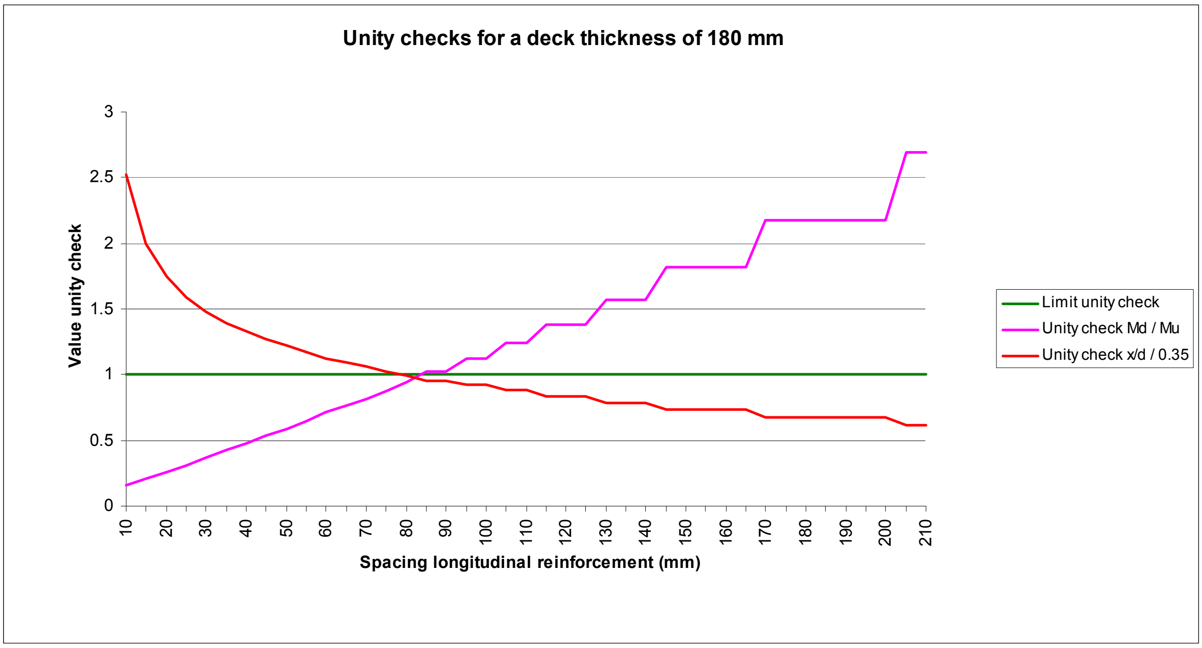

Graph 15: Unity checks for a deck thickness of 180 mm

To verify if the deck thickness can be taken smaller, the deck thickness is decreased with 10 mm to a thickness of 170 mm. The results of the calculations for a deck thickness of 170 mm are shown in Graph 16. The graph shows that this deck thickness is too thin as there are no results where both unity checks satisfy. The steps taken for the different spacings of the bars are 5 mm. The lines of the two checks cross each other at a spacing of 80 mm. Concluded can be that the minimum deck thickness is 180 mm with reinforcement bars $\phi_{reinf} = 16mm$ and a spacing of $S_{reinf} = 80mm$. Notice that this is exactly the same as what is chosen for the optimal design described in the previous chapter.

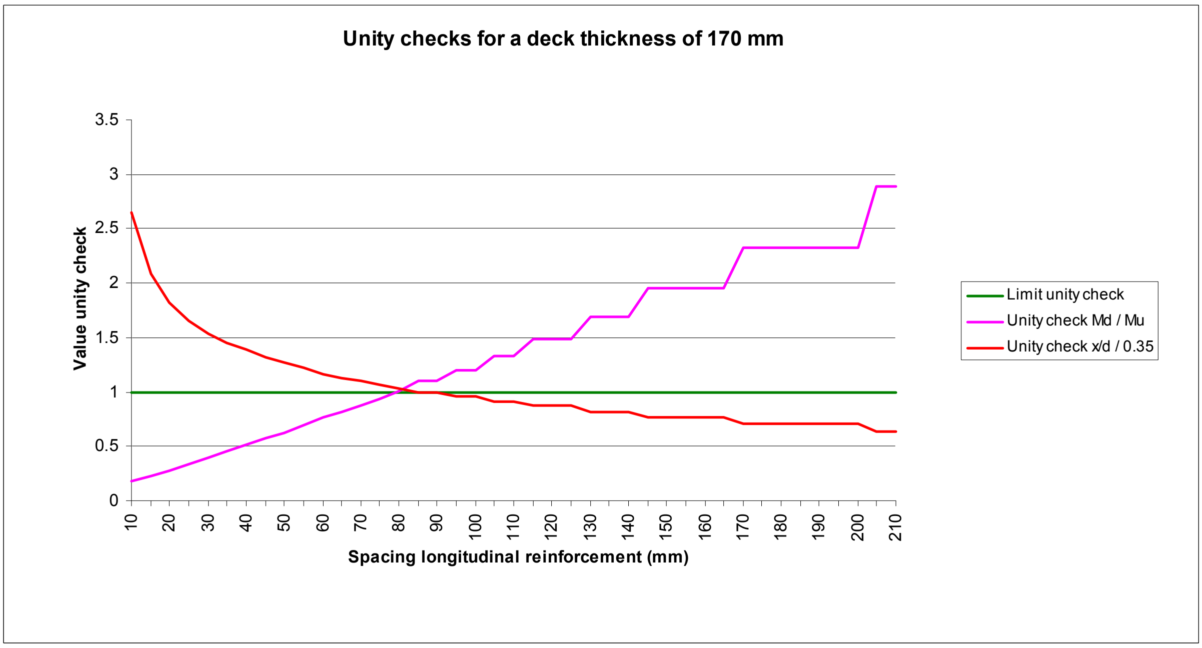

Graph 16: Unity checks for a deck thickness of 170 mm

7.3 Box girder with 6 prestressing tendons

The previous chapter, where the precast UHPC segmental box girder with six external prestressing tendons was described, showed the important structural verifications for the design: the ultimate resistance moment and rotation capacity of the deck, buckling of the webs and the ultimate resistance moment of the box girder. For a box girder with 6 tendons the minimum dead load of the girder is determined for different depths of the webs (H_{box}). The depth of the webs is changed in steps of 150 mm (height of a shear key). The result of this iterative optimisation process is shown in Table 11. Table 11 shows in each column the optimal design for a certain depth of the webs and the normative structural verifications. For the results of all the structural verifications of the different designs reference is made to Appendix D.2.1.

In Table 11 nine designs are shown. Notice that only eight designs are feasible as design 1 does not satisfy the verification of ultimate resistance moment at t=∞, see the red cell. The green cells represent the normative verification to which the bottom flange has to be adjusted and the pink cells represent the normative verification to which the width of the webs has to be adjusted. Design 2, which is the same as the design in Chapter 6, is the design with the smallest dead load and has also the smallest depth of the box girder. This is thus the optimal design for a box girder with 6 tendons.

The normative verification for design 2 is the ultimate resistance moment of the box girder at t=0. To satisfy this verification there are three options: change the thickness of the top flange, change the width of the webs and change the thickness of the bottom flange. Graph 18, Graph 19 and Graph 20 show the impact on the ultimate resistance moment of the box girder at t=0 for changing respectively the thickness of the top flange, the width of the webs and the thickness of the bottom flange of design 2. Considering the graphs it is the best to increase the thickness of the bottom flange to satisfy the verification. This adds weight to the box girder and brings down the centroidal axis of the box girder which both results in a smaller hogging moment. Notice in Graph 19 the maximum value of the unity check at a width of the webs of 0.18 m. For a small width of the webs the line increases and for widths larger than 0.18 m the line decreases. This is because the ultimate resistance moment at t=0 decreases faster than the hogging moment for increasing the web widths up to a width of 0.18 m. When the web width of 0.18 m is passed the hogging moment decreases faster than the ultimate resistance moment at t=0. The compressive strain in the box girder is smaller than the maximum elastic compressive strain in the UHPC $(\varepsilon_{c3} = 1.632‰)$ for all the widths of the webs shown in Graph 19.

The lightest box girder thus arises when the minimum top flange thickness and the minimum width of the webs are chosen and the bottom flange thickness is just enough to satisfy the verification of the ultimate resistance moment at t=0. This can be seen for design 2, where the minimum top flange thickness is 0.18 m (see Section 7.2) and the minimum width of the webs is 0.14 m, which is determined by buckling of the webs (see pink cell in Table 11). A bottom flange thickness of 0.13 m is just enough to satisfy the verification of the ultimate resistance moment at t=0, see Graph 20. Notice that increasing the top flange thickness has the least effect on the verification of the ultimate resistance moment at t=0. Unless this adds more weight and thus results in a smaller hogging moment it also brings the centroidal axis of the box girder upwards which reduces the effect of adding weight.

Table 11 shows that for more slender box girders the unity check for additional deflection increases. For design 1 this verification even becomes normative over the ultimate resistance moment at t=0. This design is however not feasible as the required stiffness to satisfy the verification of additional deflection results in a too heavy box girder. Due to this the verification of the ultimate resistance moment at t=∞ is not satisfied anymore. Graph 24 shows the result of decreasing the depth of the webs on the verification of the ultimate resistance moment at t=∞ for design 2. The ultimate resistance moment of design 1 is too small to resist the sagging moment. The only option left to satisfy the verification of the ultimate resistance moment would be to decrease the dead load of the box girder. For design 1 this is however not possible as the box girder needs its minimum bottom flange thickness to satisfy the verification of additional deflection. Increasing the bottom flange thickness is the most effective way to satisfy the verification of additional deflection, see Graph 21, Graph 22 and Graph 23 (for design 2). By increasing the bottom flange thickness the centroidal axis is brought down so that the moment of inertia of the box girder (mainly influenced by the Huygens-Steiner theorem) increases.

The distance of the deviation blocks to the supports (a), is placed at the distance from the supports where the minimum shear force in the box girder arises for t=0 and for t=∞. In Graph 25 the influence of the distance of the deviation blocks to the supports on the vertical shear + torsion in the webs is shown for design 2. As the distance a only influences the shear force and not the shear resistance, Graph 25 shows that the box girder has the minimal shear force for a distance of the deviation blocks to the supports of 17 metres. Graph 25 shows for the vertical shear at t=∞ a line with two kinks which implicates the change of the normative section of the box girder with respect to the shear force, see Figure 39. For the vertical shear at t=0 the normative section of the box girder with respect to the shear force stays the same which results in a smooth line. Notice that the unity checks for vertical shear at t=0 and at t=∞ are close to each other for all the designs in Table 11. Due to the large design compressive strength of UHPC the verification of shear + torsion in the webs is never normative for the design. The required minimum width of the webs is therefore determined by buckling of the webs.

The placement of the deviation blocks farther away from the supports results in a smaller hogging moment at the deviation blocks in the ultimate limit state at t=0. This can be seen in Graph 26 (for design 2). For larger distances of the lever arm (a) of the upward prestressing force, the unity check for the ultimate resistance moment at t=0 decreases. As this verification is normative for the bottom flange thickness, see Table 11, it is thus the best to place the deviation blocks in the middle of the span at 22.5 metres of the supports, see Graph 26. The maximum bending moment in the box girder in the ultimate limit state at t=∞ will then however not arise at mid-span but somewhere between the support and the middle of the span. The place where this maximum moment arises is variable when the cross-section of the box girder is changed. For simplification reason it is therefore chosen to place the deviation blocks at a distance to the supports where the minimum shear force arises, so that the maximum bending moment for the verification of the ultimate resistance moment at t=∞ always arises at mid-span.

The optimal design for a UHPC box girder with 6 tendons is thus design 2 from Table 11. This design is also the one that is described in Chapter 6. In Graph 17 the dead load is shown for the 8 feasible designs of Table 11. Notice that for the UHPC box girder it is assumed that the verification of fatigue of the UHPC is not normative for the design. This is however a very critical assumption which should be validated.

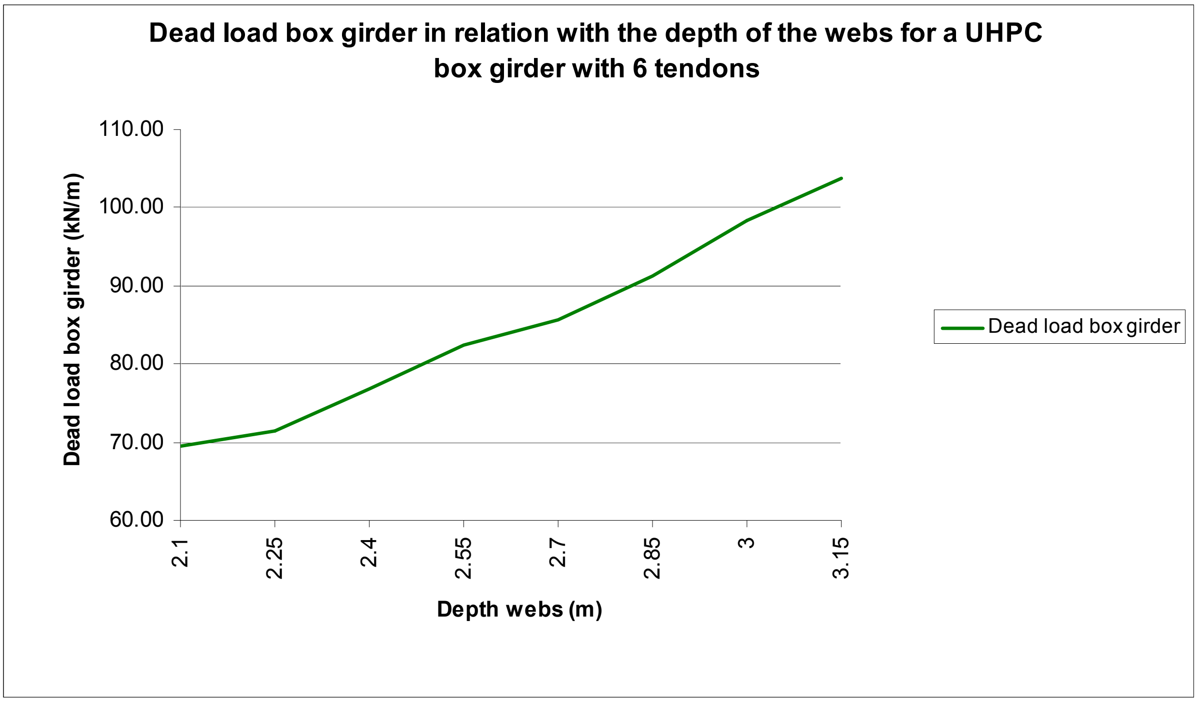

Graph 17: Dead load box girder in relation with the depth of the webs for a UHPC box girder with 6 tendons

										Unity
Design number	1	2	3	4	5	6	7	8	9	
Depth webs	1.95	2.1	2.25	2.4	2.55	2.7	2.85	3	3.15	m
Depth box girder	2.27	2.41	2.57	2.75	2.93	3.1	3.28	3.47	3.66	m
Thickness top flange	0.18	0.18	0.18	0.18	0.18	0.18	0.18	0.18	0.18	m
Width webs	0.13	0.14	0.14	0.15	0.16	0.16	0.17	0.18	0.18	m
Thickness bottom flange	0.14	0.13	0.14	0.17	0.2	0.22	0.25	0.29	0.33	m
Distance of deviation blocks to supports	15	17	18	18	18	19	19	19	19	m
Dead load box girder	68.35	69.40	71.49	76.84	82.35	85.62	91.36	98.27	103.73	kN/m
Ultimate resistance moment at t=0, bottom side	0.927842	0.979699	0.998876	0.991904	0.990612	0.996762	0.999957	0.995606	0.991634	Unity check
Ultimate resistance moment at t=∞, top side	1.055392	0.844592	0.655365	0.570374	0.510473	0.426843	0.396686	0.3872	0.362394	Unity check
Additional deflection under mobile load	0.974998	0.87138	0.726141	0.564627	0.451973	0.381982	0.316943	0.26176	0.221111	Unity check
Vertical shear in the webs at t=0	0.388812	0.334594	0.319957	0.287651	0.260832	0.247937	0.226988	0.20736	0.201948	Unity check
Vertical shear + torsion in the webs at t=∞	0.38733	0.341614	0.320151	0.285129	0.256475	0.249339	0.227391	0.21142	0.205854	Unity check
First natural bending frequency n0	3.053051	3.205052	3.459239	3.783739	4.085171	4.358157	4.631756	4.914137	5.204224	Hz
Minimum required width of the webs (buckling)	125.0441	131.5375	137.3142	144.0739	150.914	157.0092	163.6383	171.0248	177.6947	mm

Table 11: Optimal designs of the UHPC box girder for different depths of the webs and 6 prestressing tendons

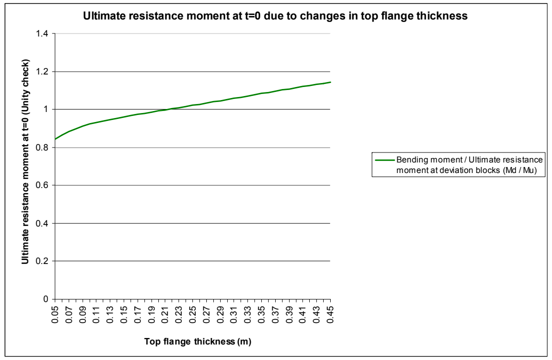

Graph 18

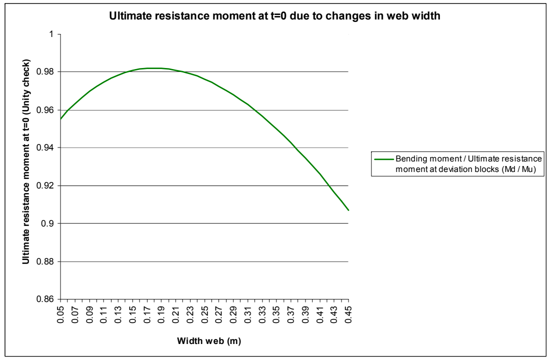

Graph 19

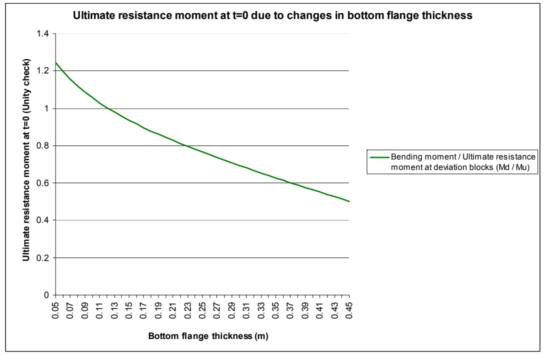

Graph 20

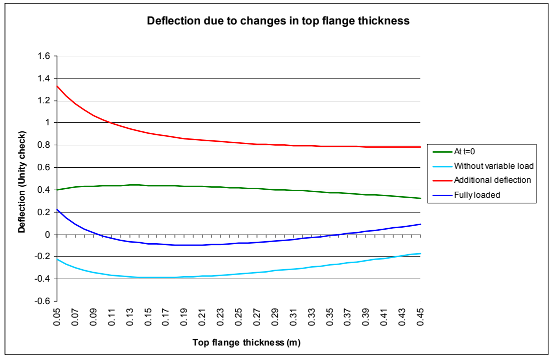

Graph 21

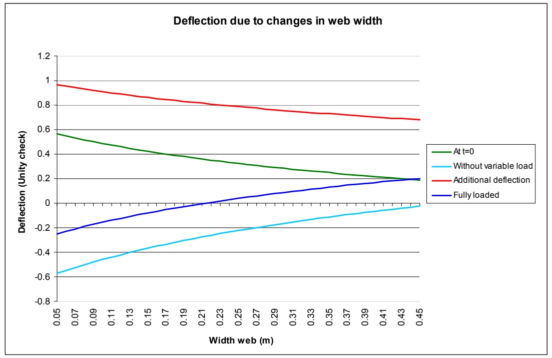

Graph 22

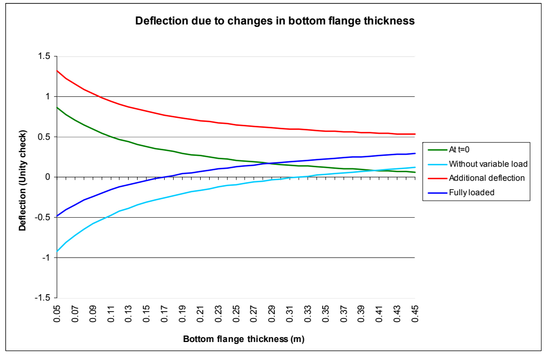

Graph 23

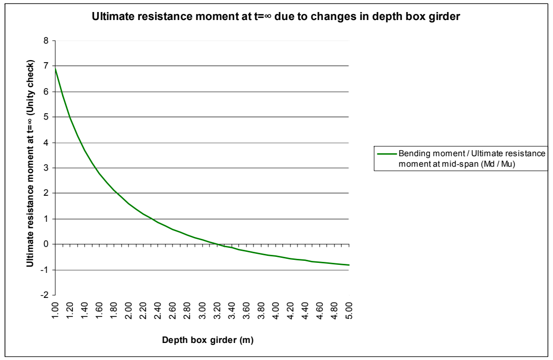

Graph 24

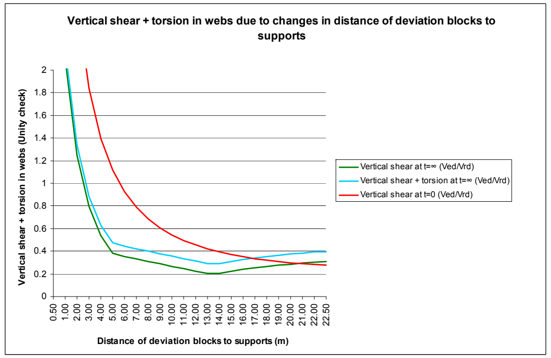

Graph 25

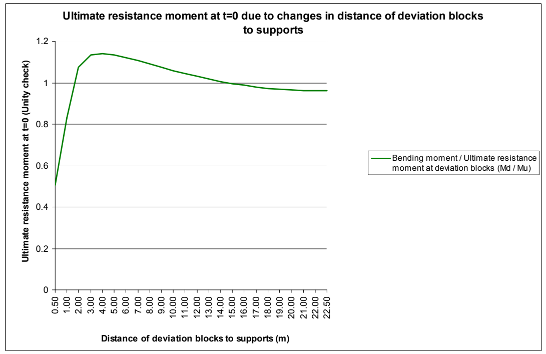

Graph 26

7.4 Box girder with 8 prestressing tendons

For a box girder with 8 tendons the minimum dead load of the box girder for different depths of the webs (H_{box}) is shown in Table 12. The depth of the webs is changed in steps of 150 mm (height of a shear key). Table 12 shows in each column the optimal design for a certain depth of the webs and the normative structural verification. For the results of all the structural verifications of the different designs reference is made to Appendix D.2.2.

In Table 12 nine designs are shown. Notice that only eight designs are feasible as design 1 does not satisfy the verification of the ultimate resistance moment at t=∞, see the red cell. The green cells represent the normative verification to which the bottom flange has to be adjusted and the pink cells represent the normative verification to which the width of the webs has to be adjusted. Design 4 is the design with the smallest dead load. This is thus the optimal design for a box girder with 8 tendons. Notice that this design not results in the most slender box girder.

The difference with a box girder with 6 tendons is the smaller depth of the designs; compare Table 11 with Table 12. Due to the larger prestressing force the verification of the ultimate resistance moment at t=∞ is easier satisfied. It is therefore possible to decrease the depth of the webs. For design 4 the verification of additional deflection is normative. This was not the case for the optimal design of a box girder with 6 tendons. The best way to satisfy this verification is to increase the thickness of the bottom flange, see Section 7.3. The lightest box girder thus arises when the minimum top flange thickness and the minimum width of the webs are chosen and the bottom flange thickness is just enough to satisfy the verification of additional deflection. This can be seen for design 4, where the minimum top flange thickness is 0.18 m (see Section 7.2) and the minimum width of the webs is 0.13 m, which is determined by buckling of the webs (see pink cell in Table 12). Table 12 shows that for designs with a larger depth the unity check for the ultimate resistance moment at t=0 increases. For design 5 the verification of the ultimate resistance moment at t=0 even becomes normative instead of additional deflection. Notice that the change of normative verification arises between a depth of the webs of 1.95 and 2.1 metres. This is also the case for a box girder with 6 tendons, see Table 11.

The optimal design for a UHPC box girder with 8 tendons is thus design 4 from Table 12. In Graph 27 the dead load is shown for the 8 feasible designs of Table 12. Notice the optimal depth of the webs of 1.95 m which results in the lightest box girder. This optimum is set by the verifications of the additional deflection. Design 4 results in a smaller dead load and depth of the railway girder than the optimal design of a box girder with 6 prestressing tendons. This is due to the larger prestressing force so that the verification of the ultimate resistance moment at t=∞ is easier satisfied. In fact design 4 is thus the optimal design for an UHPC box girder. However, in Chapter 6 the optimal design of a box girder with 6 tendons is presented as the optimal design for an UHPC box girder. This is chosen as the benefit of a UHPC box girder with 8 tendons is small (dead load: 68.35 vs. 69.4 kN/m; depth box girder: 2.27 vs. 2.41 m). The application of two extra tendons will increase the costs considerably. Besides, the dead load of the tendons and anchorage blocks is not included in the dead load of the box girder. Due to the larger prestressing force (8 instead of 6 tendons) the distance of the deviation blocks to the supports is large. The placement of the deviation blocks farther away from the supports results in a smaller hogging moment. Notice the large difference between the unity checks of the ultimate resistance moment at t=0 and at t=∞. This implies that the prestressing tendons are not used very efficiently as only at t=0 the unity check is near the limit. For the optimal design of a box girder with 6 tendons holds that the tendons are used far more efficient. Notice the small difference between the unity checks of the ultimate resistance moment at t=0 and at t=∞ for design 2 in Table 11. Considering all this, design 2 of the optimisation process with 6 prestressing tendons is presented in Chapter 6 as the optimal design.

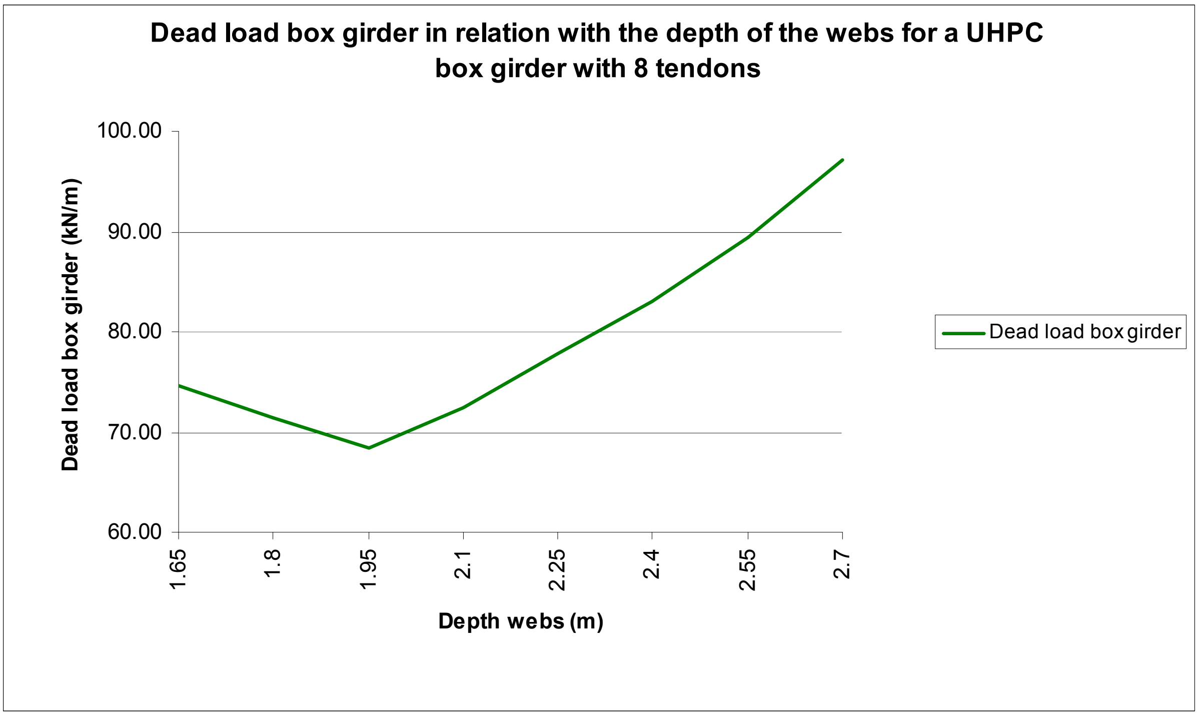

Graph 27: Dead load box girder in relation with the depth of the webs for a UHPC box girder with 8 tendons

										Unity
Design number	1	2	3	4	5	6	7	8	9	
Depth webs	1.5	1.65	1.8	1.95	2.1	2.25	2.4	2.55	2.7	m
Depth box girder	1.97	2.06	2.16	2.27	2.44	2.62	2.81	3	3.2	m
Thickness top flange	0.18	0.18	0.18	0.18	0.18	0.18	0.18	0.18	0.18	m
Width webs	0.11	0.12	0.13	0.13	0.14	0.15	0.15	0.16	0.17	m
Thickness bottom flange	0.29	0.23	0.18	0.14	0.16	0.19	0.23	0.27	0.32	m
Distance of deviation blocks to supports	11	14	18	22	22.5	22.5	22.5	22.5	22.5	m
Dead load box girder	79.14	74.70	71.44	68.35	72.46	77.74	82.97	89.50	97.20	kN/m
Ultimate resistance moment at t=0, bottom side	0.716334	0.789971	0.875696	0.978491	0.994855	0.999365	0.993497	0.996567	0.995821	Unity check
Ultimate resistance moment at t=∞, top side	1.042509	0.810971	0.570799	0.287966	0.19058	0.14499	0.116281	0.109413	0.11827	Unity check
Additional deflection under mobile load	0.983757	0.972339	0.969571	0.974998	0.769344	0.600788	0.47205	0.379063	0.305326	Unity check
Vertical shear in the webs at t=0	0.6286	0.516942	0.42731	0.401278	0.36	0.325917	0.315377	0.286404	0.260492	Unity check
Vertical shear + torsion in the webs at t=∞	0.640053	0.512597	0.446094	0.411905	0.356763	0.313982	0.298652	0.27083	0.250447	Unity check
First natural bending frequency n0	2.824662	2.924377	2.994721	3.053051	3.338155	3.646978	3.982579	4.279095	4.575062	Hz
Minimum required width of the webs (buckling)	109.6349	114.6823	121.5154	127.4723	133.7999	141.267	148.4801	155.6115	162.4677	mm

Table 12: Optimal designs of the UHPC box girder for different depths of the webs and 8 prestressing tendons

7.5 Box girder with 4 prestressing tendons

For a box girder with 4 tendons the minimum dead load of the box girder for different depths of the webs (H_{box}) is shown in Table 13. The depth of the webs is changed in steps of 150 mm (height of a shear key). Table 13 shows in each column the optimal design for a certain depth of the webs and the normative structural verification. For the result of all the structural verifications of the different designs reference is made to Appendix D.2.3.

In Table 13 nine designs are shown. Notice that only eight designs are feasible as design 1 does not satisfy the verification of the ultimate resistance moment at t=∞, see the red cell. The green cells represent the normative verification to which the bottom flange has to be adjusted and the pink cells represent the normative verification to which the width of the webs has to be adjusted. Design 2 is the design with the smallest dead load and depth of the box girder. This is thus the optimal design for a box girder with 4 tendons.

The difference with a box girder with 6 tendons is the much larger depth of the designs; compare Table 11 with Table 13. Due to the smaller prestressing force a larger depth of the webs is required in order to satisfy the verification of the ultimate resistance moment at t=∞. For design 2 the verification of the ultimate resistance moment at t=0 is normative. Due to the large angle α_t the upward prestressing force becomes very large. The hogging moment at t=0 is thus quite large, despite of the application of just 4 tendons. The best way to satisfy this verification is to increase the thickness of the bottom flange, see Section 7.3. The lightest box girder thus arises when the minimum top flange thickness and the minimum width of the webs are chosen and the bottom flange thickness is just enough to satisfy the verification of the ultimate resistance moment at t=0. This can be seen for design 2, where the minimum top flange thickness is 0.18 m (see Section 7.2) and the minimum width of the webs is 0.19 m, which is determined by buckling of the webs (see pink cell in Table 13).

The optimal design for a UHPC box girder with 4 tendons is thus design 2 from Table 13. In Graph 28 the dead load is shown for the 8 feasible designs of Table 13. The designs of the box girders with 4 prestressing tendons result in a much larger dead load than for box girders with 6 prestressing tendons. This is mainly due to the large webs of the box girder. Besides the larger dead load, the application of 4 tendons also results in an unacceptable large depth of the box girder. Concluded can be that a UHPC box girder with 4 tendons not outweighs the optimal design of a box girder with 6 prestressing tendons. Worth to notice is that for some designs the first natural frequency of the box girder exceeds the upper limit of 5.5 Hz, see Table 13. Due to the large stiffness of the box girder these designs require a dynamic analysis in order to verify if the box girder is well determined against the dynamic effects.

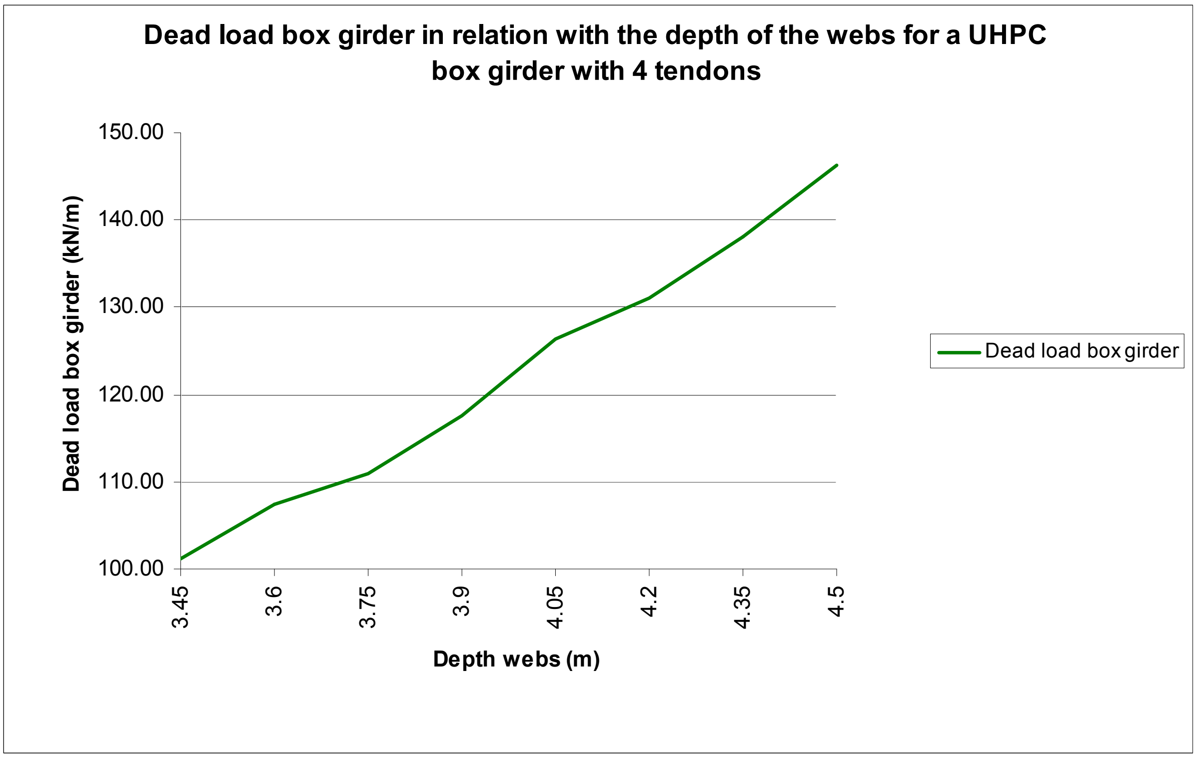

Graph 28: Dead load box girder in relation with the depth of the webs for a UHPC box girder with 4 tendons

										Unity
Design number	1	2	3	4	5	6	7	8	9	
Depth webs	3.3	3.45	3.6	3.75	3.9	4.05	4.2	4.35	4.5	m
Depth box girder	3.72	3.89	4.07	4.24	4.42	4.62	4.8	4.98	5.17	m
Thickness top flange	0.18	0.18	0.18	0.18	0.18	0.18	0.18	0.18	0.18	m
Width webs	0.18	0.19	0.2	0.2	0.21	0.22	0.22	0.23	0.24	m
Thickness bottom flange	0.24	0.26	0.29	0.31	0.34	0.39	0.42	0.45	0.49	m
Distance of deviation blocks to supports	14	14	14	14	14	13	13	13	13	m
Dead load box girder	95.92	101.10	107.45	111.02	117.60	126.38	131.12	138.08	146.22	kN/m
Ultimate resistance moment at t=0, bottom side	0.990987	0.997026	0.992394	0.998749	0.996191	0.99837	0.998272	0.999748	0.994324	Unity check
Ultimate resistance moment at t=∞, top side	1.033175	0.989082	0.962052	0.901965	0.888308	0.896784	0.86188	0.858377	0.864406	Unity check
Additional deflection under mobile load	0.239836	0.208523	0.17937	0.15947	0.13943	0.119512	0.106838	0.095402	0.084682	Unity check
Vertical shear in the webs at t=0	0.174642	0.162047	0.149475	0.147746	0.137172	0.133973	0.131775	0.123683	0.115699	Unity check
Vertical shear + torsion in the webs at t=∞	0.183255	0.169141	0.158948	0.153242	0.144842	0.132982	0.130214	0.123864	0.119304	Unity check
First natural bending frequency n0	5.196248	5.428181	5.677106	5.923294	6.154903	6.413093	6.658994	6.866847	7.082864	Hz
Minimum required width of the webs (buckling)	178.9074	185.1942	192.3364	197.7381	204.9531	210.4468	216.8954	223.2039	231.1623	mm

Table 13: Optimal designs of the UHPC box girder for different depths of the webs and 4 prestressing tendons

7.6 Conclusions

In the optimisation process it is concluded that the design of a precast UHPC segmental box girder with 6 prestressing tendons from Chapter 6 is the optimal design. However, the application of 6 tendons does not result in the lightest box girder. The optimal design of a box girder with 8 tendons results in a smaller dead load and depth of the railway girder than the optimal design of a box girder with 6 prestressing tendons. In fact design 4 for a box girder with 8 tendons is thus the optimal design for an UHPC box girder. However, in Chapter 6 the optimal design of a box girder with 6 tendons is presented as the optimal design for an UHPC box girder. This is chosen as the benefit of a UHPC box girder with 8 tendons is small (dead load: 68.35 vs. 69.4 kN/m; depth box girder: 2.27 vs. 2.41 m). The application of two extra tendons will increase the costs considerably. Besides, the dead load of the tendons and anchorage blocks is not included in the dead load of the box girder. Due to the larger prestressing force (8 instead of 6 tendons) the distance of the deviation blocks to the supports is large. The placement of the deviation blocks farther away from the supports results in a smaller hogging moment. Notice the large difference between the unity checks of the ultimate resistance moment at t=0 and at t=∞. This implies that the prestressing tendons are not used very efficiently as only at t=0 the unity check is near the limit. For the optimal design of a box girder with 6 tendons holds that the tendons are used far more efficient. Notice the small difference between the unity checks of the ultimate resistance moment at t=0 and at t=∞ for design 2 in Table 11. Considering all this, design 2 of the optimisation process with 6 prestressing tendons is presented in Chapter 6 as the optimal design.

The normative verification for the optimal design is the ultimate resistance moment at t=0. The best way to satisfy this verification is to increase the bottom flange thickness. This adds weight to the box girder and brings down the centroidal axis of the box girder which both results in a smaller hogging moment. The lightest box girder thus arises when the minimum top flange thickness and the minimum width of the webs are chosen and the bottom flange thickness is just enough to satisfy the verification of the ultimate resistance moment at t=0.

The application of 8 prestressing tendons results in a larger prestressing force. The verification of the ultimate resistance moment at t=∞ is hereby easier satisfied. For box girders with 8 prestressing tendons it is therefore possible to decrease the depth of the webs, resulting in a more slender design. The depth of the optimal design for a box girder with 8 tendons is even this small that the verification of additional deflection becomes normative instead of the ultimate resistance moment at t=0. Increasing the bottom flange thickness is the most effective way to satisfy the verification of additional deflection. By increasing the bottom flange thickness the centroidal axis is brought down so that the moment of inertia of the box girder (mainly influenced by the Huygens-Steiner theorem) increases. Graph 27 shows that in the end there is always an optimum depth of the webs which is set by the verification of the additional deflection. This verification is influenced by the moment of inertia of the box girder and not by the number of prestressing tendons. The designs of the box girders with 4 prestressing tendons result in a larger dead load than box girders with 6 prestressing tendons. This is mainly due to the large webs of the box girder in order to satisfy the verification of the ultimate resistance moment at t=∞. Besides the larger dead load, the application of 4 tendons results also in an unacceptable large depth of the box girder.

Due to the large design compressive strength of UHPC the verification of shear + torsion in the webs is never normative for the design. The required minimum width of the webs is therefore determined by buckling of the webs. The distance of the deviation blocks to the supports (a), is placed at the distance from the supports where the minimum shear force in the box girder arises for t=0 and for t=∞. Considering the optimisation process it can be concluded that the application of more than 8 or less than 4 tendons is not interesting for the design as the optimum is in the middle (6 tendons). The application of more tendons results in heavier box girders with inefficient use of the prestressing tendons. The application of 2 tendons will not even result in a feasible design as the verification of the ultimate resistance moment at t=∞ requires such a large depth of the webs so that the ultimate resistance moment at t=0 is not enough anymore. The optimal design for a precast UHPC segmental box girder is thus the one as presented in Chapter 6.

8. Fibre Reinforced Polymer sandwich girder

8.1 General

This chapter describes the design of the Fibre Reinforced Polymer sandwich girder and the method of calculation. For the extensive calculation of the sandwich girder reference is made to Appendix E: Calculations FRP. This design represents the global design for a FRP sandwich girder and is not optimal. As mentioned in the literature and preliminary study, there is a wide range of FRP producible and there is a lack of standards. In order to design an elevated metro railway made of FRP a thesis is used: "Onderzoek naar composietmaterialen in brugconstructies" [17]. This thesis provides information on FRP and also the InfraCore® concept is analysed. The InfraCore® concept is a combination of FRP and a sandwich construction and is invented by FiberCore Europe, see Figure 43 and Figure 44. From this concept an arithmetic method is derived to design FRP bridges as a sandwich construction. This arithmetic method is applicable at macro level. The micromechanics are not taken into consideration in this thesis [17], among other things because FiberCore Europe was not willing to give this information. This thesis should however give enough information to design an elevated railway made of FRP in general to determine the global dimensions and normative structural verifications. References to the specific codes and literature used for the design are also given in the Appendix.

Figure 43: An InfraCore® bridge [4]

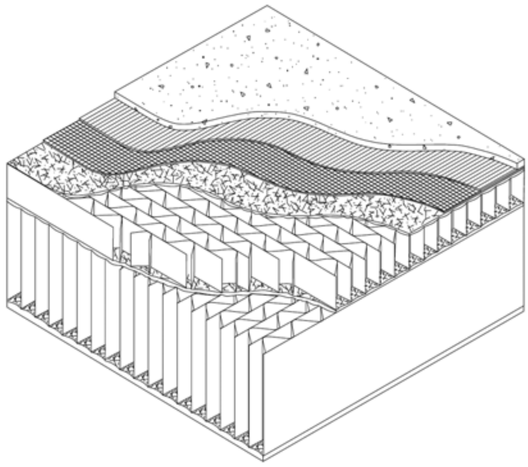

Figure 44: Cross-section of the InfraCore® concept [4]

8.2 Material characteristics

There is chosen for a carbon fibre epoxy laminate for the sandwich girder. A carbon fibre fabric offers the largest strength and stiffness for the girder compared with the other reinforcing fibres. Therefore it is the best reinforcing fibre to satisfy the verification of deflection which is considered as the normative verification for the sandwich girder. Carbon fibres are however far more expensive than glass fibres. As an elevated FRP railway girder with a span of 45 metres is already quite futuristic and most likely more expensive than a (UHP) concrete box girder, the costs are not considered as a criterion for the chosen FRP. Epoxy resins offer the best mechanical properties for FRP. The combination of these two materials results in the best FRP material for the railway girder from a structural point of view. The volume fraction of the carbon fibres is 55% (maximum fibre volume fraction for the production of woven fabrics [3]). For the material characteristics of the FRP reference is made to Appendix E.2. From now on in this design study carbon fibre epoxy laminate is meant with FRP.

8.3 Geometry sandwich girder

The cross-section of the FRP sandwich girder with the metros is shown in Figure 45. The sandwich girder consists of two thicker outer skins and five intermediate thin skins in order to limit the buckling length of the core. The core is thus divided in six parts and is made of triangles filled with foam, see Figure 46 to Figure 49. The sandwich girder is a 45 metres long simply supported statically determinate girder. A longer continuous FRP sandwich girder is not an option as the fabrication and transportation of the girder then becomes even more difficult, see Section 8.11. Because the core depth-to-skins thickness ratio is large the FRP girder is considered as a thin skin sandwich girder [7].

The cross-section of a core triangle and the FRP sandwich girder are shown in respectively Figure 50 and Figure 51, where:

Length span	L	45	m
Width sandwich girder	B	9	m
Spacing outer skins	d	3	m
Thickness outer skins	$t_{skin,out}$	0.04	m
Thickness middle skins	$t_{skin,mid}$	0.01	m
Core depth	$t_{core} = d - 2 * \frac{1}{2} * t_{skin,out}$	2.96	m
Number of core parts	nr	6	
Buckling length core parts	$L_{core} = \frac{t_{core} - (nr - 1) * t_{skin,mid}}{nr}$	0.485	m
Sandwich depth	$H = d + 2 * \frac{1}{2} * t_{skin,out}$	3.04	m
Length core triangle	L_{tria}	200	mm
Width core triangle	B_{tria}	100	mm
Thickness core triangle	t_{tria}	4	mm

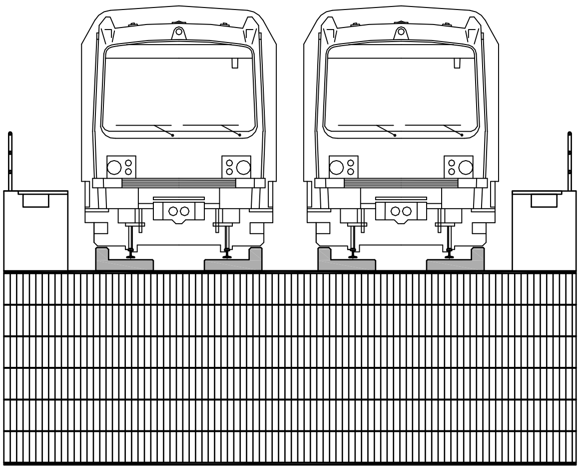

Figure 45: Cross-section of the superstructure

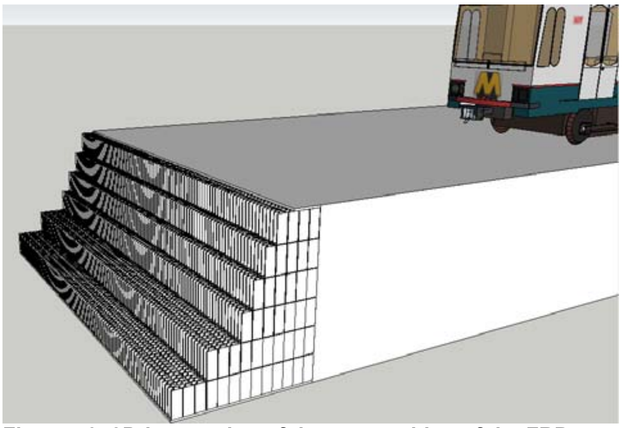

Figure 46: 3D-impression of the composition of the FRP sandwich girder

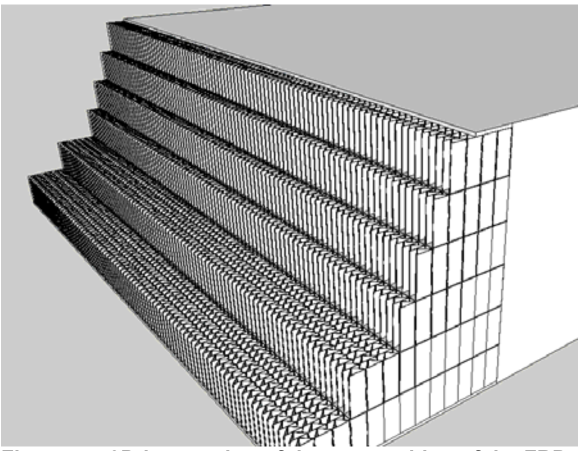

Figure 47: 3D-impression of the composition of the FRP sandwich girder

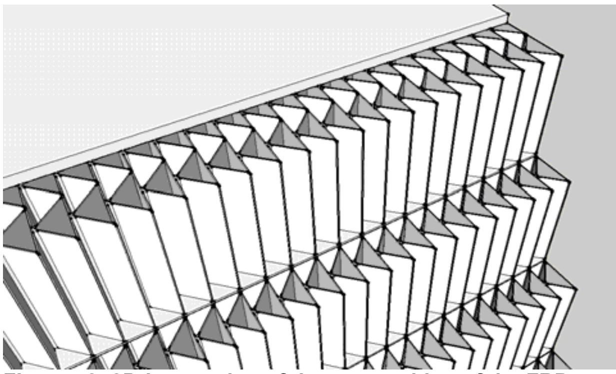

Figure 48: 3D-impression of the composition of the FRP sandwich girder

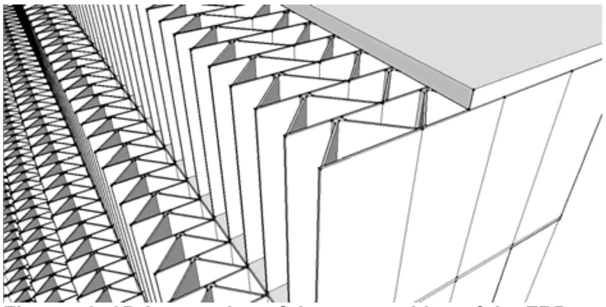

Figure 49: 3D-impression of the composition of the FRP sandwich girder (without foam)

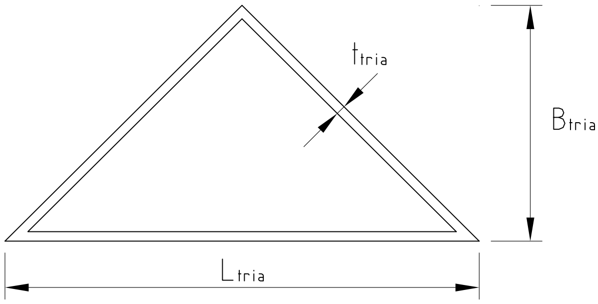

Figure 50: Cross-section of a core triangle

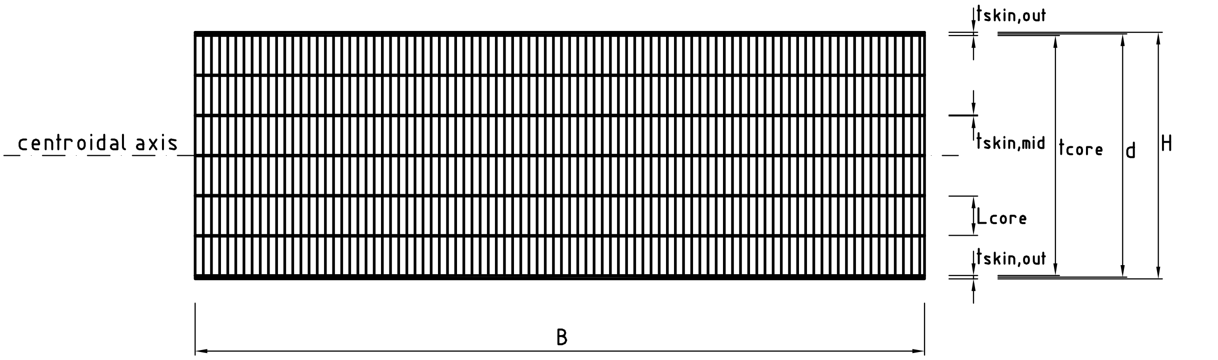

Figure 51: Cross-section of the sandwich girder

The laminate of the skins and core triangles is quasi-isotropic[2] by the orientation of the fibres in 4 directions: 0°, 45°, -45° and 90°. Every direction should have at least 15 % of the total fibre volume fraction [3]. This should exclude that fatigue, creep, impact and such is only taken by the epoxy resin. Besides it is meant to resist unexpected loads. With this condition it is possible to consider one yield value for every direction in-plane of the laminate. The remaining percentage of the total fibre volume fraction is placed in the direction where it has the largest contribution to the bending and shear stiffness:

Fibre layout in the skins:

Percentage of fibres in x-direction (0°) $v_{s0} = 55\%$

Percentage of fibres in y-direction (90°) $v_{s90} = 15\%$

Percentage of fibres in xy-direction (45°) $v_{s45} = 15\%$

Percentage of fibres in xy-direction (-45°) $v_{s-45} = 15\%$

Fibre layout in the core:

Percentage of fibres in x-direction (0°) $v_{c0} = 15\%$

Percentage of fibres in z-direction (90°) $v_{c90} = 15\%$

Percentage of fibres in xz-direction (45°) $v_{c45} = 35\%$

Percentage of fibres in xz-direction (-45°) $v_{c-45} = 35\%$

For the moment of inertia of the sandwich girder in z-direction (vertical) only the skins are taken into account. As the moment of inertia of the skins self is small, the calculation of the moment of inertia of the girder is only based on the Huygens-Steiner theorem:

Bending stiffness of the sandwich girder in x-direction (longitudinal direction of the railway girder):

$$E_x I_z = 1.966 * 10^{17}\ Nmm^2$$

[2] A quasi-isotropic laminate is a laminate that approximates isotropy by orientation of the fibres in several or more directions in-plane.

Because it concerns a thin skin sandwich girder the shear stiffness of the FRP girder is determined by only the core triangles (the skins have no fibres in z-direction):

The shear stiffness of the sandwich girder in x-direction:

$$GA_x = G_{xz} * n_{tw} * A_{1,tria,h} = 1204521813N$$

For the calculation of the cross-sectional properties reference is made to Appendix E.3.

8.4 Loads and partial factors

In Figure 52 the cross-section of the superstructure without the sandwich girder is shown.

The vertical loads in longitudinal direction of the sandwich girder are:

- Dead load of the FRP sandwich girder: $g_{dead} = 34.48kN/m$
- Permanent load of the permanent construction shown in Figure 52: $g_{perm} = 34.42kN/m$
- Variable load of the metros and snow loading: $q_{var} = 58.29kN/m$

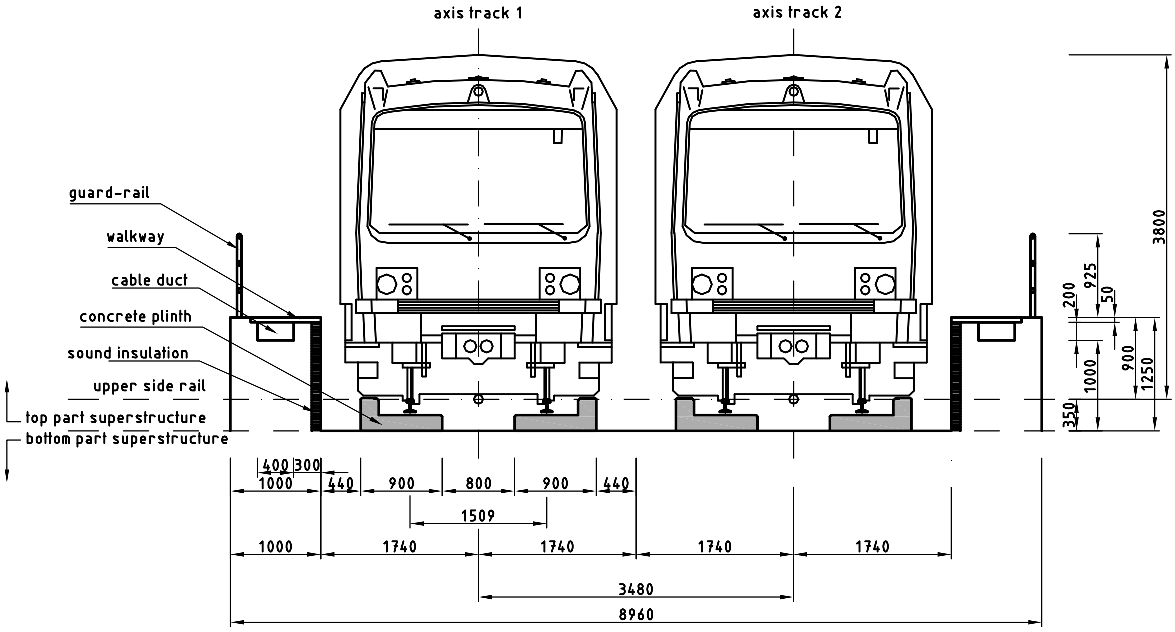

Figure 52: Cross-section top part superstructure without the sandwich girder

The dynamic loading of the metro is taken into account by multiplying the vertical metro load with a dynamic factor: $\phi = 1 + 4/(10 + L) = 1.07$.

The sandwich girder has to satisfy:

$$S * \gamma_f \leq R/(\gamma_m * \gamma_c)$$

Where:

S	Is the effect of the representative load
R	Is the representative load carrying capacity and/or strength of the structure
γ_f	Is a load factor
γ_m	Is a material factor
γ_c	Is a conversion factor

The material and conversion factors are from: "CUR-Aanbeveling 96, Vezelversterkte kunststoffen in civieltechnische draagconstructies" [3]. This CUR-recommendation can be used for designing civil structures made of glass fibre reinforced polymers. This code is also mainly used in the thesis on the InfraCore® concept [17]. In this design study as well as in the used thesis [17] it concerns a carbon fibre reinforced polymer sandwich girder. Because there is no code for carbon fibre reinforced polymer civil structures it is however chosen to take into account this CUR-recommendation. Notice the large conversion factors for some situations which sometimes even halve the strength of the structure (see Table 25 in Appendix E.4.1).

For the exact calculation of the loads in the serviceability and ultimate limit state and the partial factors per situation reference is made to Appendix E.4.

8.5 Deflection

The deflection for a simply supported FRP girder is calculated with the following formula:

$$w = \frac{5}{384} \frac{qL^4}{E_x I_z /(\gamma_m * \gamma_c)} + \frac{\eta * q * L}{8 * GA_x /(\gamma_m * \gamma_c)}$$

The deflections at mid-span and unity checks for different phases are:

Time	*Load q*	*Deflection w*	*value*	*Maximum allowed deflection* $w_{\max}$	*Unity check* $w/w_{\max}$
At t=∞ without variable load	$g_{dead} + g_{perm}$	58.8	mm	$L/500 = 90mm$	0.65
Additional deflection under mobile load	q_{var}	28.8	mm	$L/1500 = 30mm$	0.96
At t=∞ fully loaded	$g_{dead} + g_{perm} + q_{\text{var}}$	58.8 + 28.8 = 87.6	mm	$L/500 = 90mm$	0.97

Table 14: The deflections at mid-span and unity checks for different phases

As the unity checks shows, the construction satisfies with respect to deflection for all phases. The normative deflections are the additional deflection under mobile load and the deflection at t=∞ fully loaded. The deflection is mostly determined by the deflection due to bending and not by shearing. To decrease the deflection the bending stiffness should thus be increased (enlarge the moment of inertia). Notice that deflection is indeed a very important verification for FRP bridges.

For the calculation of the deflections reference is made to Appendix E.5

8.6 Vibration

Verification according Annex F [10]

The first natural bending frequency of the sandwich girder is:

$$n_0 = \frac{C_{end}}{2\pi} \sqrt{\frac{E_x I_z}{g_{dead} * L^4 / g}} = 5.84Hz$$ Without partial factors

$$n_0 = \frac{C_{end}}{2\pi} \sqrt{\frac{E_x I_z /(\gamma_m * \gamma_c)}{g_{dead} * L^4 / g}} = 3.98Hz$$ With partial factors

The velocity of the metros is:
$v = 100km/h = 27.78m/s$

The extrapolated maximum value of the velocity divided by the first natural frequency is:
$(v/n_0)_{\lim} = 10.0m$

The verification of the ratio of the velocity over the first natural frequency is:

$v/n_0 = 4.75m \leq 10.0m \rightarrow Ok$	n_0 without partial factors
$v/n_0 = 6.98m \leq 10.0m \rightarrow Ok$	n_0 with partial factors

Verification according to Figure 6.10 [10]

Limits of natural frequency n_0 (Hz) as a function of L (m)

The upper limit of natural frequency is governed by dynamic enhancements due to track irregularities and is given by:

$$n_{0\max} = 94.76 * L^{-0.748} = 5.5Hz$$

The lower limit of natural frequency is governed by dynamic impact criteria and is given by:

$$n_{0\min} = 23.58 * L^{-0.592} = 2.48Hz$$

The first natural frequency of the sandwich girder is:

$n_0 = \frac{C_{end}}{2\pi}\sqrt{\frac{E_x I_z}{g_{dead} * L^4 / g}} = 5.84Hz \rightarrow Not\ ok$	Without partial factors
$n_0 = \frac{C_{end}}{2\pi}\sqrt{\frac{E_x I_z /(\gamma_m * \gamma_c)}{g_{dead} * L^4 / g}} = 3.98Hz \rightarrow Ok$	With partial factors

Conclusion

As the FRP sandwich girder is very light, Table 27 (see Appendix E.6) does not give a solution for the maximum value of the velocity divided by the first natural frequency. Therefore there is made an extrapolation of this maximum. This extrapolation is however quite rough and the question rises if this extrapolation is valid. For this reason only the second verification is taken into account. This verification shows that the sandwich girder requires a dynamic analysis as the first natural frequency of the structure without partial factors is too high. This means that the frequency approaches the frequency due to track irregularities which causes enhancement of the dynamic loads. This way the vertical forces due to impacts on the rail become larger than just the vertical load. The dynamic factor which is taken into account so far is not sufficient anymore when the upper limit of 5.5 Hz is passed. The structure thus requires a dynamic analysis. It is however expected that the maximum frequency of the structure of 5.84 Hz, which is not much more than the limit, is not very problematic as in reality the amplitude of the acceleration of the metros is small. Besides the damping of the FRP sandwich girder (foam) is not taken into account. It is therefore expected that executing a dynamic analysis will not result in a different design. It is however recommended to make a dynamic analysis to be certain of this assumption. A dynamic analysis is not treated in this design as this is too specific and goes far beyond the purpose to design a global FRP railway girder. For a further elaboration of a FRP metro viaduct it is thus recommended to make a dynamic analysis to check whether the structure is determined against the dynamic effects.

For the vibration verifications reference is made to Appendix E.6.

8.7 Stresses

The maximum compressive and tensile stress in the sandwich girder is:

$$\sigma_{x,skin} = \frac{M_{Ed,uls} * \frac{1}{2} H}{I_z} = 37.72 N/mm^2$$

8.7.1 Stresses in the outer skins

Tension

The ultimate tensile strength of the skin is:

$$f_{t,skin} = \frac{E_{x,skin}}{\gamma_m * \gamma_c} * \varepsilon_{c\max} = 233.25 N/mm^2$$

Unity check tensile stress in the skin:

$$\boxed{\frac{\sigma_{x,skin}}{f_{t,skin}} = 0.16 \leq 1.0 \rightarrow Ok}$$

Compression

The ultimate compressive strength of the skin is (skin dimpling):

$$f_{c,\dim pling} = 0.75 * \frac{E_{x,skin}}{\gamma_m * \gamma_c} * (t_{skin,out} / L_{tria})^{3/2} = 1922.2 N/mm^2$$

Unity check compressive stress in the skin:

$$\boxed{\frac{\sigma_{x,skin}}{f_{c,\dim pling}} = 0.02 \leq 1.0 \rightarrow Ok}$$

8.7.2 Stresses in the core triangles

Tension

The ultimate tensile strength of the core is:

$$f_{t,core} = \frac{E_{x,core}}{\gamma_m * \gamma_c} * \varepsilon_{c\max} = 69.17 N/mm^2$$

Unity check tensile stress in the core:

$$\boxed{\frac{\sigma_{x,skin}}{f_{t,core}} = 0.55 \leq 1.0 \rightarrow Ok}$$

8.7.3 Flexural strength

The flexural strength of the sandwich girder is:

$$M_{Rd} = B * t_{skin,out} * t_{core} * \frac{E_x}{\gamma_m * \gamma_c} * f_{t,core} / \frac{E_{x,core}}{\gamma_m * \gamma_c} = 248548.92 kNm$$

Unity check flexural strength:

$$\boxed{\frac{M_{Ed,uls}}{M_{Rd}} = 0.18 \leq 1.0 \rightarrow Ok}$$

8.7.4 Conclusion stresses

The verifications of the stresses in the FRP sandwich girder are all easily satisfied. The verification of the stresses in the girder is therefore not considered as a normative verification for the design.

For the verifications of the stresses reference is made to Appendix E.7.

8.8 Shear

It is expected that all the shear stresses are carried in the core. The shear strength of this material with its volume fraction of fibres and fibre orientation is not known and should be determined by experiments. For this design it is however assumed that a quite conservative shear strength of:
$\tau = 50N/mm^2$ will do, considering the shear strengths given in [i7].

The design shear strength then becomes:

$$\tau_{Rd} = \frac{50}{\gamma_m * \gamma_c} = 14.76N/mm^2$$

8.8.1 Transverse shear

The transverse shear force is:

$$\tau_{Ed} = \frac{V_{Ed,uls}}{A_{1,tria,h} * n_{tw}} = 5.48N/mm^2$$

Unity check transverse shear:

$$\boxed{\frac{\tau_{Ed}}{\tau_{Rd}} = 0.37 \leq 1.0 \rightarrow Ok}$$

8.8.2 Parallel shear

The parallel shear force is:

$$\tau_{Ed} = \frac{V_{Ed,uls} * S}{I_z * \frac{A_{1,tria,h}}{t_{core}} * n_{tw}} = 10.77N/mm^2$$

Unity check parallel shear:

$$\boxed{\frac{\tau_{Ed}}{\tau_{Rd}} = 0.73 \leq 1.0 \rightarrow Ok}$$

8.8.3 Conclusion shear

Also the verifications of shear in the sandwich girder are easily satisfied. The strength of the structure is therefore not considered as a normative structural verification. The verification of deflection is normative over the strength verifications for a FRP sandwich girder.

For the verifications of shear reference is made to Appendix E.8.

8.9 Buckling of the core

The critical buckling force of the core is:

$$F_{cr} = \frac{\pi^2 * \frac{E_{z,core}}{\gamma_m * \gamma_c} * I_{tria} * n_{tw}}{L_{buc,core}^{\ 2}} = 45007.44kN$$

The maximum buckling force is:

$$V_{Ed.uls} = 0.5 * L * q_{uls} = 4060.15kN$$

Unity check buckling of the core:

$$\frac{V_{Ed,uls} * \alpha_{cr}}{F_{cr}} = 0.90 \leq 1.0 \rightarrow Ok$$

The verification of buckling of the core triangles is satisfied. The unity check is however close to the limit. The five intermediate thin skins are thus very important in order to limit the buckling length of the core triangles. Notice that the thickness of the core triangles is small (4 mm). When this verification is not satisfied more intermediate thin skins should be placed or the core triangles should be made stiffer.

For the verifications of buckling of the core reference is made to Appendix E.9.

8.10 Optimisation

The design presented in this chapter is a global design of a FRP sandwich girder. As mentioned before, this is not the optimal design. The schematisation and dimensions of the sandwich girder with its intermediate skins and core triangles is just one of the many possibilities for the girder. It is for instance possible to change the dimensions of the core triangles or the thickness of the skins. There are many variables involved to find the optimal design. The minimal thickness of the triangles and skins is most likely determined by the manufacturing process in order to create a strong connection between the cores and skins (thick enough to interweave the fibres of both parts). The maximum thickness of the laminates is probably limited by the chance of delamination. Besides, the costs for a certain thickness of the laminate should be taken into consideration. In this design the core consists of triangles. Another shape of the core could however result in a better design than the one described in this chapter. It can be concluded that it is quite difficult to find the optimal design of a FRP sandwich girder for an elevated metro structure. The design in this chapter shows however the global dimensions and normative structural verifications which apply to a FRP sandwich girder.

The calculations of the FRP sandwich girder showed the normative structural verifications. These normative verifications are the verifications of the additional deflection of the girder under mobile load, the deflection of the girder at $t=\infty$ fully loaded and buckling of the core triangles. Besides, the verification of vibration is a point of interest as the first natural frequency of the girder exceeds the upper limit. It is however expected that a dynamic analysis will not result in a different design, see Section 8.6. Despite it is hard to determine the optimal design there is made a small optimisation process for the design. In this optimisation process there is searched for the optimal design (smallest dead load) by changing only two parameters:

- Thickness of the outer skins $t_{skin,out}$, steps of 10 mm
- Spacing of the outer skins d , steps of 100 mm

For the relations of these two parameters with other parameters reference is made to Section 8.3. The spacing of the outer skins is changed in steps of 100 mm. For each spacing of the outer skins the thickness of the outer skins is adjusted in such a way that the sandwich girder just satisfies all the structural verifications. The result of this iterative optimisation process is shown in Table 15. Table 15 shows in each green frame the optimal design for a certain spacing of the outer skins and the normative structural verifications (green cell). Notice that the verifications of deflection are normative for the designs. In Graph 29 the dead load of the FRP girder is shown for all the designs of Table 15. The design presented in this chapter has a spacing of the outer skins of 3 metres. However, Graph 29 shows that this is not the lightest design. The lightest design has a spacing of the outer skins of 3.4 metres. Notice that this design does not satisfies the verification of buckling of the core, see Table 15. To satisfy this verification the design requires an extra intermediate skin. This will however increase the weight of the girder so that it is not lighter anymore than the design with a spacing of the outer skins of 3 metres presented in this chapter. Notice the large dead load and thickness of the outer skins for the smaller spacings, see Table 15. The slope of the dead load increases fast for smaller spacings, see Graph 29. This small optimisation process shows the results of changing the spacing and thickness of the outer skins, which has the most effect on the bending stiffness of the girder. But, as mentioned before this does not result in the optimal design for an FRP sandwich girder.

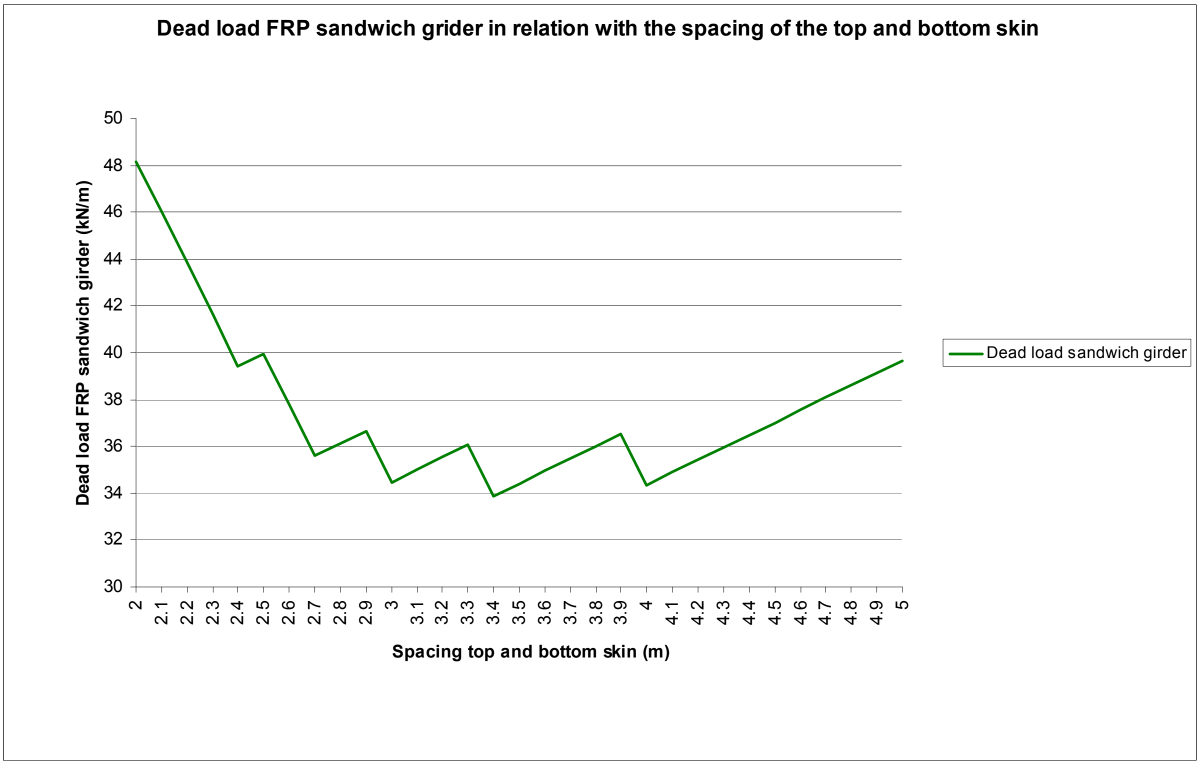

Graph 29: Dead load FRP sandwich girder in relation with the spacing of the top and bottom skin

Spacing outer skins	2	2.1	2.2	2.3	2.4	2.5	2.6	2.7	m
Thickness outer skins	0.11	0.1	0.09	0.08	0.07	0.07	0.06	0.05	m
Dead load sandwich girder	48.17502	45.99031	43.80561	41.6209	39.4362	39.96797	37.78326	35.59856	kN/m
Additional deflection under mobile load	26.00481	25.76948	25.87863	26.37841	27.35657	25.23533	26.80564	29.22994	mm
Deflection at t=∞ fully loaded	89.69766	87.21644	85.90932	85.85951	87.27104	80.90195	84.19957	89.92094	mm
Buckling of the core	0.397627	0.43997	0.483619	0.528448	0.57433	0.628215	0.676832	0.726183	Unity check
First natural bending frequency n0	5.242153	5.384947	5.500447	5.582964	5.625002	5.820686	5.800184	5.713303	Hz
Spacing outer skins	2.8	2.9	3	3.1	3.2	3.3	3.4	3.5	m
Thickness outer skins	0.05	0.05	0.04	0.04	0.04	0.04	0.03	0.03	m
Dead load sandwich girder	36.13033	36.66211	34.4774	35.00918	35.54095	36.07272	33.88802	34.41979	kN/m
Additional deflection under mobile load	27.19818	25.3725	28.79751	26.98513	25.33963	23.84111	28.63873	27.03805	mm
Deflection at t=∞ fully loaded	84.09946	78.85438	87.63319	82.5435	77.90976	73.67833	86.64948	82.23282	mm
Buckling of the core	0.786207	0.848846	0.902107	0.969012	1.038567	1.110797	1.169039	1.24548	Unity check
First natural bending frequency n0	5.88145	6.047457	5.842686	5.991648	6.138707	6.283923	5.902374	6.029012	Hz
Spacing outer skins	3.6	3.7	3.8	3.9	4	4.1	4.2	4.3	m
Thickness outer skins	0.03	0.03	0.03	0.03	0.02	0.02	0.02	0.02	m
Dead load sandwich girder	34.95157	35.48334	36.01512	36.54689	34.36218	34.89396	35.42573	35.95751	kN/m
Additional deflection under mobile load	25.56863	24.21648	22.96943	21.81685	28.68516	27.31232	26.03617	24.84784	mm
Deflection at t=∞ fully loaded	78.16696	74.41513	70.94527	67.72936	87.19331	83.45101	79.96241	76.70464	mm
Buckling of the core	1.324631	1.406517	1.491164	1.578596	1.643927	1.735535	1.829963	1.927237	Unity check
First natural bending frequency n0	6.154066	6.277585	6.399616	6.520205	5.848465	5.948902	6.048162	6.146281	Hz
Spacing outer skins	4.4	4.5	4.6	4.7	4.8	4.9	5		m
Thickness outer skins	0.02	0.02	0.02	0.02	0.02	0.02	0.02		m
Dead load sandwich girder	36.48928	37.02105	37.55283	38.0846	38.61638	39.14815	39.67993		kN/m
Additional deflection under mobile load	23.73945	22.70396	21.73512	20.82732	19.97553	19.17524	18.42235		mm
Deflection at t=∞ fully loaded	73.6574	70.80258	68.12399	65.60712	63.23894	61.00772	58.90286		mm
Buckling of the core	2.027382	2.130425	2.236389	2.345301	2.457186	2.572069	2.689976		Unity check
First natural bending frequency n0	6.243294	6.339231	6.434126	6.528006	6.6209	6.712836	6.803839		Hz

Table 15: Designs of the FRP sandwich girder for different spacings of the outer skins

8.11 Manufacturing process and transportation

The FRP sandwich girder design satisfies the verifications at macro level. However, the micromechanics and also the manufacturing process are not taken into consideration. The feasibility of the design is therefore not guaranteed. The InfraCore® concept is applied for small bridges for pedestrians and cyclists. The FRP girder in this chapter is however much larger in size and has to resist larger forces. The question is if the sandwich girder can handle these forces at micro level. Besides the question is how to build such a large railway girder. FiberCore Europe has patented its product and manufacturing process, see [i3] [i4]. For the InfraCore® principle reference is made to

Appendix F: Infracore principle. The layout of the fibres and foam is placed in a closed mould and is then injected with resin using Vacuum-Assisted Resin Injection (VARTM), see Figure 53. Vacuum-Assisted Resin Injection is a closed process in which resin is pulled into the mould by negative pressure and impregnates the fibres already laid out in the mould. The FRP sandwich design in this study can be considered as a combination of six InfraCore® sandwiches. The size of the railway girder is large so that it requires quite some negative pressure to inject the whole girder at once. The question is if this manufacturing process is applicable for such a large sandwich girder. Maybe it is necessary to inject the sandwich girder in multiple phases.

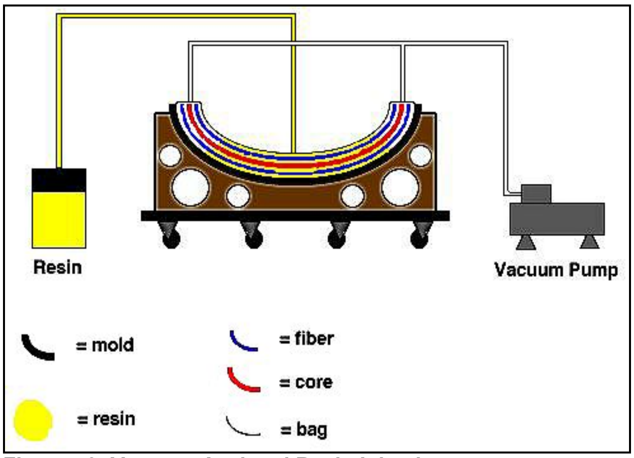

Figure 53: Vacuum-Assisted Resin Injection

Besides the manufacturing process also the transportation and placement of the girder should be taken into account. The InfraCore® bridges are small compared with the FRP railway girder. These small bridges can be placed by mobile cranes, see Figure 54. The designed FRP girder is however much larger and heavier. Due to its large length, width and dead load it requires exceptional transport. To place the sandwich girder multiple cranes are needed. Fact is that the transportation and placement of a FRP railway girder will result in much hindrance for the surrounding area. A solution to minimize the hindrance could be to make the girder floating and transport it by water.

Figure 54: Placement InfraCore® bridge

8.12 Conclusions and recommendations

The design presented in this chapter is a global design of a FRP sandwich girder. As mentioned before, this is not the optimal design. The schematisation and dimensions of the sandwich girder with its intermediate skins and core triangles is just one of the many possibilities for the girder. The normative verifications for the design are the verifications of the additional deflection of the girder under mobile load, the deflection of the girder at $t=\infty$ fully loaded and buckling of the core triangles. Besides, the verification of vibration is a point of interest as the first natural frequency of the girder exceeds the upper limit. It is however expected that a dynamic analysis will not result in a different design.

The FRP sandwich girder has to be fail-safe. This has resulted in the application of large conversion factors. The capacity of the railway girder is therefore expected to be much larger than the design strength. In this design, the verifications at macro level are considered and not the micromechanics. The feasibility of the design is therefore not guaranteed. Because FRP is often applied in the aerospace engineering (many stress changes) it is however expected that it should not be impossible to satisfy the verification of the micromechanics of the design. For the same reason fatigue of the FRP is not considered as a critical verification for the design.

To produce the designed sandwich girder using Vacuum-Assisted Resin Injection (VARTM) a large negative pressure is required to inject the whole girder at once. The question is if this manufacturing process is applicable for such a large sandwich girder. Maybe it is necessary to inject the sandwich girder in multiple phases. Due to the large length, width and dead load of the girder exceptional transport is required. Fact is that the transportation and placement of a FRP railway girder will result in much hindrance for the surrounding area. A solution to minimize the hindrance could be to make the girder floating and transport it by water.

For a further elaboration of the FRP railway girder it is recommended to:

- Execute a dynamic analysis to check whether the structure is determined against the dynamic effects.
- Take into account the micromechanics of the FRP sandwich girder.
- Take into account the manufacturing process of the FRP sandwich girder.

For more information on FRP structures reference is made to [17], [7] and [3].

9. Substructure

9.1 General

This chapter describes the designs of the substructure (column + foundation) for the three designed railway girders. The schematisation and verifications of the substructure are given in paragraph 2. In the next paragraph a clear overview of the characteristics and verifications of the three designs is shown. This includes the most important aspects of the designs in order to compare them. For the extensive calculations of the substructure reference is made to Appendix G: Calculations column + foundation. The latest paragraph deals with some alternative solutions and assumptions for the design of the substructure. The extensive calculations of the substructure for the concrete box girder, the UHPC box girder and the FRP sandwich girder can be found in respectively Appendix G.1, G.2 and G.3. References to the specific codes and literature used for the designs are also given in the Appendix.

9.2 Schematisation and verifications substructure

The schematisation of the substructure is shown in Figure 55. The column is a square cast in-situ concrete (C50/60) column with a drainage tube in the middle, see Figure 56. A square column is preferable over a circular column as it results in a larger moment of inertia for the column. The column is made as slender as possible so that it just satisfies the verifications of stability and stiffness. The foundation slab is considered as an infinite stiff slab. The piles underneath the foundation slab have a spring stiffness of $k = 100000 kN/m$ and a maximum allowed compressive pile force of $P_{\max,allow} = -1200 kN\ \ per\ \ pile$ (both are assumptions). The spacing of the piles is 2 metres. For the stability of the structure two critical buckling modes are considered, see Figure 57. The total critical buckling force is calculated out of these two buckling modes: $\frac{1}{F_{cr,tot}} = \frac{1}{F_{cr,1}} + \frac{1}{F_{cr,2}} \rightarrow F_{cr,tot}$

Where:

$F_{cr,1} = \frac{\pi^2 * E_{c,eff} * I_{column}}{l_c^2}$ Critical buckling force mode 1

$F_{cr,2} = \frac{C_y}{H}$ Critical buckling force mode 2

In order to satisfy the verification of stability the structure should satisfy: $n = \frac{F_{cr,tot}}{F_{v,viaduct,uls}} \geq 10$

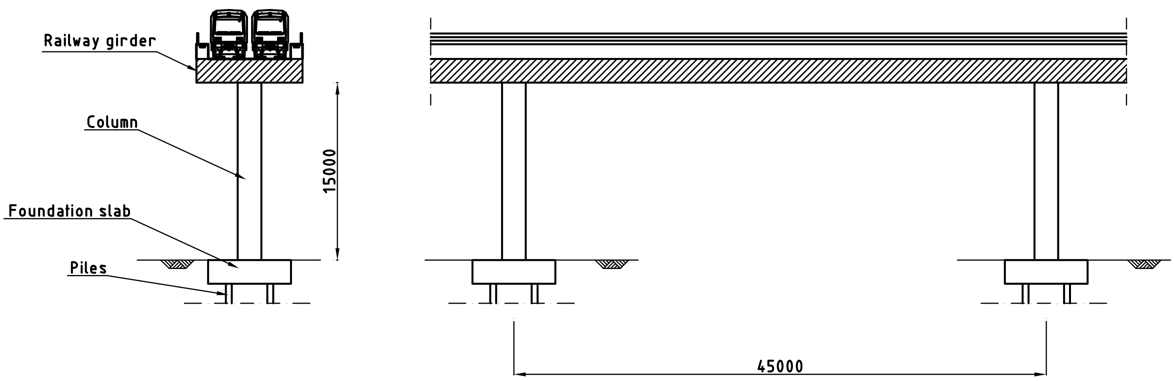

Figure 55: Schematisation elevated metro structure, cross-section and side-view of the structure

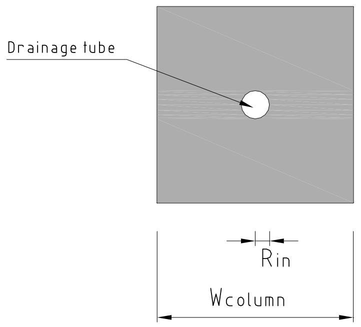

Figure 56: Cross-section column

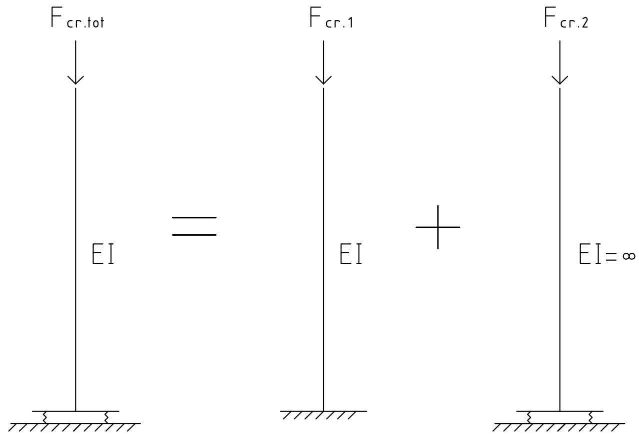

Figure 57: Structural model

The stiffness of the structure is considered in the transversal direction of the viaduct as this is the normative direction. The maximum allowed deflection at the top of the column is $\delta_{\max} = \frac{H}{500} = 0.03m$. The total deflection at the top is the summation of three deflections multiplied by the 2nd degree magnification factor:

- Deflection at the top due to horizontal force at the top of the column $\delta_h = \frac{F_{h,trans} * H^3}{3 * E_{c,eff} * I_{column}}$
- Deflection at the top due to wind load at the column $\delta_q = \frac{q_{wind} * w_{column} * H^4}{8 * E_{c,eff} * I_{column}}$
- Deflection at the top due to rotation of the foundation slab $\delta_c = \frac{M_y}{C_y} * H$

The maximum and minimum pile force arises in the corner piles of the foundation slab. The pile force is determined by the vertical forces and the moments in longitudinal and transversal direction of the girder: $P_{\max} = P_v - P_{my} - P_{mx} \geq P_{\max,allow} = -1200kN$ and $P_{\min} = P_v + P_{my} + P_{mx}$.

Where:

$P_v = \frac{-F_{v,piles}}{n_p}$	Load on piles due to the vertical load
$P_{my} = \frac{M_y}{C_y} * ny_{\max} * k$	Load on the outside piles in transversal direction due to the moment in the transversal direction
$P_{mx} = \frac{M_x}{C_x} * nx_{\max} * k$	Load on the outside piles in longitudinal direction due to the moment in the longitudinal direction

The foundation consists of just enough piles so that the maximum allowed compressive pile force of $P_{\max,allow} = -1200kN$ is not exceeded. When more piles are required they are placed on the edge of the foundation where it has the largest contribution to the rotation stiffness of the foundation in the transversal direction (normative direction). The layout of the piles should be in balance as much as possible.

Besides the pile force, the piles are also subjected to a pile head moment due to the horizontal forces. For this verification the pile is schematised as a beam of infinite length on one side and is fixed in the foundation slab on the other side. The pile which is supported by linear elastic springs (soil) is subjected to a concentrated horizontal force at the foundation slab. The structural model for a pile subjected to the horizontal force is shown in Figure 58.

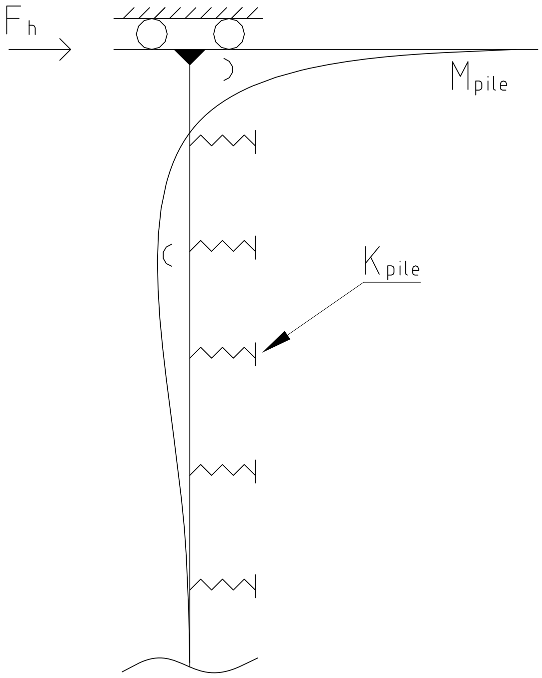

Figure 58: Structural model piles

The maximum pile head moment in the pile is:

$$M_{pile} = \frac{\frac{1}{2} * \frac{F_h}{n_p}}{2 * \beta}$$

Where:

$$\beta = \sqrt[4]{\frac{k_{pile}}{4E_{pile} I_{pile}}}$$

$k_{pile} = k * w_{pile} * c_{effectivewidth}$	Modulus of subgrade reaction of pile
$k = 3000 kN/m^3$	Modulus of subgrade reaction (assumption)
$c_{effectivewidth} = 1.5$	Factor for determining the effective width of the pile (assumption)
$w_{pile} = 0.42m$	Width of the pile (assumption)
$h_{pile} = 0.42m$	Depth of the pile (assumption)

The required reinforcement at one side of the pile to resist the pile head moment is:

$$\frac{M_{pile}}{z} = A_s * f_{yd} \rightarrow A_s$$

The total required reinforcement in a pile then becomes:

$$A_{s,tot} = 4 * A_s$$

The maximum reinforcement percentage in a column/pile is 4%, so:

$$\omega_0 \leq \omega_{\max} = 4\%$$

Finally, the stresses in the column are calculated.
The maximum compressive stress in the column is:

$$\sigma_{c\max} = \sigma_n - \sigma_m$$

The minimum compressive stress in the column is:

$$\sigma_{c\min} = \sigma_n + \sigma_m$$

Where:

$\sigma_n = \dfrac{-F_{v,tot,bot,column}}{A_{column}}$ Is the compressive stress in the column due to the vertical load

$\sigma_m = {}^{+}\!/\!_{-}\dfrac{M_y}{W_{column}}$ Is the stress in the column due to the moment in transversal direction

9.3 Comparison of the three designs

The verifications mentioned in the previous paragraph are taken into account for the designs of the substructure for the three designed girders. The results of the calculations are shown in the overviews below. For the extensive calculations of the substructures reference is made to Appendix G: Calculations column + foundation.

	Concrete C50/60	UHPC C180	FRP
Cross-section of the elevated metro structure in transversal direction	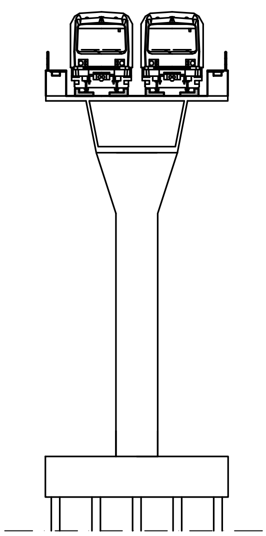	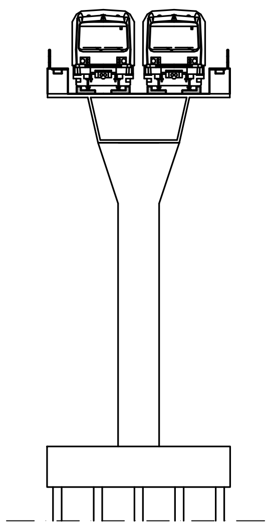	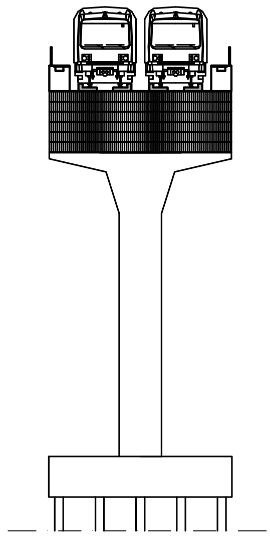
Pile foundation, top- and side-view	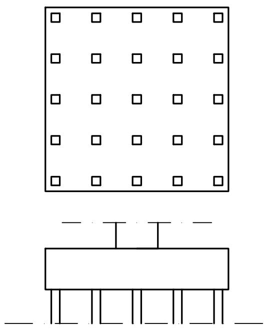	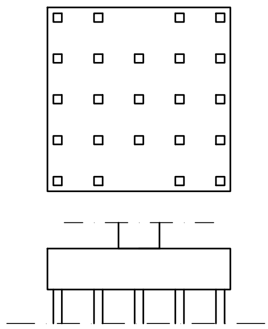	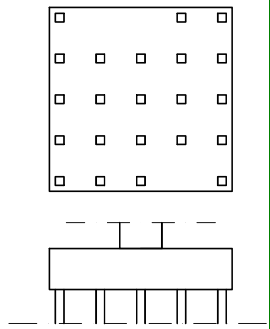

Table 16: Comparison of the three designs, drawings

		Concrete C50/60	UHPC C180	FRP	Unity
Depth railway girder	H	2.8	2.41	3.04	m
Dead load railway girder	g_{dead}	102.02	69.4	34.48	kN/m
Permanent load at the girder	g_{perm}	34.42	34.42	34.42	kN/m
Variable load at the girder	q_{var}	58.29	58.29	58.29	kN/m
Vertical force at the top of the column	$F_{v,viaduct}$	9,320	7,834.34	6,165	kN
Horizontal force at the top of the column in longitudinal direction of the viaduct	$F_{h,long}$	326.25	326.25	326.25	kN
Horizontal force at the top of the column in transversal direction of the viaduct	$F_{h,trans}$	485.63	459.3	505.88	kN
Width of the column	w_{column}	2.06	2.02	2.08	m
Number of piles	n_p	25	23	22	
Length foundation slab	L_{fs}	9	9	9	m
Width foundation slab	W_{fs}	9	9	9	m
Thickness foundation slab	T_{fs}	2	2	2	m
The rotation stiffness of the foundation in transversal direction	C_y	20,000,000	20,000,000	19,200,000	kNm/rad
The rotation stiffness of the foundation in longitudinal direction	C_x	20,000,000	16,800,000	15,200,000	kNm/rad
Critical buckling force mode 1	$F_{cr,1}$	278,777.87	257,742.18	289,765,79	kN
Critical buckling force mode 2	$F_{cr,2}$	1,333,333.33	1,333,333.33	1,280,000	kN
Total critical buckling force	$F_{cr,tot}$	230,569.59	215,989.90	236,277.42	kN
Factor n	n	17.77	19.69	27.11	
2nd degree magnification factor:	$\frac{n}{n-1}$	1.06	1.05	1.04	
Deflection at the top due to the horizontal force at the top of the column	δ_h	0.0215	0.0220	0.0215	m
Deflection at the top due to wind load at the column	δ_q	0.0008	0.0008	0.0007	m
Deflection at the top due to rotation of the foundation slab	δ_c	0.0057	0.0054	0.0062	m
Total 2nd order deflection at the top	δ_{tot}	0.0297	0.0297	0.0296	m
Total vertical force at the piles, ULS	$F_{v,piles}$	20,411.41	18,324.78	16,193.35	kN
Total horizontal force at the piles, ULS	F_h	797.96	757.13	829.01	kN
Total moment at the foundation slab in transversal direction, ULS	M_y	11,832.76	11,171.73	12,166.5	kNm
Total moment at the foundation slab in longitudinal direction, ULS	M_x	7,340.56	7,340.56	7,340.56	kNm
Load on piles due to the vertical load	P_v	-816.46	-796.73	-736.06	kN

Load on the outside piles in transversal direction due to the moment in the transversal direction	P_{my}	+/- 236.66	+/- 223.43	+/- 253.47	kN
Load on the outside piles in longitudinal direction due to the moment in the longitudinal direction	P_{mx}	+/- 146.81	+/- 174.78	+/- 193.17	kN
The maximum pile force in the corner piles of the foundation slab	$P_{\max}$	-1,199.92	-1,194.94	-1,182.7	kN
The minimum pile force in the corner piles of the foundation slab	$P_{\min}$	-432.99	-398.52	-289.42	kN
The pile head moment in a pile	M_{pile}	30.18	31.12	35.63	kNm
The reinforcement percentage in a pile	ω_0	0.46	0.47	0.54	%
The compressive stress in the column due to the vertical load	σ_n	-3.61	-3.23	-2.54	N/mm^2
The stress in the column due to the moment in transversal direction	σ_m	+/- 8.12	+/- 8.13	+/- 8.11	N/mm^2
The maximum compressive stress in the column	$\sigma_{c\max}$	-11.73	-11.37	-10.66	N/mm^2
The minimum compressive stress in the column	$\sigma_{c\min}$	4.52	4.90	5.57	N/mm^2

Table 17: Comparison of the three designs, characteristics and verifications

The comparison between the three designs shows that a lighter girder does not result in a large reduction of the number of piles. The difference between the concrete and the FRP design is just three piles. The dimensions of the foundation slab are the same for the three designs. The normative structural verification for the width of the column is stiffness and not stability of the whole structure. The stiffness of the column is just large enough so that the deflection at the top is smaller than $\delta_{\max} = 0.03m$, see the green cells in Table 17. Stiffness is normative over stability due to the large horizontal force in transversal direction $(F_{h,trans})$ at the top of the column, which causes the largest contribution to the deflection. This horizontal force is not taken into account in the verification of stability. The horizontal force $F_{h,trans}$ includes the wind load and the sideward force due to the metro. Especially the wind load is determining for the magnitude of this force. Due to the larger depth of the FRP girder the horizontal force $F_{h,trans}$ is larger for the FRP design. This results in a larger width of the column to satisfy the verification of stiffness. For the FRP design holds that the total moment at the foundation slab in transversal direction (ULS) is larger because of this force. This results in a larger pile force due to the moment in longitudinal direction (P_{my}) in the corner piles of the foundation. The maximum pile force is for the three designs just below the maximum pile force of $P_{\max,allow} = -1200kN$, see the red cells in Table 17. The application of fewer piles for the designs will cross this limit. Furthermore, the required reinforcement percentage in a pile to resist the pile head moment is small just as the stresses in the column. This should not give any trouble.

In first instance one should expect a larger difference between the three designs considering the large differences in the dead load of the girders: concrete $g_{dead} = 102.02kN/m$; UHPC $g_{dead} = 69.4kN/m$ and FRP $g_{dead} = 34.42kN/m$. The reason for the small difference between the substructures of the three designs is the small weight contribution of the railway girder to the total vertical load at the piles. For the weight contribution of the different elements of the structure to the total vertical load at the piles reference is made to Table 18. This table shows that the dead load of the concrete railway girder is 33.06% of the total vertical load at the piles. A weight reduction of 66.26% of the railway girder (FRP girder $g_{dead} = 34.42kN/m$ instead of concrete C50/60 girder $g_{dead} = 102.02kN/m$) therefore does not result in a total vertical load reduction at the piles of the same extent. The vertical load reduction at the piles is 21.07% by using FRP instead of concrete for the railway girder $\left(100\% - \frac{11703.62kN}{14828.12kN} * 100\% = 21.07\%\right)$. Besides, the moments at the foundation have a large contribution to the pile forces, which are almost irrespective of the dead load of the girder, see P_{my} and P_{mx} in Table 17. Only the depth of the girder, the width of the column (wind load) and the 2nd order moment $\left(\delta_{tot} * F_{v,viaduct,uls}\right)$ influence the differences between the moments M_y at the foundations of the three designs. Because the FRP sandwich girder has the largest depth this results in a larger moment at the foundation $\left(M_y\right)$ and a larger width of the column to limit the deflection at the top. Notice the larger dead load of the column for the FRP design in Table 18. This is due to the larger width of the column and the cross-girder to support the FRP sandwich girder.

A rough division of the contribution of the elements to the total vertical load at the piles for the concrete design is (see Table 18):

- 30% dead load girder
- 30% permanent and variable load at the girder
- 10% dead load column
- 30% dead load foundation slab

The permanent and variable load is the same for the three designs. The dead load of the column has a relative small contribution to the total vertical load at the piles. So optimising the column is not as effective as optimising the girder and the foundation slab (both have a contribution of 30%). The dimensions of a foundation slab are however from a practical and financial point of view already quite determined. The best way to optimise the elevated metro structure is thus indeed to optimise the girder of the structure as was assumed in Chapter 2. However, due to the small weight contribution of the girder to the total vertical load at the piles and the large contribution of the moments at the foundation to the pile forces, the application of a lighter girder results in a small benefit considering the required number of piles for the substructures of the three designs. The differences between the widths of the columns to satisfy the verification of stiffness are also small as the differences between the depths of the girders (wind load) are relative small. Because of these small differences between the substructures of the designs the choice between the three designs will probably be based on the construction/fabrication, costs and aesthetics (depth and shape) of the railway girder.

For a 3D-impression of the three designs reference is made to Appendix H: 3D-impressions three designs.

		Concrete C50/60	UHPC C180	FRP	Unity
Dead load railway girder	$g_{dead} * L + (Q_{v,tendons} + Q_{v,anchorage})$	4,902.76	3,417.14	1,551.6	kN
Percentage of the total vertical load at the piles		33.06	25.73	13.26	%
Total load railway girder fully loaded	$q_{tot} * L + (Q_{v,tendons} + Q_{v,anchorage})$	9,074.71	7,589.09	5,723.55	kN
Percentage of the total vertical load at the piles		61.2	57.14	48.9	%
Dead load column	$F_{v,column} + Q_{v,widening}$	1,780.36	1,720.32	2,007.02	kN
Percentage of the total vertical load at the piles		12.01	12.95	17.15	%
Dead load foundation slab	$F_{v,fs}$	3,973.05	3,973.05	3,973.05	kN
Percentage of the total vertical load at the piles		26.79	29.91	33.95	%
Total vertical load at the piles	$q_{tot} * L + (Q_{v,tendons} + Q_{v,anchorage} +)$ $F_{v,column} + Q_{v,widening} + F_{v,fs}$	14,828.12	13,282.46	11,703.62	kN
Percentage of the total vertical load at the piles		100	100	100	%

Table 18: Comparison of the three designs, weight contribution of the elements

9.4 Alternative solutions and assumptions

The columns in the designs presented in the previous paragraph are made of in-situ concrete C50/60. It is however possible to create a more slender elevated metro structure by applying UHPC columns. But as mentioned before it is hard to control the curing/quality of in-situ UHPC. For constructing in UHPC it is better to utilize precast UHPC elements as this ensures a better quality. For the columns it is however more practical and economical to use in-situ concrete. Besides, the dead load of the column has a relative small contribution to the total vertical load at the piles. So optimising the columns (applying UHPC) is not very effective as optimising the girder and it is even the question if this will result in a better and/or cheaper design. For the three designs it is therefore chosen to apply concrete (C50/60) columns.

For the elevated metro structure with the concrete box girder there are made some designs with alternative solutions and assumptions. This is done in order to give an impression on how the substructure changes under different conditions. For the concrete box girder three aspects are considered:

- The application of columns made of UHPC instead of conventional concrete
- Changing the spring stiffness of the piles: k = 50000, 100000 and 150000 kN/m
- Changing the height of the columns: H = 5 m, 10 m, 15 m, 20 m and 40 m

The results of these designs can be found in Appendix I: Alternative solutions and assumptions for the substructure. The calculations of these designs are not included in this design study. This is just attached to give an impression on how the structure changes under different conditions and is not taken into further consideration in this design study.

10. Costs

To make the comparison between the three designs more complete there is made an indication of the construction costs of the three designs. The calculations are performed by a construction cost expert of the engineering office of Rotterdam Public Works. The calculations include the costs of the elevated metro structure without the walkways, rails and metros. For a detailed overview of the construction costs of the designs reference is made to Appendix J: Costs.

The direct construction costs for the elevated metro structure with a concrete box girder are: €443,553 per span of 45 metres, see Appendix J.1. When also the indirect, the unforeseen, the engineering and the additional costs as well as the costs for specifying details are taken into account the total investment cost is: € 1,049,322 per span. The contribution of indirect costs consists of costs which are not directly linked to the construction of the structure. These costs are for instance general company costs and risk percentages. For the comparison only the direct costs are considered as the investment cost is derived form the direct costs by multiplying it with estimated percentages. It is assumed that these estimated percentages are the same for the three designs, so only the direct costs are of importance.

For conventional concrete the unit price is € 175/m^3. This unit price includes processing fees. The unit price of UHPC C180 (Ductal®-AF) is however not known. For this reason the maximum unit price of UHPC is determined at which the UHPC box girder design still competes with the concrete box girder design. To result in the same direct construction costs for the elevated metro structure the unit price of UHPC should be about € 450/m^3 including processing fees, see Appendix J.2. Whether the UHPC box girder design is cheaper than the concrete box girder design is thus dependent on the market price of UHPC. When the unit price of UHPC is lower than € 450/m^3, the UHPC box girder becomes a serious competitor of the conventional concrete box girder from a financial point of view. Besides, it should be noticed that the application of UHPC results in a more slender railway girder. This aesthetical criterion can also be a reason to choose for the UHPC box girder instead of the cost criteria.

There is little known about the specific construction costs of the FRP sandwich girder. The large size of the FRP sandwich girder makes it thereby almost impossible to determine the direct costs of the girder. Therefore the unit price per square metre is determined for the FRP sandwich girder design at which it still competes with the concrete box girder design. In order to compete with the concrete box girder design the unit price of the FRP sandwich girder should be about € 720/m^2 including processing fees and transport and assembly costs, see Appendix J.3. At the engineering office of Rotterdam Public Works there is some general information available about the costs of small InfraCore® bridges for pedestrians and cyclists. To give an idea about the material costs for such a bridge: the material costs excusive labour costs are about € 4200/m^2 for a FRP sandwich bridge of carbon fibre and vinyl ester (dimensions: span 24 m, width 4 m, depth 0.37 m, skin thickness 30 mm). This is far more than the unit price of € 720/m^2 which is required to be competitive with the concrete design. Besides, such a bridge easily fits about eight times in the designed railway girder. Imagine the total investment cost for an elevated metro structure with FRP girders. For the small InfraCore® bridges hold in general that they are competitive in price with concrete and steel bridges as the foundation can be made lighter. The benefit of a lighter foundation then outweighs the larger material costs of FRP. The designed FRP railway girder results however in a very small benefit on the foundation compared with the other two designs. This is due to the small weight contribution of the girder to the total vertical load at the piles and the large contribution of the moments at the foundation to the pile forces. Considering all this it can be concluded that the costs for an elevated metro structure with FRP girders becomes far too high compared with the two other designs. Only when the market price of FRP is drastically decreased it can be considered to build a FRP viaduct. For now it is out of the question to apply FRP for the railway girders.

11. Conclusions and recommendations

11.1 Conclusions

In this design study the accent is on the optimal structural design in relation to the costs and less on the aesthetical design. For the designs of the elevated metro structure made of conventional concrete, UHPC or FRP the focus is therefore on the lightest railway girder and not on the minimum depth of the girder. The conclusions of the design study are described below:

11.1.1 Concrete concepts

- The best concept for the concrete and UHPC railway girder is the precast segmental box girder with external prestressing tendons.
- The best construction method for the precast segmental box girder is the span-by-span construction.

11.1.2 Concrete box girder

- For the dimensions of the optimal concrete box girder reference is made to Section 4.3.
- The dead load of the optimal concrete box girder is: $g_{dead} = 102.02kN/m$
- The optimal concrete box girder has 6 prestressing tendons.
- The normative structural verification of the optimal concrete box girder is fatigue[3] of the concrete at the deviation blocks at the bottom side.
- The minimum deck thickness is set by the verifications of the ultimate resistance moment and the rotation capacity of the deck.
- The minimum depth of the webs is set by the verification of the ultimate resistance moment of the box girder at t=∞.
- The minimum width of the webs of the optimal design is set by the verification of buckling of the webs.

11.1.3 UHPC box girder

- For the dimensions of the optimal UHPC box girder reference is made to Section 6.3.
- The dead load of the optimal UHPC box girder is: $g_{dead} = 69.4kN/m$
- The optimal UHPC box girder has 6 prestressing tendons.
- The normative structural verification of the optimal UHPC box girder is the ultimate resistance moment of the box girder at t=0.
- The minimum deck thickness is set by the verifications of the ultimate resistance moment and the rotation capacity of the deck.
- The minimum depth of the webs is set by the verification of the ultimate resistance moment of the box girder at t=∞.
- The minimum width of the webs is set by the verification of buckling of the webs.

[3] The concrete box girder is verified for fatigue of the concrete according to Annex NN.3.2 NN.112 [12] (Eurocode). This is a simplified approach for railway bridges which results in a conservative fatigue verification. Other fatigue verifications show however that fatigue of the concrete is not normative for the design. When the fatigue verification is not normative for the box girder the verification of the ultimate resistance moment of the box girder at t=0 becomes normative. The change of normative structural verification for the design results however not in a radically different design of the elevated metro structure. For the comparison of the different fatigue verifications for concrete reference is made to Appendix K: Comparison fatigue verifications for concrete.

11.1.4 FRP sandwich girder

- For the dimensions of the FRP sandwich girder reference is made to Section 8.3.
- The dead load of the FRP sandwich girder is: $g_{dead} = 34.48 kN / m$
- The normative structural verifications of the FRP sandwich girder are deflection of the girder and buckling of the core triangles.
- "CUR-Aanbeveling 96, Vezelversterkte kunststoffen in civieltechnische draagconstructies" [3] applies large conversion factors in order to design fail-safe FRP structures.

11.1.5 Substructure

- For the dimensions of the substructures of the three designs reference is made to Section 9.3.
- The application of a lighter railway girder does not result in a large reduction of the number of piles. This is due to:
    - The small weight contribution of the railway girder to the total vertical load at the piles.
    - The large contribution of the moments at the foundation to the pile forces.

- The normative structural verification of the columns is stiffness of the viaduct.

11.1.6 Costs

- The direct construction costs for the elevated metro structure with a concrete box girder are: € 443,553 per span of 45 metres.
- When the unit price of UHPC is lower than € 450/m^3, the UHPC box girder becomes a serious competitor of the conventional concrete box girder from a financial point of view.
- Currently FRP is far too expensive to result in a railway girder which competes with the (UHP) concrete box girder design.

11.2 Recommendations

Some recommendations are made concerning a further detailing of the designs:

11.2.1 Concrete box girder

- Execute an accurate calculation of the prestressing losses to check whether the verification of fatigue of the concrete is still satisfied.

11.2.2 UHPC box girder

- Examine the fatigue behaviour of UHPC and determine the fatigue verification of UHPC.

11.2.3 FRP sandwich girder

- Execute a dynamic analysis to check whether the structure is determined against the dynamic effects.
- Take into account the micromechanics of the FRP sandwich girder.
- Take into account the manufacturing process of the FRP sandwich girder.

References

Literature

[1] Bruijn, H.J. de (2005). Master thesis: *Literatuur- en voorstudie: hogere sterkte beton nader belicht.* Delft: Delft University of Technology and Holland Railconsult.

[2] Carter, H. (2002). *Modulus of symmetrical filament wound carbon fibre tubes*. University of Exeter and The Czech Technical University.

[3] CUR-commissie C 124 “VVK in civiele draagconstructies” (2003). *CUR-aanbeveling 96, Vezelversterkte kunststoffen in civiele draagconstructies*. Gouda: Stichting CUR.

[4] Haasnoot composieten BV (2009). *Productinformatie: InfraCore® brug*. Rijnsburg.

[5] International Federation for Structural Concrete (fib), Task Group 6.4, Precast bridges (2004). *Precast concrete bridges.* Bulletin no. 29.

[6] Kenter, R.J.A. (2010). Master thesis: *The elevated metro structure in concrete, UHPC and composite, Literature and preliminary study*. Delft: Delft University of Technology and Rotterdam Public Works.

[7] Kolstein M.H. (2008). *Fibre Reinforced Polymer (FRP) structures, CT5128*. Delft: Delft University of Technology.

[8] Kuiper, R.R. & Feijen, Th.A. (1997). *Richtlijnen Metro Viaduct: Richtlijnen voor de berekening van de viaducten en bovengrondse stations t.b.v. de metro*. Rotterdam: Ingenieursbureau Gemeentewerken Rotterdam, Beton- en Staalbouw.

[9] Normcommissie 351 001 “Technische Grondslagen voor Bouwconstructies” (2006). *NEN-EN 1990/A1, Eurocode: Basis of structural design*. Delft: Nederlands Normalisatie-instituut.

[10] Normcommissie 351 001 “Technische Grondslagen voor Bouwconstructies” (2003). *NEN-EN 1991-2, Eurocode 1: Actions on structures – Part 2: Traffic loads on bridges*. Delft: Nederlands Normalisatie-instituut.

[11] Normcommissie 351 001 “Technische Grondslagen voor Bouwconstructies” (2005). *NEN-EN 1992-1-1, Eurocode 2: Design of concrete structures – Part 1-1: General rules and rules for buildings*. Delft: Nederlands Normalisatie-instituut.

[12] Normcommissie 351 001 “Technische Grondslagen voor Bouwconstructies” (2005). *NEN-EN 1992-2, Eurocode 2: Design of concrete structures – Concrete bridges: Design and detailing rules*. Delft: Nederlands Normalisatie-instituut.

[13] Normcommissie 351 001 “Technische Grondslagen voor Bouwconstructies” (2009). *Draft NEN-EN 1992-2/NB, Eurocode 2: Design of concrete structures – Concrete bridges: Design and detailing rules*. Delft: Nederlands Normalisatie-instituut.

[14] Normcommissie 351 001 “Technische Grondslagen voor Bouwconstructies” (2009). *NEN 6723, Regulations for concrete – Bridges – Structural requirements and calculation methods*. Delft: Nederlands Normalisatie-instituut.

[15] Peperkamp, W.J.M. (2008). *Case study Prestressed Concrete CT4160, Programme 2007/2008*. Delft: Delft University of Technology.

[16] Schmidt, M. & Fehling, E. (2004). *Ultra-High-Performance Concrete: Research, Development and Application in Europe*. Kassel: International Symposium on UHPC in 2004.

[17] Schutte W.D. & Sayed M. (2009). Bachelor thesis: *Onderzoek naar composietmaterialen in brugconstructies.* Rotterdam: Hogeschool Rotterdam and Rotterdam Public Works.

[18] SETRA and AFGC (2002). *Ultra High Performance Fibre-Reinforced Concrete, Interim Recommendations*.

[19] Simone, A. (2007). *Analysis of slender structures, CT3110*. Version 0.1. Delft: Delft University of Technology.

[20] Smith, K.B. & Shust, W.C. (2004). *Bounding Natural Frequencies in Structures I: Gross Geometry, Material and Boundary Conditions*. Southwest Research Institute® and Objective Engineers, Inc.

[21] Spanbeton BV. *Infra bouwoplossingen Spanbeton, de verbindende factor*. Koudekerk a/d Rijn.

[22] Tender, R.E.M. de & Pols, D. (2001). *Gegevens Metrobouw*. Rotterdam: Ingenieursbureau Gemeentewerken Rotterdam, Beton- en Staalbouw.

[23] Tol, A.F. van (2003). *Funderingstechnieken, ontwerpaspecten, CT2330*. Delft: Delft University of Technology.

[24] Walraven, J.C. (2006). *Prestressed Concrete, CT4160*. Delft: Delft University of Technology.

Internet

[i1] http://groupsci.com/skytrain_-_vancouver.htm (9-8-2010)

[i2] http://tet.rdw.nl/nl/nederlandse_tet_site/ (9-8-2010)

[i3] http://v3.espacenet.com/publicationDetails/biblio?CC=NL&NR=2001830C2&KC=C2&FT=D&date=20100121&DB=EPODOC&locale=nl_nl (9-29-2010)

[i4] http://v3.espacenet.com/publicationDetails/biblio?CC=WO&NR=2010059048A2&KC=A2&FT=D&date=20100527&DB=EPODOC&locale=nl_nl (9-29-2010)

[i5] http://www.ductal-lafarge.com/wps/portal/Ductal/Technology/MechanicalPerformances (7-13-2010)

[i6] http://www.gakei.com/th1/bts.htm (8-30-2010)

[i7] http://www.performance-composites.com/carbonfibre/mechanicalproperties_2.asp (9-8-2010)

[i8] http://www.skyscrapercity.com/showthread.php?t=326914 (12-15-2009)

List of figures

Figures

Tables

Graphs